Engineering

Journal of Research

of the

National Bureau of Standards

FEBRUARY 1934

VOLUME

U. S. DEPARTMENT OF COMMERCE
Charles Sawyer, Secretary
NATIONAL BUREAU OF STANDARDS
A. V. Astin, Director

FEBRUARY • 1954
VOLUME • 52
NUMBER • 2

JOURNAL OF RESEARCH

of the

NATIONAL BUREAU OF STANDARDS

PERIODICALS OF THE NATIONAL BUREAU OF STANDARDS

The National Bureau of Standards is engaged in fundamental and applied research in physics, chemistry, mathematics, and engineering. Projects are conducted in thirteen fields: electricity, optics and metrology, heat and power, atomic and radiation physics, chemistry, mechanics, organic and fibrous materials, metallurgy, mineral products, building technology, applied mathematics, electronics, and radio propagation. The Bureau has custody of the national standards of measurement and conducts research leading to the improvement of scientific and engineering standards and of techniques and methods of measurement. Testing methods and instruments are developed; physical constants and properties of materials are determined; and technical processes are investigated.

JOURNAL OF RESEARCH

Internationally known as a leading scientific periodical, the Journal presents research papers by authorities in the specialized fields of physics, mathematics, chemistry, and engineering. Complete details of the work are presented, including laboratory data, experimental procedures, and theoretical and mathematical analyses. Annual subscription: domestic, $5.50; foreign, $6.75.

TECHNICAL NEWS BULLETIN

Summaries of current research at the National Bureau of Standards are published each month in the Technical News Bulletin. The articles are brief, with emphasis on the results of research, chosen on the basis of their scientific or technological importance. Lists of all Bureau publications during the preceding month are given, including Research Papers, Handbooks, Applied Mathematics Series, Building Materials and Structures Reports, and Circulars. Each issue contains 12 or more type-volume pages; illustrated. Annual subscription: domestic, $1.00; foreign, $1.25.

BASIC RADIO PROPAGATION PREDICTIONS

The Predictions provide the information necessary for calculating the best frequencies for communication between any two points in the world at any time [illegible] month. The data are important to all users of high-frequency radio communications and [illegible] broadcasting, aviation, commercial and [illegible] communications, as well as for investigators of [illegible] and ionosphere. Each issue, covering a period of one month, is published three months in [illegible] Annual subscription: [illegible]

[illegible] publications [illegible] Government Printing [illegible] Washington [illegible]

[illegible] of this publication has been approved [illegible] of the Bureau [illegible] may be made

Journal of Research of the National Bureau of Standards Vol. 52, No. 2, February 1954 Research Paper 2472

Synthesis and Physical Properties of Several Acetylenic Hydrocarbons

Philip Pomerantz, Abraham Fookson,[1] Thomas W. Mears, Simon Rothberg,[2] and Frank L. Howard

As a part of researches conducted on hydrocarbons as jet-fuel components under the auspices of the National Advisory Committee for Aeronautics, a number of acetylenic hydrocarbons and their intermediates have been prepared. The details of these syntheses and the physical constants measured on the compounds are presented.

1. Introduction

The work described herein is the continuation of hydrocarbon research conducted at the Bureau since 1937 under the administrative sponsorship of the National Advisory Committee for Aeronautics. Previous papers [5, 12] [3] have described the preparation and physical properties of a number of aliphatic hydrocarbons and their intermediates; these were used mainly in researches on the detonation properties of fuels for reciprocating engines. More recently, attention has been directed to fuels for reaction engines. The emphasis at the Bureau was thereby shifted to hydrocarbons useful in investigations of basic problems in jet-fuel combustion. The hydrocarbons selected for synthesis were alkynes, alkadiynes, and an alkenyne, and were chosen in order to ascertain the effects of structure on flame speed and other properties. These compounds and the intermediates used in their syntheses are listed in table 1, in which are enumerated the physical constants of the material prepared, the purities of selected hydrocarbons, and the melting points of the mercury derivative of the 1-acetylenes [6].

[1] Present address, Frankl Photographic Services, Washington, D. C.
[2] Present address, National Institutes of Health, Bethesda, Md.
[3] Figures in brackets indicate the literature references at the end of this paper.

TABLE 1. *Physical properties of compounds prepared*

Compound	Boiling point at 760 mm Hg	Freezing point in air	Density at 20° C	Refractive index at 20° C	Melting point of mercury derivative [6]	Purity [a]
	° C	° C	g/ml	n_D^{20}	° C	Mole percent
Propyne					208 to 210	97.6 MS
1-Butyne		−125.87			161.5 to 162	
2-Butyne	26.97	−32.33	0.6906	1.3918		99.88 FP
1-Pentyne	40.233	−106.5	.69400	1.38476	117 to 118	99.5 MS
2-Pentyne	56.12	−109.45	.71040	1.40336		
3-Methyl-1-butyne	29.0	[b] nf	.6727	1.3756	[c] 76.5 to 77	
1-Hexyne	71.38	−132.4	.7149	1.3986	95.7 to 96.7	
2-Hexyne	84.52	−89.58	.73146	1.41382		
3-Hexyne	81.43	−103.16	.7226	1.4112		
3-Methyl-1-pentyne	57.7	nf	.7037	1.3916	74 to 75	
4-Methyl-1-pentyne	61.3	−105.3	.7047	1.3932	100 to 100.5	
4-Methyl-2-pentyne	73.13	−110.37	.7157	1.4057		
3,3-Dimethyl-1-butyne	37.72	−78.21	.6678	1.3736	92.5 to 93.0	
4-Methyl-2-hexyne	99.54	−107.63	.73855	1.4170		99.8 MS
5-Methyl-2-hexyne	102.46	[d] −92.91	.73776	1.41762		99.89 LTC
2-Methyl-3-hexyne	95.2	−116.7	.7249	1.4120		
1-Octyne	126.20	−79.6	.7468	1.4163	80.5 to 81.0	
1-Pentyne-3-ene(*cis* and *trans*)[e]	43.8 to 44.0		.7304 to .7297	1.4293 to 1.4340		
1-Pentyne-3-ene(*trans*)[e]	51.9		.7270	1.4377	155.3 to 157	
1,3-Butadiyne	10 to 11					99.8 MS
1,5-Hexadiyne	87.858	−4.266	.79943	1.43934	Polymer	
1-Pentyne-4-ol	27.3	nf	.8957	1.4388		
1,1-Dichloro-3-methylbutane	[f] 129.6	nf	1.0473	1.4342		
1,1-Dichloro-3-methylpentane	[g] 157.2	nf	1.0373	1.4426		
1,1-Dichloro-3,3-dimethylbutane	[h] 146.0	−60.3	1.0272	1.4388		
4-Methyl-2-chloro-1-pentene	102 to 103					
1,2,5,6-Tetrabromohexane		49 to 50				

[a] FP, purity from freezing curve analysis [16]; LTC, purity by low-temperature calorimetry (by G. T. Furukawa, Thermodynamics Section [4]); MS, purity by mass spectrometry (by V. H. Dibeler and F. L. Mohler, Mass Spectrometry Section.)
[b] nf is nonfreezing, glassy at low temperatures.
[c] On freshly prepared material. After standing for 4 days, material became yellow and did not melt at 150° C.
[d] Triple point, measured in calorimeter by G. T. Furukawa of Thermodynamics Section. Molar heat of fusion = 10,600 joules.
[e] *cis* and *trans* designations from infrared spectrometry, performed and interpreted by F. A. Smith and J. E. Stewart.
[f] 90° C at 240 mm.
[g] 92° C at 100 mm.
[h] 85° C at 104 mm.

2. Equipment

2.1. Reaction Vessels

Large-scale reactions were carried out in a commercial 50-gal stainless-steel reaction vessel designed to permit any jacket temperature from 5° to 150° C to be maintained. This kettle is described in a previous publication [5].

For experimental runs and for small-scale work, a 5-gal brass kettle was used. This was made of 12-in. brass tubing with a sheet-brass bottom brazed into place and a removable flanged top to facilitate emptying and cleaning. The top was equipped with openings for stirrer, addition vessel, reflux condenser, and observation hole, and was held in place by means of C-clamps and sealed by means of a neoprene gasket pressed between the flanges. This reactor was of sufficiently small size to allow immersion in a bath for heating or cooling, as necessary. Because of the relatively high heat conductivity of the metal, this apparatus permitted highly exothermic reactions, such as halide condensations (see sec. 3.4), to be run with appreciable savings of time and much greater safety than prevails with the use of glass equipment of equal capacity. Glass equipment was used only for very small-scale preliminary reactions.

For reactions using liquid ammonia as a solvent (see sec. 3.2 and 3.3), a 10-gal stainless-steel reaction vessel was installed. This was jacketed for temperature control and equipped with appropriate valves and flanged openings; on the bottom was a 2-in. drain valve, on the top were openings for a 2-in. peephole, gas inlet, and reflux condenser. The peephole was normally stoppered, but when necessary, it could be used for observation of the reaction or addition of reagents. Acetylene and other gases were introduced through a ¼-in. steel pipe brazed through a flange and extending almost to the bottom of the vessel. The condenser consisted of a 30-gal open-top insulated cylinder, through which passed two intertwined coils made of 20-ft lengths of ¾-in. steel pipe welded into a 1-in. tee at the bottom. The 1-in. tee connected to a sight-glass for observation of reflux and thence to the kettle. Stirring was effected by means of a built-in stirrer driven by an explosion-proof motor. The kettle was insulated on all sides with a 6-in. layer of ground cork. When in continuous operation, it was necessary to fill the condenser with dry ice only at 8-hr intervals.

2.2. Distillation Equipment

There were seven stills available for this work. These were used for purification of reagents, for the fractionation of final hydrocarbons and some of the intermediates, and have been described previously [5]. For convenience, the salient features of each are listed in table 2.

TABLE 2.

Still	Type	Size	Packing	Pot capacity
		cm		ml
5	Total reflux variable takeoff.	150 by 2.2	3/32-in. stainless steel helices from 0.010-in. wire.	200 to 5,000.
6	do	150 by 2.2	3/16-in. glass helices	200 to 5,000.
17	Podbielniak Hypercal.	127 by 0.8	Heli-grid	250 to 5,000.
19	do	250 by 2.5	do	250 to 5,000.
21	Total reflux variable takeoff.	120 by 3.5	3/16-in. glass helices	22,000.
22	do	183 by 2.5	3/32-in. stainless steel helices from 0.010-in. wire.	500 to 5,000.
28	do	35 by 2.5	¼-in. glass helices	2,000.

3. Methods and Technique

3.1. Preparation of Grignard Reagents

The Grignard reagents necessary for some of the syntheses were prepared in the 50-gal stainless-steel kettle according to the methods used previously [5]. In all cases the Grignard reagent was then reacted in place.

3.2. Preparation of Sodium Acetylide

For the preparation of many of the acetylene homologs, the starting material was monosodium or disodium acetylide. The flow sheets of the several synthetic schemes, using these compounds as starting materials, are given as methods A to C in table 3, in which are enumerated the several different synthetic routes used in this work and the compounds prepared thereby. The technique of preparing sodium acetylide was adapted from that used by K. W. Greenlee and his associates at Ohio State University, Columbus, Ohio. These sodium acetylides were conveniently prepared in the 10-gal stainless-steel reactor and alkylated in place to the desired alkyne. A typical preparation of 60 moles of monosodium acetylide is described below.

About 10 kg of commercial anhydrous ammonia was added in the liquid phase to the reactor through the gas-inlet tube, the cold refluxing ammonia being sufficient to cool the pot. Then 15 g of ferric chloride was added deftly in 3 portions through the peephole. The reaction was quite violent, and after the reflux had subsided, about 60 g of sodium cut in small pieces was added. After the sodium had dissolved, a stream of dry air was passed through the gas-inlet tube for about 1½ min, in order to form a catalyst, which would be effective in converting the sodium into the amide rapidly. Sodium cut into approximately ½-in. cubes was then added in portions with stirring until a total of 1,389 g (60 g-atoms) was added The reaction was vigorous, and a continuous

TABLE 3. *Flow sheet of alkyne syntheses*

Method A. Alkylation of monosodium acetylide:

$$Na \xrightarrow[NH_3]{\text{liquid}} NaNH_2 \xrightarrow{CH\equiv CH} NaC\equiv CH \xrightarrow{RX^*} RC\equiv CH$$

R=CH_3, C_2H_5, *n*-C_3H_7, *n*-C_4H_9, *n*-C_6H_{13}.

Method B. Symmetrical alkylation of disodium acetylide:

$$Na \xrightarrow[NH_3]{\text{liquid}} NaNH_2 \xrightarrow{CH\equiv CH} NaC\equiv CNa \xrightarrow{RX} RC\equiv CR$$

R=CH_3, C_2H_5

Method C. Unsymmetrical alkylation of acetylene (in situ):

$$Na \xrightarrow[NH_3]{\text{liquid}} NaNH_2 \xrightarrow{CH\equiv CH} NaC\equiv CH \xrightarrow{RX} RC\equiv CH \xrightarrow[NaNH_2]{\text{powdered}} RC\equiv CNa \xrightarrow{R'X} RC\equiv CR'$$

R=C_2H_5, *n*-C_3H_7

R′=CH_3

Method D. Alkylation of 1-alkynes:

$$Na \xrightarrow[NH_3]{\text{liquid}} NaNH_2 \xrightarrow{RC\equiv CH} RC\equiv CNa \xrightarrow{R'X} RC\equiv CR'$$

R=*i*-C_3H_7, *i*-C_4H_9, *s*-C_4H_9

R′=CH_3, C_2H_5

Method E. Vinylation and dehydrohalogenation reactions:

$$RCl \xrightarrow{CH_2=CHCl} RCH_2CHCl_2 \xrightarrow[90°\text{-}100°C]{NaNH_2} RC\equiv CH$$

R=*i*-C_3H_7, *s*-C_4H_9, *t*-C_4H_9

Method F. Alkylation and dehydrohalogenation reactions:

$$RMgX + CH_2=CClCH_2Cl \longrightarrow RCH_2CCl=CH_2 \xrightarrow[150°C]{NaNH_2} RCH_2C\equiv CH$$

R=*i*-C_3H_7

Method G. Dehydrohalogenation and isomerization reactions:

$$HOCH(R)C\equiv CCH(R)OH \xrightarrow{SOCl_2} ClCH(R)C\equiv CH(R)Cl \xrightarrow{KOH} RC\equiv CC\equiv CR$$

R=H

Method H. Halogenation and dehydrohalogenation:

$$CH_2=CHCH_2CH_2CH=CH_2 \xrightarrow{Br_2} CH_2BrCHBrCH_2CH_2CHBrCH_2Br \xrightarrow[NH_3(l)]{NaNH_2} CH\equiv C-CH_2CH_2C\equiv CH$$

Method I. Alkynation and dehydration reactions:

$$Na \xrightarrow[NH_3]{\text{liquid}} NaNH_2 \xrightarrow{CH\equiv CH} NaCC\equiv CH \xrightarrow[-33°C]{RCHCH_2\ (O)} CH\equiv CCH_2CH(R)OH \xrightarrow[\text{chloride}]{p\text{-toluene sulfonyl}}$$

$$CH\equiv CCH_2CH(R)-OSO_2C_6H_4CH_3(p) \xrightarrow[110°C]{KOH} CH\equiv C-CH=CH-R$$

R=CH_3

*RX indicates alkyl halide or alkyl sulfate.

stream of hydrogen was evolved. The solution was then stirred for 2 hr before the addition of acetylene. In several cases the conversion of sodium to sodium amide was extremely slow, the sodium merely dissolving in the ammonia. This was evidenced by the persistent, intense blue color of the liquid. In such cases the solution was permitted to stand overnight, or until it attained a characteristic black hue and the blue coloration was completely gone.

Commercial acetylene gas was then passed into the sodium-amide solution through the gas-inlet tube after it had passed through a sulfuric acid scrubber to remove entrained acetone. Disodium acetylide was formed first and imparted a milky-white appearance to the liquid. For the preparation of disodium acetylide, the gas addition was stopped when the molal ratio of acetylene to sodium was one-half. Upon continued addition of acetylene, the disodium salt was converted to the monosodium acetylide, and as the theoretical quantity for monosodium-acetylide formation was approached, the color of the solution regained its black appearance. Thus, from 60 g-atoms of original sodium, 30 moles of disodium acetylide were formed with 780 g of acetylene, whereas the addition of 1,560 g of acetylene caused formation of 60 moles of monosodium acetylide.

3.3. Alkylation Reactions

The alkylation of the sodium acetylides and their homologs was carried out in the 10-gal stainless-steel reactor. Because of the variation in the technique, representative alkylations illustrating methods A to D in table 3 are described below. A résumé of the preparation of each acetylene made thereby is given in table 4.

(a) *Method A.* Propyne was prepared in 65-percent yield by treatment of monosodium acetylide with dimethyl sulfate in liquid ammonia. Sixty theoretical moles of monosodium acetylide was prepared from 1.70 kg of acetylene (65 moles), 1.61 kg of sodium (70 g-atoms), and 18 g of ferric chloride in 11 kg of liquid ammonia, using a modification of the previously described method (see sec. 3.2). Because of the difficulty in separating acetylene from propyne, care had to be taken to avoid an excess of acetylene; consequently, only enough acetylene was added to make 60 moles of monosodium acetylide and 5 moles of disodium acetylide. In this case, the 2-butyne formed as a by-product from the disodium acetylide present offered no problem in the purification step.

To this acetylide solution was added 8.8 kg (70 moles) of dimethylsulfate over a period of 3 hr. The reaction was quite vigorous but easily controllable. The mixture was stirred overnight, after which it was treated with 11.5 liters of water. The condenser was then blocked off at the sight glass, and a delivery tube attached through the peephole flange. The evolved gas was passed through a train consisting of a water trap with a constant-level continuous-flow siphon, cold 10-percent sulfuric acid, a calcium-chloride drying tower, a dry-ice condenser, and was caught in a chilled steel cylinder containing a small amount of acetone. The product from two runs was fractionated in column 19 to recover 3.25 kg (81 moles) of purified 1-propyne (65-percent yield).

(b) *Method B.* 2-butyne was prepared by the reaction of dimethylsulfate with disodium acetylide in liquid ammonia. Forty moles of disodium acetylide were prepared from 1,840 g of sodium (80 g-atoms), 1.05 kg (40 moles) of acetylene, and 20 g of ferric chloride in 14.5 kg of liquid ammonia, by the technique previously described (see sec. 3.2). To this mixture was added 10.6 kg (84 moles) of dimethylsulfate over a period of 6 hr; the reaction was vigorous, but controllable. The solution was stirred for 16 hr, and the 2-butyne was recovered in the same manner used for propyne. In this case, however, most of the 2-butyne condensed in the chilled dilute sulfuric acid, and was distilled from this flask through a calcium-chloride tower into a steel bomb by heating the flask with an electric heating mantle. This run

TABLE 4. *Alkynes by alkylation*

Hydrocarbon	Preparative method	Reactants				Alkylation agents				Product yield	
		Na	C_2H_2	$FeCl_3$	$NH_3(l)$	RX (first)		R′X (second)			
		g-atoms	*Moles*	*g*	*kg*	*Compound*	*Moles*	*Compound*	*Moles*	*Moles*	*Percent*
Propyne	A	70	65	18	11.0	CH_3Br	60			40.5	65
1-Butyne	A	70	65	18	11.0	$(C_2H_5)_2SO_4$	60			43.7	67
2-Butyne	B	80	40	20	14.5	CH_3Br	84			17.0	42
1-Pentyne	A	21	[a]	5.5	3.5	n-C_3H_7Cl	21			7.4	35
2-Pentyne	C	45	45	12	9.1	C_2H_5Br	45	CH_3Br	[b] 48	36.3	81
1-Hexyne	A	60	60	15	10.3	n-C_4H_9Br	60			28.8	48
2-Hexyne	C	45	45	12	9.1	n-C_3H_7Br	45	$(CH_3)_2SO_4$	[b] 48.5	27	60
3-Hexyne	B	80	40	20	10.0	$(C_2H_5)_2SO_4$	80.5			25.6	[c] 64
4-Methyl-2-pentyne	D	63	[d]	15	10.0	$(CH_3)_2SO_4$	63			24	42
4-Methyl-2-hexyne	D	40	[e]	9	7.5	CH_3Br	40			25	[f] 69
5-Methyl-2-hexyne	D	35	[e]	12	9.1	CH_3Br	40			28.4	81
2-Methyl-3-hexyne	D	48	[b]	12	9.1	C_2H_5Br	50			38.6	80
1-Octyne	A	30	30	7	5.5	n-$C_6H_{13}Br$	30			11.2	38

[a] Sufficient to attain black color. [b] Preceded by 46 moles of sodium amide. [c] One run, using ethyl bromide gave 93 percent yield. [d] 57 moles of 3-methyl-1-butyne used. [e] 36 moles of 3-methyl-1-pentyne used. [f] Purified through azeotrope with ethanol, bp 74° C [10]. [g] 35 moles of 4-methyl-1-pentyne used. [h] 45 moles of 3-methyl-1-butyne used.

produced a total of 0.91 kg (17 moles) of crude 2-butyne; yield, 42 percent. The crude was fractionated through column 19 to yield 2-butyne with the properties listed in table 1.

(c) *Method C.* 2-pentyne was prepared by the treatment of monosodium acetylide with ethyl bromide in liquid ammonia, followed by the reaction of methyl bromide with the sodium derivative (formed in situ) of the resulting 1-butyne. Monosodium acetylide (45 moles) was formed from 1,035 g (45 g-atoms) of sodium, 1.17 kg (45 moles) of acetylene and 12 g of ferric chloride in 9.1 kg of ammonia by the usual technique (see sec. 3.2). To this solution was added 4.91 kg of ethyl bromide (45 moles) over a period of 2½ hr, during which the reaction was quite vigorous. After the addition was completed, the reaction mixture was stirred for 1½ hr before adding 1.82 kg of commercial sodium amide over a period of 45 min. The solution was stirred for 1 hr, and then 4.58 kg of methyl bromide was added to the reaction in the liquid phase. The mixture became quite viscous and was allowed to stand overnight. The next morning it had solidified and the stirrer would not operate. To loosen it, 2.7 kg of liquid ammonia was added. This was followed by 3.8 liters of isooctane [4] as solvent and 15 liters of water. There was no vigouous reflux during this decomposition. The organic layer was separated, washed twice with cold water, once with dilute hydrochloric acid, and dried over anhydrous sodium carbonate.

On distillation there was obtained 2.47 kg (36.3 moles) of pure 2-pentyne with the properties listed in table 1. This recovery corresponds to a yield of 81 percent.

(d) *Method D.* 5-methyl-2-hexyne was formed by the methylation of 4-methyl-1-pentyne prepared by method E. To a solution of sodium amide prepared in the usual way from 805 g (35 g-atoms) of sodium, 12 g of ferric chloride, and 9.1 kg of ammonia, was added 2.87 kg (35 moles) of 4-methyl-1-pentyne. The addition took 1 hr and did not cause very vigorous refluxing. After 2 hr of stirring, 3.64 kg (38 moles) of methyl bromide was added rapidly through the gas-inlet tube. The reaction mixture was stirred overnight, after which it was treated with 19 liters of water. The organic layer was filtered and washed three times with water, and then dried over anhydrous sodium carbonate. Distillation of the crude through column 6 yielded 2.73 kg of material, boiling at 102° to 103° C (yield, 81 percent). Redistillation in still 19 yielded a product with the properties listed in table 1.

[4] Isooctane is the trivial name for 2,2,4-trimethylpentane.

3.4. Preparation of Halides—Methods E to H

Direct alkylation of sodium acetylide is not successful with branched-chain adducts. Therefore, it was necessary to prepare branched acetylenes by dehydrohalogenation of appropriate halogen compounds [17]. Several dihalides used in method E (see table 3) were prepared by adaptations of the vinylation method of Schmerling [15]; one chlorolefin was prepared by the Grignard reaction [9]. Dehydrohalogenation reactions were also used for the syntheses of two diacetylenes (methods G and H). The halides for these were made by chlorination of a polyalcohol and by addition of bromine to a diolefin. In table 5 are given data on typical syntheses of the intermediate halides used in preparing 3-methyl-1-butyne, 3-methyl-1-pentyne, 3,3-dimethyl-1-butyne, 4-methyl-1-pentyne, 1,3-butadiyne, and 1,5-hexadiyne, respectively, some of which were used in additional preparations utilizing alkylation techniques (see table 4).

(a) *Halides for method E.* Inasmuch as the quantities involved in these syntheses were many times greater than those used by Schmerling, it was necessary to develop techniques for the addition of reagents and control of the reaction in order to assure adequate yield. Typical of the several vinylation reactions is the preparation of 1,1-dichloro-3-methylbutane, which proceeds according to the reaction

$$i\text{-}C_3H_7Cl + CH_2{=}CHCl \xrightarrow[-30^\circ \text{ to } -40^\circ \text{ C}]{AlCl_3} (CH_3)_2CHCH_2CHCl_2.$$

To the 5-gal brass reactor equipped with stirrer, condenser cooled to −78° C, thermometer, and inlet tube were added 3.92 kg (50 moles) of isopropyl chloride and 340 g (2.5 moles) of aluminum chloride. Effervescence and darkening of the liquid began immediately upon this addition; the former ceased after a short time and did not resume during the subsequent addition of vinyl chloride. After the initial heat of reaction had been dissipated, the contents of the pot was cooled to −30° C, and 3,286 g (53 moles)

TABLE 5. *Halide intermediates*

Compound prepared	Method (see table 3)	Reactants			Yields	
					Moles	*Percent*
$(CH_3)_2CHCH_2CHCl_2$	E	$(CH_3)_2CHCl$(50 moles)	$CH_2{=}CHCl$(53 moles)	$AlCl_3$(340 g)	36	72
$CH_3CH_2CH(CH_3)CH_2CHCl_2$	E	$CH_3CH_2C(CH_3)Cl$(60 moles)	$CH_2{=}CHCl$(60 moles)	$AlCl_3$(351 g)	40.7	68
$(CH_3)_3CCH_2CHCl_2$	E	$(CH_3)_3CCl$(50 moles)	$CH_2{=}CHCl$(53 moles)	$AlCl_3$(454 g)	35	70
$(CH_3)_2CHCH_2CCl{=}CH_2$	F	$CH_2{=}CClCH_2Cl$(153 moles)	[a]$(CH_3)_2CHMgCl$		70	[b]59
$ClCH_2C{\equiv}CCH_2Cl$	G	$HOCH_2C{\equiv}CCH_2OH$(4.7 moles)	$SOCl_2$(8.4 moles)		3.3	70
$CH_2BrCHBrCH_2CH_2CHBrCH_2Br$	H	$CH_2{=}CHCH_2CH_2CH{=}CH_2$(24 moles).	Br_2(48 moles)		20.4	84

[a] Prepared from 170 moles of isopropylchloride, 170 g-atoms of magnesium in 52 liters of ether.
[b] Based on dichloride consumed.

of vinyl chloride was bubbled rapidly into the stirred solution. This reaction is extremely exothermic, and rapid removal of heat is essential to prevent its becoming violent. In this case the addition required about 2 hr with the temperature at −30° to −40° C. The solution was stirred for 90 min after the addition was completed; the entire brownish reaction mixture was then poured onto cracked ice. After the colors of the aluminum-chloride complexes disappeared, a yellow liquid, heavier than water, remained. About 2,000 ml of ligroin was added as solvent; the resulting organic solution was washed once with dilute sodium carbonate and twice with water, dried over anhydrous sodium carbonate, and fractionated through column 6. After the ligroin forerun, there was collected a main product of 1,600 ml, boiling 127° to 130.5° C. The yield was 72 percent.

(b) *Halide for method F.* The chloroolefin used in method F was prepared by the reaction of isopropylmagnesium chloride on 2,3-dichloro-1-propene, according to the equation

$$(CH_3)_2CHMgCl + CH_2Cl{-}CCl{=}CH_2 \longrightarrow (CH_3)_2CH{-}CH_2{-}\underset{\displaystyle Cl}{\underset{|}{C}}{=}CH_2.$$

Isopropylmagnesium chloride was prepared in the usual manner from 13.4 kg (170 moles) of isopropyl chloride, 4.09 kg of magnesium turnings (170 g-atoms), and 52 liters of anhydrous ether in the 50-gal stainless-steel kettle. To this stirred solution 16.95 kg (153 moles) of 2,3-dichloro-1-propene dissolved in 16 liters of ether was added over a period of 3 days. At the end of this time, the reaction mixture was treated in the usual manner with 5.45 kg of concentrated hydrochloric acid in 75 liters of water. The ether layer was washed four times with water and dried over anhydrous sodium carbonate. On distillation through column 6, the organic layer yielded 3.82 kg (34 moles) of unreacted 2,3-dichloro-1-propene (bp 88° to 96° C) and 8.27 kg (70 moles) of 4-methyl-2-chloro-1-pentene (bp 100° to 104° C). The yield, based on material consumed, was 59 percent.

(c) *Halide for method G.* The 1,4-dichloro-2 butyne used in this work was prepared by reaction of commercial 1,4-dihydroxy-2-butyne with thionyl chloride [1]. To a 5-liter flask fitted with stirrer, dropping funnel, and reflux condenser, and containing 400 g of pulverized 1,4-butynediol was added 1,000 g of pure thionyl chloride; during this addition, the temperature of the mixture decreased to about −15° C. The mixture was warmed to 10° C with stirring for 12 hr and was then heated to 60° C, as long as sulfur dioxide evolved. The direct vacuum distillation of this mixture yielded 399 g of 1,4-dichloro-2-butyne, bp 50° to 70° C at 6.5 mm Hg (yield, 70 percent).

(d) *Halide for method H.* The tetrabromide for this synthesis was made by addition of bromine to 1,5-hexadiene in several runs. In one of these, 800 ml of chloroform and 490 g (6 moles) of 1,5-hexadiene were added to a 5-liter 3-necked ice-cooled flask equipped with stirrer, addition vessel, and condenser. Approximately 0.98 kg (6 moles) of bromine was added slowly over a period of 2 hr, followed by 100 ml of additional chloroform and then by another charge of 0.98 kg (6 moles) of bromine. After the addition was complete, the mixture was filtered. The first crop of crystals weighed 517 g; when the filtrate was cooled to −20° C, an additional 502 g of crystals were obtained in the second crop, and 228 g in the third. From four such runs, a total of 8,104 g of 1,2,5,6-tetrabromohexane was prepared, representing an over-all yield of 85 percent.

3.5. Dehydrohalogenation Reactions

Some of the dehydrohalogenations of dichlorides and of the chloroolefin to the corresponding acetylenes were carried out in the 50-gal stainless-steel vessel. Table 6 lists some of the compounds prepared in this manner. The most convenient method of dehydrohalogenation utilized sodium amide suspended in refined light mineral oil at about 100° to 150° C [2]. The technique employed in dehydrochlorinations in methods E and F is illustrated by the conversion of 1,1-dichloro-3-methylbutane to 3-methyl-1-butyne.

(a) *Large-scale dehydrohalogenations in methods E and F.* The top of the condenser of the kettle was connected to another condenser kept at −20° C and thence to a 5-liter trap at −20° C. To the 50-gal stainless-steel kettle was added 26.5 liters of

TABLE 6. *Hydrocarbons by dehydrohalogenation*

Hydrocarbon	Synthetic method (see table 3)	Halide		Sodium amide	Dispersion medium		Yield	
		Formula	Quantity		Volume	Temperature		
			Moles	*Moles*	*Liters*	*°C*	*Moles*	*Percent*
3-Methyl-1-butyne	E	$(CH_3)_2CHCH_2CHCl_2$	80	281	[a]26.5	94	49	62
3-Methyl-1-pentyne	E	$CH_3CH_2CH(CH_3)CH_2CHCl_2$	107	375	[a]38	100	62.5	59
3,3-Dimethyl-1-butyne	E	$(CH_3)_3CCH_2CHCl_2$	60	210	[a]19	90 to 95	28.5	45
4-Methyl-1-pentyne	F	$(CH_3)_2CHCH_2CCl{=}CH_2$	67.3	168	[a]38	140	53.7	80
1,3-Butadiyne	G	$CH_2ClC{\equiv}CCH_2Cl$	[b]1.5	[c]7.0	[d]0.80	[e]75	0.9	60
1,5-Hexadiyne	H	$CH_2BrCHBrCH_2CH_2CHBrCH_2Br$	[f]6.6	58	[g]17.5	−33	4.16	63

[a]Mineral oil. [b]Dissolved in 1,200 g of 95% ethanol. [c]KOH. [d]Water. [e]Inverse addition. KOH-in-water solution added to heated ethanol solution. [f]Dissolved in 7 liters of diethylether. [g]Liquid ammonia.

light oil and 4.5 kg of sodium amide. The suspension was heated to 140° C, and an initial 200 ml of 1,1-dichloro-3-methylbutane was started to initiate the reaction; dehydrochlorination began immediately, as evidenced by the evolution of ammonia. The temperature of the suspension was reduced to 94° C, and 3,630 g of the dihalide was added over a period of 3 hr. Ammonia was evolved during the entire course of the addition.

The next day, the contents of the kettle were cooled and an additional 6.36 kg of sodium amide was added to the pot (total 281 moles). Again the reaction mixture was heated to 94° C, and the remainder of the dihalide, total 11.4 kg (80 moles), was added over a 7-hr period. There was a continuous evolution of ammonia during the addition, and the reaction mixture assumed the consistency of a thick grease. The mixture was then heated for 48 hr, and it was noted that refluxing had ceased.

After cooling the reaction mixture, 7.5 liters of water was added cautiously with stirring. Only slight amounts of ammonia were evolved at this stage. Then there was added 3,500 ml sulfuric acid (63 moles) in 95 liters of water. The reaction mixture was then distilled from the kettle until the distillate reached a temperature of 95° C. The distillate was caught in isooctane, dried, and redistilled to recover 3.36 kg (49 moles) of 3-methyl-1-butyne, bp 27° to 32° C, yield, 62 percent.

For the preparation of butadiyne and 1,5-hexadiyne, this method of dehydrohalogenation was not used; the data on these dehydrohalogenations are given in table 6, and the description of the syntheses of these compounds are given below. Because of the ease of polymerization and peroxidation of these compounds, the syntheses and purifications were conducted in an inert atmosphere, and the final products sealed under their own vapor pressure.

(b) *Dehydrochlorination in method G.* The starting material for the synthesis of 1,3-butadiyne was 1,4-dihydroxy-2-butyne [14] purchased from a commercial source. This alcohol was converted to 1,4-dichloro-2-butyne [5], as described in section 3.4(c). The dichloride was converted to butadiyne by reaction with potassium hydroxide [7]. To a solution of 195 g of 1,4-dichloro-2-butyne in 1,200 g of 95-percent ethanol at 75° C was added with stirring a solution of 400 g of potassium hydroxide and 800 g of water. The evolved 1,3-butadiyne was scrubbed with dilute potassium hydroxide and dried with calcium chloride. The yield in this step was 60 percent. The product from several such runs was fractionated in still 28. Mass-spectrometer analysis of the center cut indicated this distillate to be 99.8 percent pure.

(c) *Dehydrobromination in method H.* 1,5-Hexadiyne was obtained from the dehydrobromination of 1,2,5,6-tetrabromohexane with sodium amide in liquid ammonia.

As a starting material for this synthesis, large quantities of 1,5-hexadiene were prepared in the stainless-steel reactor in two identical runs. One of these is described below.

To 2.83 kg (118 moles) of magnesium in the kettle was added 3 liters of a solution prepared by mixing 15.2 kg (200 moles) of allyl chloride and 60 liters of ether. After reaction had started, 20 liters of ether and the remainder of the allyl chloride-ether mixture were added while the kettle jacket was kept cold. The reaction was not a very violent one, but as the addition proceeded, the mixture thickened considerably and became milky-white. Stirring was continued for 3 days; the mixture was then treated with 49 liters of water and about 3.6 kg of hydrochloric acid. The ether layer was washed three times with water and dried over anhydrous sodium carbonate. The products of two such runs were combined and distilled in column 6 to give 11.31 kg (138 moles) diallyl boiling 56° to 63° C. This recovery corresponds to a 69-percent yield.

The 1,5-hexadiene was converted to the tetrabromide by treatment with bromine, as described in section 3.4(d); the 1,2,5,6-tetrabromohexane was then converted to 1,5-hexadiyne by an adaptation of the method of Raphael and Sandheimer [13]. One of the four dehydrobrominations is described.

To 12 kg of liquid ammonia in the 10-gal stainless-steel kettle was added 2.27 kg (58 moles) of powdered sodium amide. To this stirred solution was added 2.63 kg (6.6 moles) of 1,2,5,6-tetrabromohexane dissolved in 7 liters of ether, and the solution stirred for 2 days. During this period the dry-ice condenser was allowed to warm up, permitting some of the ammonia to boil off. At the end of this time the reaction mixture was treated with 20 moles of ammonium chloride and 15 liters of water. The organic layer was siphoned, washed three times with water, and dried over anhydrous sodium carbonate. After the bulk of the ether had been stripped, the organic layer was distilled in column 19, and 313 g of a fraction boiling 86° to 88° C was obtained, along with a forerun boiling 50° to 86° C. The total yield was 63 percent. Continued distillation past 90° C resulted in an explosion. The combined yield (bp 80° to 88° C) from four such runs was redistilled in column 19, under a nitrogen atmosphere, to give the material with the properties listed in table 1 for this diacetylene.

3.6. Miscellaneous Reactions—Method I

The reactions illustrated by method I in table 3 were used for the preparation of 1-pentyne-3-ene. Because of its reactivity, the compound was sealed in the absence of air.

(a) *1-Pentyne-3-ene.* This compound was prepared by treating the *p*-toluenesulfonate of 1-pentyne-4-ol with potassium hydroxide [3]. The 1-pentyne-4-ol was prepared by reacting propylene oxide with monosodium acetylide [8].

Sodium acetylide was prepared in the usual manner from 1,172 g of sodium, 15 g of ferric chloride, and 1.36 kg of acetylene in 10 ky of liquid ammonia. To this was added 2,500 g (43 moles) of propylene oxide, and the mixture was stirred all night. The ammonia was allowed to evaporate, and 6 liters of water were added slowly. The reaction mixture was transferred to a glass vessel, made slightly acid

with acetic acid, and steam distilled. The distillate was saturated with potassium carbonate and the organic layer separated, dried, and distilled. The portion boiling at 127.3° to 127.5° C was collected as 1-pentyne-4-ol. The yield was 1,377 g (38 percent).

A solution of 1,656 g of *p*-toluenesulfonyl chloride in 1,120 ml of warm pyridine was cooled rapidly to obtain small crystals. To this slurry was added slowly 675 g (8.05 moles) of 1-pentyne-4-ol. The solution was well stirred and the temperature kept below 30° C with external cooling. After the vigor of the reaction had subsided, it was allowed to stand at room temperature for 20 hr, after which 1 liter of water was added with cooling. The reaction mixture was extracted with 2 liters of ether and the extract washed 4 times with 1.5 liters of 30-percent sulfuric acid, 3 times with 1 liter of saturated sodium-bicarbonate solution, and, finally, 2 times with water and dried. The ether was removed by vacuum until a final pressure of 4 mm Hg was reached. The yield was 1,876 g (98 percent).

To a stirred solution of 600 g of potassium hydroxide in 2 liters of water was added slowly 1,876 g (7.85 moles) of the *p*-toluene-sulfonate of 1-pentyne-4-ol. The reaction temperature was kept at 110° C, and a small amount of wetting agent was added to facilitate the reaction. The evolved vapors were collected in a trap at −25° C; the frozen distillate was melted periodically and the layers separated. The organic material amounted to 486 g (7.36 moles), representing a yield of 94 percent. This material was dried with calcium chloride and distilled in column 19. The distillation gave first a mixture of *cis* and *trans* forms (bp 43.8° to 43.9° C, $n_D^{20}=1.4289$ to 1.4316) and then the pure *trans* form (bp 51.9° C, $n_D^{20}=1.4375$). Identification [5] of the distillate fractions was made by infrared analysis, which demonstrated the presence of these two species and the absence of other isomers.

3.7. Measurements of Physical Properties

Because of the extremely reactive nature of several of the prepared compounds, final distillations of these were conducted from hydroquinone under a nitrogen atmosphere and bottled under their own vapor pressures [11]. This method of packaging reduced the amount of peroxides present and yielded samples suitable for physical-constants measurements. In general, the properties of the hydrocarbons measured included melting point or triple point, boiling point, refractive index, and density. The methods and techniques used in these determinations have been given previously [12].

Where feasible, the purities of samples were measured by mass spectrometry, calorimetrically [4], or by freezing-curve analysis [16]. For a more complete characterization of some of the 1-acetylenes, mercury derivatives of these hydrocarbons were prepared according to the directions of Johnson and McEwen [6]. The data obtained on some of the compounds are listed in table 1, which is a summary of data obtained on the several compounds prepared.

[5] Determined and interpreted by F. A. Smith and J. E. Stewart of the Bureau's Gas Chemistry Section.

4. Conclusions

Seventeen acetylenes, 1 olefin-acetylene, and 2 diacetylenes have been prepared in high states of purity. Physical constants are reported for these compounds; where feasible, the purity of the compound was determined.

Grateful acknowledgment is made to E. A. Cadwallader, R. L. Alexander, J. A. Cogliano, J. Todorov, and E. H. Rich for their assistance in preparing some of the compounds made in this work.

We thank G. T. Furukawa of the Thermodynamics Section for making the low-temperature calorimeter measurements, and V. H. Dibeler and F. L. Mohler of the Mass Spectrometry Section for the mass-spectrograph determinations, and F. A. Smith and J. E. Stewart of the Gas Chemistry Section for the infrared-absorption data and their interpretation.

5. References

[1] P. Bauman, Chemische Werke Hüls, GMBH, Marl, Germany, private communication.
[2] M. Bourguel, Ann. Chim. [10] **3,** 191, 325 (1925).
[3] G. Eglinton, and M. C. Whiting, J. Chem. Soc. 3650 (1950).
[4] G. T. Furukawa, D. C. Ginnings, R. E. McCoskey, and R. A. Nelson, J. Research NBS **46,** 195 (1951) RP2191.
[5] F. L. Howard, T. W. Mears, A. Fookson, P. Pomerantz, and D. B. Brooks, J. Research NBS **38,** 365 (1947) RP1779.
[6] J. R. Johnson, and W. L. McEwen, J. Am. Chem. Soc. **48,** 469 (1926).
[7] E. Keyssner, and E. Eichler, German Patent 740,637.
[8] O. R. Kreimeier, U. S. Patent 2106182.
[9] Lespieau, Bul. Soc. Chim. France [4] **29,** 528 (1921).
[10] B. J. Mair, A. R. Glasgow, Jr., and F. D. Rossini, J. Research NBS **27,** 39 (1941) RP1402.
[11] B. J. Mair, D. J. Termini, C. B. Willingham, and F. D. Rossini, J. Research NBS **37,** 229 (1946) RP1744.
[12] T. W. Mears, A. Fookson, P. Pomerantz, E. H. Rich, C. S. Dussinger, and F. L. Howard, J. Research NBS **49,** 229 (1950) RP2079.
[13] R. A. Raphael, and F. Sandheimer, J. Chem. Soc., 120 (1950).
[14] W. Reppe, A. Steinhofer, H. Spaenig, and K. Locher, U. S. Patent 2306969.
[15] L. Schmerling, J. Am. Chem. Soc. **68,** 1650 (1946).
[16] Selected values of properties of hydrocarbons, NBS Circular 461 (1947).
[17] H. Van Risseghem, Bul. Soc. Chim. Belg. **42,** 229 (1933).

WASHINGTON, August 19, 1953.

Journal of Research of the National Bureau of Standards Vol. 52, No. 2, February 1954 Research Paper 2473

Synthesis and Physical Properties of Several Aliphatic and Alicyclic Hydrocarbons

Philip Pomerantz, Abraham Fookson,[1] Thomas W. Mears, Simon Rothberg,[2] and Frank L. Howard

The synthesis and purification of four paraffins, three cycloparaffins, six olefins, and five diolefins, and their intermediates are described. These compounds were prepared by standard reactions or modifications thereof, and purified by fractional distillation. Physical properties of the hydrocarbons are presented, and purity data are given for some of them.

1. Introduction

At its outset the hydrocarbon research program at the National Bureau of Standards was concerned with compounds of interest as fuel components in high-compression spark-ignition engines. Therefore, the emphasis was upon highly branched paraffin hydrocarbons [8].[3] With the advent of reaction engines, the researches were directed to the syntheses of alicyclic hydrocarbons and the less highly branched aliphatics with various degrees of unsaturation. The work on the acetylenic hydrocarbons is described in a previous paper [12]. The work described herein is the part of this program, sponsored by the National Advisory Committee for Aeronautics, dealing with the syntheses and purification of 4 paraffins, 6 olefins, 5 diolefins, and three alicyclic hydrocarbons.

2. Apparatus

2.1. Reaction Vessels

Large-scale reactions were carried out in two commercial 50-gal jacketed reaction kettles designed to permit any temperature from 5° to 150° C to be maintained. One of these was stainless steel, the other was glass-lined steel; both are described in a previous publication [8]. In general, preparations of Grignard reagents were carried out in the stainless-steel vessel; the more corrosive reactions, such as acid oxidations, were conducted in the glass-lined one.

For reactions involving liquid ammonia as a solvent (see sec. 4.9 and 4.10), a 10-gal stainless-steel kettle was used. This reactor was jacketed and insulated with a 6-in. layer of ground cork. There were appropriate facilities for the addition of reagents or observation of reflux. This equipment has been described previously [12].

2.2. Hydrogenation Equipment

Commercial rocking autoclaves of 1-, 3-, and 20-liter capacity were used for this work. A commercial nickel-on-kieselguhr catalyst was used, and the hydrogenations were usually carried out at 140° to 180° C and at a maximum pressure of 2,500 lb/in^2. This equipment is described in a previous publication [8].

2.3. Dehydration Equipment

The dehydrator consisted of a 2- by 48-in. stainless-steel tube placed in a furnace made by winding 35 ft of nichrome wire (1 ohm/ft) around a 3.25-ft length of 2-in. pipe. Aluminum-oxide catalyst was contained in the tube and activated by heating for 4 hr at 250° C in a stream of nitrogen. The feed of material to the apparatus was controlled either by a constant-level device made by modification of an automobile carburetor or by means of a commercial sylphon pump whose rate could be regulated. Dehydrations in this work were conducted in the vapor phase at 300° to 320° C. Details of the dehydrator have been given previously [11].

2.4. Stills

Six stills were used in this work. These have been described previously [8], but for convenience, the salient features of each are given in table 1.

[1] Present address, Frankl Photographic Services, Washington, D. C.
[2] Present address, National Institutes of Health, Bethesda, Md.
[3] Figures in brackets indicate the literature references at the end of this paper.

TABLE 1. *Distillation columns*

Still	Type	Size	Material of construction	Packing	Pot capacity
		cm			*ml*
11	Total reflux-variable takeoff	240 by 2	Monel	3/32-in. stainless-steel helices made from 0.010-in. wire.	60,000.
12	do	1,500 by 10	Galvanized steel	3/4-in. unglazed-porcelain raschig rings	210,000.
13	do	1,500 by 10	do	do	210,000.
18	Podbielniak Hypercal	127 by 2.5	Glass	Heli-grid	250 to 5,000.
19	do	250 by 2.5	do	do	250 to 5,000.
21	Total reflux-variable takeoff	120 by 3.5	do	3/16-in. glass helices	22,000.

283819—54——2

3. Methods and Techniques

3.1. Preparation of Grignard Reagents

The Grignard reagents necessary for the large-scale syntheses in this work (up to 300 moles) were prepared in the 50-gal stainless-steel kettle. The details of the preparation of these reagents have been reported previously [8]. In all cases, these reagents were reacted in place.

3.2. Reductions with Sodium in Liquid Ammonia

For conversion of acetylenic hydrocarbons to olefins, reduction with sodium in liquid ammonia was used; the product obtained was almost exclusively the *trans* isomer [7]. The description of the preparation of several alkynes is given in a previous paper [12], and some of these were used in the present work. The technique used for these reactions is illustrated by the preparation of *trans*-2-hexene from 2-hexyne (see sec. 4.9). In order to minimize the formation of peroxide catalysts, which induce sodium-amide formation, the sodium metal was freshly cut and immediately added to the liquid ammonia.

3.3. Determination of Physical Properties

The properties measured on the compounds prepared included boiling point, freezing point, refractive index, and density. The methods used for the determination of these properties have been reported previously [11]. Where feasible, purities were determined on selected hydrocarbons by mass spectrometry, low-temperature calorimetry [6], or freezing-curve analysis [13]. The low-boiling compounds and some of the unsaturates were sealed under their own vapor pressure [10]. The physical properties measured on the compounds prepared in this work and on their intermediates are listed in table 2, along with purity determinations, where made. When the purities were measured calorimetrically, the triple point and the molar heat of fusion of the substance [6] were also obtained.

4. Preparation of Materials

4.1. n-Octane

This paraffin was prepared by hydrogenation of purified 1-octene obtained from a commercial source (see sec. 4.11 for description of the purification of the

TABLE 2. *Physical properties of compounds prepared*

Compound	Boiling point at 760 mm Hg	Freezing point in air	Density at 20° C	Refractive index at 20° C	Purity [a]
	°C	°C	g/ml	n_D^{20}	Mole percent
n-Octane	125.668	−56.864	0.70264	1.39770	99.7 FP
3-Methyloctane	144.214	[b] nf	.7205	1.40630	
4-Methyloctane	142.425	−53.528	.72017	1.40624	
4-Ethyloctane	163.637	nf	.73811	1.41506	
Methylcyclopropane		[c] −177.51			99.30 LTC
Ethylcyclopropane	36.2	[d] −149.60	.6840	1.3788	98.79 LTC
Cyclobutane		[e] −90.59			99.91 LTC
2-Pentene (*cis* and *trans*)	36.7		.6545	1.3812 to 1.3823	99.4 MS
trans-2-hexene	67.87	−133.07	.67853	1.39351	
trans-3-hexene	67.15	−114.28	.67718	1.39410	
1-Octene	121.26	−101.84	.71486	1.40875	99.2 FP
4-Ethyl-2-octene	163.5 to 165.0	nf	.7531	1.4300	
4-Ethyl-3-octene	160 to 162	nf	.7457	1.4242	
Propadiene	−34.5	[f] −136.56			99.13 LTC
2,3-Pentadiene	48.2	−125.72	.6957	1.4266	
1,5-Hexadiene	59.46		.69115	1.40386	
2-Methyl-1,3-pentadiene	75.76	nf	.72391	1.44529	
2,5-Dimethyl-1,5-hexadiene	114.472	−74.829	.7420	1.4287	
2-Pentanol	119.3	nf	.8098	1.4065	
3-Pentanol	115.5	nf	.8207	1.4111	
3-Methyl-3-octanol		nf	.8331	1.4298	
4-Methyl-4-octanol	113 (50 mm)		.8284	1.4316	
2-Pentanone	102.4		.8095	1.3903	
1,1-Dicarbethoxycyclobutane	226.3	nf	1.0420	1.4351	
Cyclobutane carboxylic acid	135 to 138 (110 mm)	−7.1	1.0610	1.4430	
Cyclobutylbromide	107.4			1.4794	

[a] FP, purity from freezing-curve analysis [13]; LTC, purity by low-temperature calorimetry [6] (performed by G. T. Furukawa); MS, purity by mass spectrometry (determined by V. H. Dibeler and F. L. Mohler).
[b] nf, nonfreezing, glassy at low temperatures.
[c] Triple point, measured in calorimeter. Molar heat of fusion = 2,800±100 joules.
[d] Triple point, measured in calorimeter. Molar heat of fusion = 5,600±100 joules.
[e] Triple point, measured in calorimeter. Molar heat of fusion = 1,095±50 joules.
[f] Triple point, measured in calorimeter. Molar heat of fusion = 4,400±100 joules.

olefin). Hydrogenation of 4.32 kg of the 1-octene was effected smoothly, and the crude paraffin was percolated through silica gel and distilled through column 18. The center fraction was reserved for measurements of physical constants.

4.2. 3-Methyloctane

This hydrocarbon was prepared by hydrogenation of the olefins resulting from the dehydration of 3-methyl-3-octanol. The carbinol was prepared by the reaction between ethylmagnesium bromide and methyl-*n*-amyl ketone.

Ethylmagnesium bromide was prepared from 7.2 kg (300 g-atoms) of magnesium and 32.7 kg (300 moles) of ethyl bromide as described previously [8]. After preparation of the Grignard reagent, it was found that the stock of 2-heptanone was only 17.1 kg (150 moles) due to partial delivery of an order. This quantity was added to the Grignard reagent. In order to avoid wasting the excess Grignard reagent and to diminish the working hazards, it was decided to add 19.3 kg (150 moles) of 2-ethylhexaldehyde. This compound was chosen because it would yield 4-ethyl-3-octanol, a compound also needed in another synthesis. Because of the difference in molecular weight and structure, it was presumed the two final paraffins or their intermediates could easily be separated.

Six hours were required to effect the total addition, and the mixture was allowed to stand overnight. The reaction mixture was worked up in the usual manner to obtain 68 liters of ether-carbinol solution. The ether was removed from this by distillation on column 21 to leave a carbinol concentrate.

Considerable difficulty was experienced in attempting to distill the carbinol mixture. This was principally due to dehydration. Since the hydrocarbons were the desired products, it was finally decided to dehydrate the mixture of carbinols and separate the resulting olefins.

The carbinol mixture (13.9 kg) was dehydrated over alumina at 300° C during a period of 150 hr. The crude olefin was separated roughly into two fractions on columns 18 and 21. The first fraction, bp 130° to 150° C, consisted principally of 3-methyloctenes, and the second fraction, bp 150° to 170° C, principally of 4-ethyloctenes. The 3-methyloctenes fraction was redistilled to yield 5,760 ml of material boiling 135° to 150° C. The 4-ethyloctenes fraction was redistilled to give 450 ml of material boiling at 135° to 150° C and 4,325 ml of material boiling 150° to 170° C. Material of like boiling points were combined for a total of 6,210 ml (4.62 kg, 36.7 moles) of 3-methyloctenes, bp 135° to 150° C, and 4,325 ml (3.27 kg, 23.4 moles) of 4-ethyloctenes, bp 150° to 170° C. A considerable amount of high boiling residue remained that was not investigated but was probably aldol formed from 2-ethylhexaldehyde.

A charge of the 135° to 150° C cut was refractionated in column 19 in order to obtain samples for physical properties. However, no sharp "plateau" was obtained; the major portion boiled at 146.5° to 150° C, but the refractive index, n_D^{20}, rose from 1.4238 to 1.4258.

The mixed 3-methyloctenes (3.5 kg, 28.2 moles) were hydrogenated, and the resulting crude 3-methyloctane (4,000 ml) was distilled in column 19. From this distillation there was obtained 3,160 ml of a 3-methyloctane plateau. A center portion of this had a 20 to 80 percent boiling-point spread of 0.007° C. This was the sample chosen for the determination of the physical constants.

4.3. 4-Methyloctane

This hydrocarbon was prepared by a series of reactions, beginning with the oxidation of 2-pentanol to the corresponding ketone. The 2-pentanone was reacted with *n*-butylmagnesium chloride to yield 4-methyl-3-octanol, which was dehydrated, and the resulting olefins hydrogenated to 4-methyloctane.

Commercial mixed secondary amyl alcohols (190 liters) were fractionated in column 11 to yield 38 liters of 3-pentanol, bp 115.3° to 115.7° C, n_D^{20}= 1.4104 to 1.4106, and 40 liters of 2-pentanol, bp 119.1° to 119.5° C, n_D^{20}=1.4062 to 1.4068.

The 2-pentanol was oxidized, using sulfuric acid-sodium dicromate as the oxidizing agent [15]. Sulfuric acid (13.8 kg) was added with stirring and cooling to 30 liters of water in the glass-lined kettle. To this solution was added 16.5 kg (188 moles) of 2-pentanol, followed by slow addition of a solution of 18.79 kg of sodium dichromate in 37 liters of 4 *N* sulfuric acid. During this addition the solution was stirred and the temperature maintained at 25° to 30° C. After completion of the oxidation step, 56 liters of water was added and the solution steam-distilled until no more organic layer came over. From this operation there was obtained about 19 liters of crude ketone, which was distilled in column 21 to give 15 liters (1.21 kg, 141 moles, 75 percent) of 2-pentanone, bp 103° to 105° C.

n-Butylmagnesium chloride was prepared from 13.9 kg (150 moles) of *n*-butyl chloride and 3.65 kg (156 g-atoms) of magnesium in the conventional manner [8]. The addition of the halide required 3 hr, followed by 2 hr of stirring. To this was added 11.8 kg (138 moles) of 2-pentanone over a period of 2½ hr. The reaction mixture was treated in the usual way, and the ether stripped off in column 21. From this reaction there was obtained about 22 liters of crude 4-methyl-4-octanol. This material was distilled in columns 18 and 19, which gave 13.5 kg (93.8 moles, 68 percent) of purified carbinol, bp 105° to 112° C at 50 mm Hg. A sample of the best material was reserved for the measurement of physical constants.

The 4-methyl-4-octanol (13.3 kg, 92.5 moles) was dehydrated by passage over alumina at 300° to 320° C at the rate of 120 to 130 ml/hr. From this step there was obtained 15.6 liters of organic layer and 1.6 liters of water (96 percent dehydration). The olefin was distilled in columns 18 and 19, to yield 10.5

kg (83.4 moles, 90 percent) of mixed 4-methyloctenes, bp 142° to 150° C. A part of the olefin was redistilled in column 19, and almost all the charge distilled over a boiling range of 144.2° to 146.2° C. This was to be expected, because the major olefins would be the very similar *cis*- and *trans*-4-methyl-3-octene and *cis*- and *trans*-4-methyl-4-octene, together with a lesser amount of 2-*n*-butyl-1-pentene. None of the samples taken was considered sufficiently pure to warrant the determinations of physical properties.

A charge of 4.05 kg (32 moles) of the 4-methyloctenes was hydrogenated to give 3.92 kg (30.5 moles, 96 percent) of 4-methyloctane. Four liters of the crude paraffin was distilled in column 18 to recover 2,840 ml of material of suitable purity.

4.4. 4-Ethyloctane

The synthesis of the olefin precursors of this paraffin (4,325 ml of mixed 4-ethyl-2-octene and 4-ethyl-3-octene) is described in section 4.2. The mixture was redistilled on column 19 to yield two plateaus. The first plateau, bp 160° to 162° C, was tentatively identified as 4-ethyl-3-octene; the second plateau, bp 163.5° to 165° C, was probably *cis*- and *trans*-4-ethyl-2-octene. Physical properties measured on these compounds are listed in table 2. The 4-ethyloctenes were hydrogenated, and the resulting crude paraffin was distilled through still 19 to yield 4-ethyloctane.

4.5. Methylcyclopropane

This cycloparaffin was prepared by the reaction of zinc with 1,3-dibromobutane, according to the method of Bartleson, Burk, and Lankelma [3]. Several runs were made; a typical preparation is described below.

A mixture of 100 g of water, 196.5 g of zinc dust (3 g-atoms), and 3,000 ml of *n*-propyl alcohol was cooled with an ice-bath. Over a 90-min period there was added 216 g (1.0 mole) of 1,3-dibromobutane to the stirred mixture. The ice-bath was then removed and the flask permitted to warm up. After reaching room temperature, the reaction mixture warmed spontaneously with a brisk evolution of gas, until the flask temperature was 60° to 70° C. When the reaction was completed, the mixture was allowed to cool to room temperature, 250 ml water added, and a stream of nitrogen passed gently through the system for flushing. There collected in the receiver 51 g of product, yield 91 percent. This material was percolated through a silica-gel column kept at −78° C and distilled into a brass bomb for storage. The yield from four such runs totaled 136 g.

4.6. Ethylcyclopropane

This hydrocarbon was prepared by a Wolff-Kishner reduction of the hydrazone of methylcyclopropylketone [1].

To a mixture of 1,285 ml of diethylene glycol, 473.4 g (5.63 moles) of methylcyclopropylketone and 25 ml glacial acetic acid in a 5-liter flask, was added 656 g of 64-percent commercial hydrazine hydrate. The solution was refluxed for about 1 hr and then distilled through a packed column until the head temperature reached 120° C. The residue was cooled and then added dropwise to a mixture (at 180° to 200° C) of 1,350 ml of diethyleneglycol and 420 g sodium hydroxide. The decomposition products were condensed in a trap cooled to −78° C. The crude hydrocarbon was washed successively with water, dilute hydrochloric acid, again with water, and then dried over anhydrous sodium sulfate before distillation in column 19. The distillate boiled 35.5° to 36.5° C and amounted to 152 g, yield 39 percent. This material was redistilled on column 19, and a center cut of 125 ml, bp 35.9° to 36.2° C, was chosen for measurement of physical properties and purity.

4.7. Cyclobutane

Cyclobutane was prepared by a series of reactions that are a modification of the procedure described by Cason and Way [6] and Cason and Allen [5]. In this method, 1,1-dicarbethoxycyclobutane was prepared from diethyl malonate and 1,3-dibromopropane by condensation. The ester was hydrolyzed and decarboxylated by heating with aqueous hydrochloric acid. The silver salt of cyclobutane carboxylic acid was then added to bromine in carbon tetrachloride at −20° C to give cyclobutyl bromide. This was converted to cyclobutane through the Grignard reaction.

(a) *1,1-Dicarbethoxycyclobutane.* To a solution prepared from 13.6 kg (85.0 moles) of diethylmalonate and 4.4 kg of sodium methoxide in 37 liters of absolute alcohol there was added concurrently 13.8 kg (68.5 moles) of 1,3-dibromopropane and a solution of 2.9 kg of sodium methoxide in 25 liters of absolute ethanol. The time of addition was 5½ hr. When the addition was completed, the reaction mixture was refluxed for 45-min, after which the ethanol was removed by distillation. To the cooled residue was added with stirring 26 liters of water and 18 liters of isooctane [4] as solvent. The two layers were separated, and the aqueous layer was stirred again with 7.6 liters of water and 7.6 liters of isooctane. The layers were again separated and the organic layers combined and dried over anhydrous sodium carbonate. The solvent and other low-boiling material were stripped off in columns 18 and 19. The residues were combined and distilled under reduced pressure in column 6. The fraction boiling at 125° to 133° C at 50 mm Hg was collected as 1,1-dicarbethoxycyclobutane. The yield was 7.38 kg (54 percent).

The residue was a very high-boiling material and was not treated further. It probably consisted of 1,1,5,5-tetracarbethoxypentane.

(b) *Cyclobutane carboxylic acid.* The ester was hydrolyzed and decarboxylated in 12 identical runs. In each, a mixture of 900 ml of water, 1,800 ml of concentrated hydrochloric acid, and 600 g (3 moles) of 1,1-dicarbethoxycyclobutane was refluxed until

[4] Isooctane is the trivial name for 2,2,4-trimethylpentane.

the mixture became homogeneous. This took 3 to 4 hr. The water and acid were then distilled, using a short rectifying column. When all the aqueous material was removed, the residue was heated more strongly until the temperature at the head of the column reached 185° C. The evolution of carbon dioxide proceeded smoothly and was complete in less than 1 hr.

The residues from all the runs were combined and distilled in column 18. The portion boiling at 135° to 138° C at 110 mm Hg was collected as cyclobutane carboxylic acid. The yield was 2,681 g (74 percent).

(c) *Cyclobutyl bromide.* This compound was prepared by a series of several similar reactions. Because of its instability, the silver salt was prepared, dried, and reacted with bromine as rapidly as possible.

To a mixture of 200 g (2 moles) of cyclobutane carboxylic acid in 560 ml of water was added with vigorous stirring 2 *N* potassium-hydroxide solution until the solution was faintly basic. To this was added slowly 344 g (2.02 moles) of silver nitrate in 1,100 ml of water. A thick white precipitate of silver cyclobutane carboxylate was obtained. This was stirred for about 1 hr and then filtered. The precipitate was returned to the reaction vessel, stirred with 1,600 ml of water for ½ hr, and again filtered with suction until dry. The final precipitate was washed with methanol, dried by suction again, and then placed in an oven at 100° to 110° C for 24 hr. The silver salt was then cooled in a desiccator over phosphorous pentoxide.

To 2,000 ml of anhydrous carbon tetrachloride cooled to −25° C was added the stoichiometric quantity of bromine for reaction with the silver salt. To this was added the previously prepared silver salt over a period of 1½ to 2 hr, keeping the temperature at −20° to −25° C. The solution was stirred at this temperature for 1 hr and then slowly warmed to room temperature. The precipitated silver bromide was filtered off with suction and washed with carbon tetrachloride. The filtrate was washed with 2 *N* potassium hydroxide and with water and then dried with calcium chloride. The solvent was removed, using column 6, and the residue from this operation was distilled through a 1.2- by 25-cm Hempel column packed with glass helices.

This reaction is peculiar in that an occasional run failed to yield cyclobutyl bromide. It was noted in the successful runs that during the warming-up period of the bromination step, there was a sharp rise in temperature at about −10° C. This break was not evident in runs in which no yield was obtained. The average yield on the successful runs was 43 percent.

The crude cyclobutyl-bromide samples were combined, washed with water, dried with sodium carbonate, and distilled in column 19. A total of 754 g of purified cyclobutyl bromide was obtained.

(d) *Cyclobutane.* To 48.6 g (2 moles) of magnesium turnings were added 100 ml of dibutyl ether and 6.7 g cyclobutyl bromide. The flask was warmed to 60° C in a water bath until the reaction started. To this was added over a period of 3 hr 264 g (1.96 moles) of cyclobutyl bromide in 1,250 ml of dibutyl ether. The mixture was stirred for 1¼ hr at 55° to 60° C, after which it was cooled with ice, and 460 ml of *n*-butyl alcohol added slowly. When the addition was complete, the temperature of the mixture was raised slowly until reflux temperature was reached. The escaping gas was passed through the water condenser, an 85-percent sulfuric-acid wash, a 5-percent potassium-hydroxide wash, and a calcium-chloride drying tower, and condensed into a receiver at −30° C. The reaction vessel and purification train were flushed out with dry nitrogen. The yield of cyclobutane in this step was 94 g (84 percent).

From three runs there was obtained a total of 252 g of cyclobutane (about 85-percent yield). The combined samples were fractionated through column 18 and sealed in vacuum [10].

4.8. 2-Pentene

This olefin was prepared by the dehydration of 3-pentanol, obtained by fractionation of a commercial alcohol mixture (see sec. 4.3). A total of 3,080 ml of purified 3-pentanol was passed over the alumina at 300° to 320° C. There was obtained 2,850 ml of organic material and 438 ml of water. The amount dehydrated, based on water recovered, was 86 percent. The organic layer was washed with water, dried over anhydrous sodium carbonate, and distilled in column 19. The center cut was selected for measurement of physical properties and purity shown in table 2 for this compound.

4.9. trans-2-Hexene

This compound was prepared by reduction of 2-hexyne with sodium in liquid ammonia. The 2-hexyne was prepared by alkylation of acetylene, and its synthesis is described in a previous paper [12]. The reduction yielded *trans*-2-hexene almost exclusively, in 69-percent yield.

To 10 kg of liquid ammonia (200 g/mole of reactant) in the 10-gal stainless-steel kettle was added with stirring 1,220 g (53 g-atoms) of sodium. No violent exothermic reaction was evident; the sodium dissolved and colored the ammonia a deep blue. The 2-hexyne (1,917 g, 23 moles) was then added as rapidly as the condenser capacity permitted. The solution was allowed to stir for ½ hr after all the material was added, then 6 lb of solid ammonium chloride (50.5 moles) was added in portions to destroy the sodium amide formed. The contents of the pot were stirred for 15 min, after which 5-gal of water was slowly added with stirring. After the layers settled, the organic layer was washed three times with water and dried over anhydrous sodium carbonate.

Distillation of the organic layer on still 19 yielded a 2,000-ml fraction boiling 67° to 69° C (yield 69 percent). The physical constants measured on a center cut of the final distillation are reported in table 2.

4.10. trans-3-Hexene

This compound was prepared by reduction of 3-hexyne with sodium in liquid ammonia, as described in section 4.9 for *trans*-2-hexene. For this preparation there was used 8 kg of liquid ammonia, 1,143 g of sodium (50 g-atoms), 1,904 g (23.2 moles) of 3-hexyne, and 2.8 kg (52 moles) of ammonium chloride. The dried organic layer from this run was distilled in column 19 to give 1,608 g (19.2 moles) of product, bp 67° to 68° C. This corresponds to 82-percent yield. The physical properties measured on a middle cut of this compound are given in table 2.

4.11. 1-Octene

This compound was obtained in high purity by careful fractionation of commercial 1-octene. Distillation of 4,000 ml of the crude olefin on column 19 gave 3,500 ml of 1-octene with the properties listed in table 2. A portion of the purified 1-octene was hydrogenated to yield *n*-octane (see sec. 4.1).

4.12. Propadiene

This diolefin was made from the reaction of zinc with 2,3-dichloro-1-propene in methylcellosolve. When this dechlorination was attempted in ethanol [9], no reaction took place.

To a 3-liter flask equipped with stirrer, addition vessel and reflux condenser was added 300 g of zinc dust and 1,000 ml of methylcellosolve. To this mixture at its boiling point (135° C) was added dropwise 325 g (3 moles) of 2,3-dichloro-1-propene. There was an immediate reaction and sufficient evolution of heat to maintain the mixture at its boiling point with the heating mantle removed. The evolved gases were collected in a flask cooled to −78° C. The yield from three such runs was 180 g (50-percent yield). The product was dissolved in 500 ml of *n*-pentane and distilled in column 19. The fraction boiling at −34.5° C was reserved for measurements of the physical properties listed in table 2.

4.13. 2,3-Pentadiene

This compound was obtained by fractional distillation of a sample obtained from a commercial source.

Distillation of 3,000 ml in column 19 yielded a middle cut of 2,200 ml, bp 48° to 49° C. The properties of this material are reported in table 2.

4.14. 2-Methyl-1,3-Pentadiene

This diolefin was prepared from the dehydration of 4-methyl-2-pentene-4-ol.

To prepare the starting material (ethyl crotonate) for this synthesis, a mixture of 5,326 g (62 moles) of crotonic acid, 18.5 liters of 95-percent ethanol, and 172 ml of concentrated sulfuric acid was heated at 95° C in the glass-lined kettle for 8.5 hr. After the mixture had cooled, the contents of the kettle were diluted with 34 liters of water; the organic layer was washed with sodium carbonate solution and then dried over anhydrous sodium carbonate. Distillation of this crude gave 3.47 kg of ethyl crotonate, bp 137° to 137.5° C, yield 50 percent.

The ethyl crotonate (3.47 kg, 30 moles) was reacted for 2 days at reflux temperature with methylmagnesium bromide made from 7.5 kg of methyl bromide (79 moles) and 1.92 kg of magnesium (79 g-atoms) in 24 liters of ether. At the end of this time, 3 gal of water was added, the ether layer siphoned, washed once with water, and dried over sodium carbonate. The sludge was treated with 11 gal of water containing 9.5 kg of ammonium chloride; the resulting organic layer was washed until neutral to litmus and added to the main batch. The combined ether solution was distilled at atmospheric pressure on column 21. After the ether was stripped, dehydration of the carbinol started at a head temperature of 65° C. When the distillate temperature continued to rise and reached 78° C, the column was placed on total reflux until the temperature fell to 65° C; the takeoff was then continued until a head temperature of 78° C was reached. At this point the column was placed on total reflux again. The operation of the still in this manner between the head temperatures of 65° to 78° C resulted in the dehydration of the carbinol and distillation of the diolefin. About 2 liters of crude diolefin boiling 65° to 78° C was obtained. This material was dried and redistilled in column 18 to obtain 1,710 ml of material boiling 74° to 77° C. For the final pure material needed for this work, the 74° to 77° fraction was redistilled on column 19 under an atmosphere of nitrogen. A center cut was then bottled in vacuum.

The physical constants measured on this compound are listed in table 2. The extremely narrow boiling range of the center-cut sample (0.011 deg C) indicates this material to be of high purity. Chemical tests were used to establish the identity of this diolefin. Treatment with maleic anhydride according to the method of Bachman and Goebel [2] gave a 98-percent yield of 3, 5-dimethyl-Δ^4 tetrahydrophthalic anhydride, mp 57° C. Oxidation of the diolefin with potassium permanganate [2] did not yield acetone, which would arise from the presence of isomeric 4-methyl-1,3-pentadiene, a compound that could be formed in the dehydration process and would be inseparable by ordinary fractional distillation.

4.15. 1,5-Hexadiene

This compound was prepared by the reaction of allyl chloride with magnesium [14]. Two identical 200-mole runs were made in the 50-gal stainless-steel reactor, in each of which 15.2 kg (200 moles) of allyl chloride, 2.82 kg (116 moles) of magnesium, and 60 liters of ether were used. The combined product, after distillation on column 11 (bp 56° to 63° C), amounted to 11.31 kg (138 moles), yield 69 percent. A 2,000-ml portion of the crude hydrocarbon was redistilled on column 19 at a reflux ratio of 100 to 1, under nitrogen, to obtain a pure sample for the determination of the physical properties.

4.16. 2,5-Dimethyl-1,5-Hexadiene

This compound was prepared by the reaction of methallyl chloride with magnesium.

To the stainless-steel kettle was added 778 g (32 g-atoms) of magnesium and about 4 liters of ether. About 200 ml of methallyl chloride was then added, along with a few crystals of iodine to start the reaction. The remainder of the ether (14 liters) was added when the reaction was well under way, following which the addition of the remaining methallyl chloride (total 6.0 kg, 65 moles) was accomplished in 1 hr. The mixture was allowed to stand over night, and the product recovered in the usual way. Distillation on still 6 yielded 2.94 kg of 2,5-dimethyl-1,5-hexadiene, yield 75 percent.

5. Conclusions

Four paraffins, 6 olefins, 5 diolefins, and 3 alicyclic hydrocarbons have been prepared in high states of purity for use in jet-fuel researches. The details of the syntheses and the purification process are given, along with the physical properties measured on the hydrocarbons and their intermediates.

We thank D. B. Brooks, R. L Alexander, J. A. Cogliano, and E. H. Rich for their advice and assistance in preparing some of the compounds made in this work.

Acknowledgment is made to G. T. Furukawa of the Thermodynamics Section for determining the purity of some of these hydrocarbons by low-temperature calorimetry, and to V. H. Dibeler and F. L. Mohler of the Bureau's Mass Spectrometry Section who performed the mass spectrographic analyses reported.

6. References

[1] American Petroleum Institute Research Project 45, monthly report (April 1947).
[2] G. B. Bachman and C. G. Goebel, J. Am. Chem. Soc. **64,** 787 (1942).
[3] J. D. Bartleson, R. E. Burk, and H. P. Lankelma, J. Am. Chem. Soc. **68,** 2513 (1946).
[4] J. Cason and C. F. Allen, J. Org. Chem. **14,** 1036 (1949).
[5] J. Cason and R. L. Way, J. Org. Chem. **14,** 31 (1949).
[6] G. T. Furukawa, D. C. Ginnings, R. E. McCoskey, and R. A. Nelson, J. Research NBS **46**, 195 (1951) RP2191.
[7] A. L. Henne and K. W. Greenlee, J. Am. Chem. Soc. **65,** 2020 (1943).
[8] F. L. Howard, T. W. Mears, A. Fookson, P. Pomerantz, and D. B. Brooks, J. Research NBS **38,** 365 (1947) RP1779.
[9] G. B. Kistiakowsky, J. R. Ruhoff, H. A. Smith, and W. E. Vaughn, J. Am. Chem. Soc. **58,** 146 (1936).
[10] B. J. Mair, D. J. Termini, C. B. Willingham, and F. D. Rossini, J. Research NBS **37,** 229 (1946) RP1744.
[11] T. W. Mears, A. Fookson, P. Pomerantz, E. H. Rich, C. S. Dussinger, and F. L. Howard, J. Research NBS **44,** 299 (1950) RP2079.
[12] P. Pomerantz, A. Fookson, T. W. Mears, S. Rothberg, and F. L. Howard, J. Research NBS **52**, 51 (1954) RP2472.
[13] Selected values of properties of hydrocarbons, Cir. NBS 461 (1947).
[14] A. Turk and H. Chanan, Org. Syntheses **27, 7** (1949).
[15] G. R. Yohe, H. U. Louder, and G. A. Smith, J. Chem. Educ. **10,** 374 (1933).

WASHINGTON, August 19, 1953.

Journal of Research of the National Bureau of Standards Vol. 52, No. 2, February 1954 Research Paper 2474

Vibrational Spectra of Tetrafluoroethylene and Tetrachloroethylene [1, 2]

D. E. Mann, Nicolo Acquista, and Earle K. Plyler

The infrared spectra of gaseous tetrafluoroethylene from 22 to 52 μ and liquid tetrachloroethylene from 3 to 52 μ have been determined. Several hitherto unobserved bands were found. New and satisfactory assignments, for which a detailed discussion is given, have been achieved. The out-of-plane force constants are discussed and used to predict the wagging and torsion frequencies of tetrabromoethylene. Tables of the thermodynamic functions for tetrafluoro- and tetrachloroethylene are presented.

1. Introduction

As part of a more general investigation of the vibrational spectra and force constants of halogenated ethylenes, it was found desirable to reexamine the assignments for tetrafluoroethylene and tetrachloroethylene.[3] Despite a considerable body of earlier work, several fundamentals in each molecule have remained in doubt or unobserved. The availability of a cesium iodide prism [1] [4] has made convenient the extension of the observable spectral range to about 52 μ, with the result for TFE and TCE that several hitherto unsuspected and otherwise unattainable bands have been revealed. These new data, in conjunction with the recently determined value of the entropy of TFE [2] and some preliminary force-constant calculations, indicate the need, and provide the basis, for achieving more satisfactory assignments.

Although TCE has been subjected to much more spectroscopic investigation, analysis, and discussion than TFE, its assignment has remained the more questionable. This seems to have been due, at least in part, to the greater inaccessibility of the low-frequency infrared-active fundamentals of TCE. Its successful analysis may also have been impeded by the lack of adequate data for other molecules closely enough related to TCE to render some correlations useful. Tetrafluoroethylene bears a sufficiently close resemblance, both spectrally and structurally, to its chlorine analogue to make it profitable to consider them together. Moreover, the entropy data lend additional credibility to the present TFE assignment, so that its use as a guide may be at least partially justified.

2. Experimental Methods

The general method of measurement has been described previously [3, 4]. To ensure adequate resolution over the range 3 to about 52 μ, prisms of NaCl, KBr, and CsI were employed in appropriate regions. The first two were used in Perkin-Elmer model 21 and Baird Associates instruments, respectively, and the cesium iodide prism was used with a Perkin-Elmer model 12C spectrometer.

A pure sample of gaseous TFE was examined only in the region 22 to 52 μ because the earlier investigation by Nielsen, Claassen, and Smith [5] of its infrared spectrum between 2 and 22 μ is satisfactory. Recent studies of the infrared spectrum of TCE have been made by Plyler [6], who reported four bands in the region 23 to about 40 μ, and by Bernstein [7], who investigated the region between 2.5 and 25 μ. It was thought desirable to reexamine the previously studied range, using a highly purified sample of TCE, as well as to extend it to 52 μ. There are some discrepancies between the spectrum presented here and that displayed in [7]. These may be largely due to differences in purity and resolution. The sample of TCE used in this work had been specially purified by distillation through a 40-plate Piros-Glover spinning band still, and by passage through a 10-in. column of silica gel.

The spectral curves for TFE and TCE are displayed in figures 1 and 2, respectively. A complete tabulation of the observed data for the chloro compound, together with its assignment, is given in table 1.

3. Discussion

3.1. Spectra of Tetrafluoroethylene

The infrared spectrum of gaseous TFE has been examined by Torkington and Thompson [8], and more thoroughly by Nielsen, Claassen, and Smith [5] from 2 to 22 μ. The region between 22 and 37 μ was covered by Plyler with the aid of a KRS-5 prism [5]. Raman spectra of gaseous TFE, including depolarization factors, were also obtained by Nielsen, Claassen, and Smith. Monfils and Duchesne [9] have reported Raman spectra for the liquid but did not give polarization data.

The infrared band at 406 cm^{-1} observed by Plyler, was reported in [5] to have a type C contour. From figure 1 it is evident that this observation is confirmed despite the appearance of an overlapped band in the R branch. Apart from the very weak peak adjacent to the P branch of the 406 cm^{-1} band, the intermediate region is quite barren until the strong absorption around 218 cm^{-1} is reached. The resolu-

[1] Presented before the American Physical Society at its meeting in Washington, D. C., on May 1, 1953.

[2] This work has been supported in part by the ONR under contract NAonr 112-51.

[3] Hereafter in this paper tetrafluoroethylene, $F_2C{:}CF_2$, will be abbreviated to TFE, and tetrachloroethylene, $Cl_2C{:}CCl_2$, will be contracted to TCE.

[4] Figures in brackets indicate the literature references at the end of this paper.

TABLE 1. *Infrared and Raman spectra of* $Cl_2C{:}CCl_2$ *(liquid)*

Raman		Infrared [a]		Interpretation
ν	(I, ρ)	ν	I	
cm^{-1}		cm^{-1}		
218	(00,–)	------	------	$2\times110=220(A_g)$
		224	w	$\nu_7(b_{1u};\ \beta\text{-}CCl_2)$
235	(10,0.62)	------	------	$\nu_3(a_g;\ \delta\text{-}CCl_2)$
		288	w	$\nu_{12}(b_{1u};\ \delta\text{-}CCl_2)$
		310	vw	$288+\nu_1-\nu_i$
		328	vw	$777-447=330(B_{1u})$
		345	vw	(ν_6) [b]
[b] 347	(4,0.83)	------	------	$\nu_5(b_{1g};\ \rho\text{-}CCl_2)$
		405	vw	$176+235=411(B_{2u})$
		433	vw	$777-347=430(B_{2u})$
447	(15,0.14)	------	------	$\nu_2(a_g;\ \nu\text{-}CCl)$
464	(1/2,–)	------	------	$2\times235=470(A_g)$
		465	vw	$224+235=459(B_{1u});\ 908-447=461(B_{2u})$
512	(4,0.77)	------	------	$\nu_8(b_{2g};\ \beta\text{-}CCl_2)$
		513	vw	$176+347=523(B_{2u})$
		526	vw	$235+288=523(B_{1u})$
		540	vw	$777-235=542(B_{1u})$
		559	vw	$908-347=561(B_{1u})$
574	(0,–)	------	------	$2\times288=576(A_g)$
		620	vw	$176+447=623(B_{2u})$
631	(00,–)	------	------	$908-288=620(B_{1g})$
		641	vw	$288+347=635(B_{2u})$
		679	w	$224+447=671(B_{1u})$
726	(00,–)	------	------	$2\times347=694(A_g);\ 235+512=747(B_{2g})$
		755	s	$224+512=736(B_{1u});\ 288+447=735(B_{1u})$
		777	vs	$\nu_{11}(b_{1u};\ \nu\text{-}CCl)$
784	(00,–)	------	------	$347+447=794(B_{1g})$
		800	s	$288+512=800(B_{1u})$
		908	vvs	$\nu_9(b_{2u};\ \nu\text{-}CCl)$
		979	m	$224+235+512=971(B_{1u})$
		994	m	$235+777=1012(B_{1u})$
1000	(00,–)	------	------	$\nu_5(b_{1g};\ \nu\text{-}CCl)$
1025	(1,p)	------	------	$2\times512=1024(A_g)$
		1102	m	$224+347+512=1083(B_{2u})$
		1121	m	$347+777=1124(B_{2u})$
		1142	m	$235+908=1143(B_{2u})$
		1171	w	$176+1000=1176(B_{1u})$
		1200	w	$224+447+512=1183(B_{1u})$
		1222	w	$447+777=1224(B_{1u})$
		1253	w	$347+908=1255(B_{1u})$
		1355	m	$447+908=1355(B_{2u})$
		1392	vw	$176+235+1000=1411(B_{1u})$
1441	(0?,–)	------	------	$447+1000=1447(B_{1g})$
		1481	vw	$2\times288+908=1484(B_{2u})$
1571	(10,0.36)	------	------	$\nu_1(a_g;\ \nu\text{-}CC)$
		1577	w	$347+447+777=1571(B_{2u})$
		1733	vw	$288+447+1000=1735(B_{2u})$
		1751	w	$176+1571=1747(B_{2u})$
		1773	w	$777+1000=1777(B_{2u})$
		1795	vw	$224+1571=1795(B_{1u})$
1819	(0,–)	------	------	$2\times908=1816(A_g)$
		1862	w	$288+1571=1859(B_{1u})$
		1887	w	$908+1000=1908(B_{1u})$
1998	(1/2,–)	------	------	$2\times1000=2000(A_g)$
		2475	w	$908+1571=2479(B_{2u})$
		2717	vw	$235+908+1571=2714(B_{2u})$
		2755	vw	$777+2\times1000=2777(B_{1u})$
		2890	vw	$908+2\times1000=2908(B_{2u})$
		3448	vw	$908+1000+1571=3479(B_{1u})$

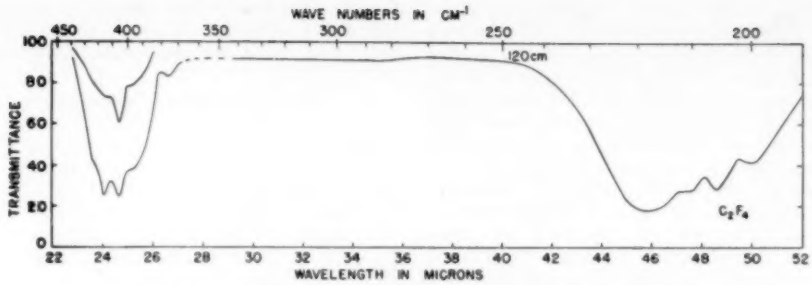

FIGURE 1. *Infrared spectrum of gaseous* $F_2C{:}CF_2$ *from 22 to 52μ.*

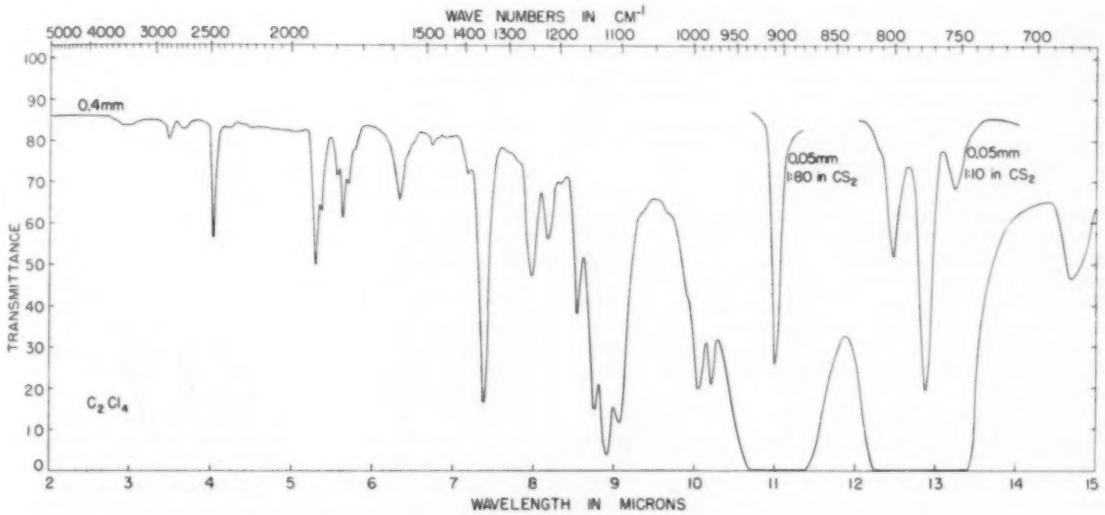

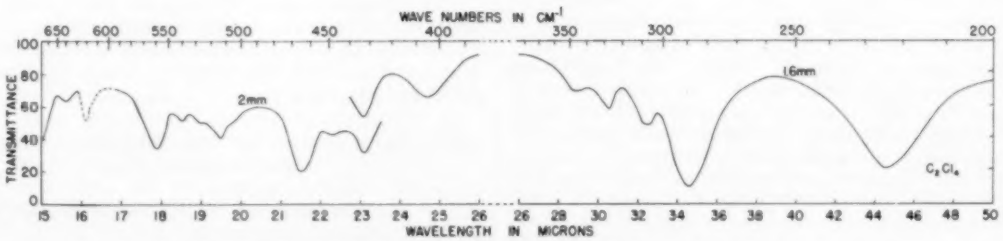

FIGURE 2. *Infrared spectrum of liquid* $Cl_2C{:}CCl_2$ *from 2 to 52μ.*

---

[a] The infrared bands at 176 and 152 cm⁻¹ observed by Pitzer (see footnote 6) may be interpreted as $\nu_{18}(b_{2u}; \rho\text{-}CCl_2)$, and $\nu_{19}+\nu_4-\nu_4$, respectively. Before Professor Pitzer's results were made known to present authors, the ν_{19} fundamental used in this table had been assigned the value ~170 cm⁻¹. This has now been corrected to 176 cm⁻¹ to accord with the new data.

[b] For lack of a better explanation, the 347cm⁻¹ infrared band is interpreted as ν_8 appearing in virtue of the partial breakdown of selection rules in the liquid. It should be noticed that there are a number of other coincidences between infrared and Raman frequencies: 464 and 465, 512 and 513, 1000 and 994, 1571 and 1577. Fortunately, these can be explained otherwise.

tion of the cesium iodide prism is not sufficient to reveal much structure in this region, and the bumps on the low-frequency shoulder should be regarded with some scepticism. Though they appear to be real, they may derive at least in part from some uncertainty in the background-absorption correction.

The band at 218 cm^{-1} undoubtedly represents the hitherto unobserved b_{2u} rocking fundamental. It had been placed at 245 cm^{-1} by Nielsen, Claassen, and Smith on the basis of their interpretation of several combination bands. A value of 250 cm^{-1} was deduced by Monfils and Duchesne [9] from a force-constant analysis. Inasmuch as 406 and 558 cm^{-1} have been unambiguously established as representing the b_{1u} wagging and b_{3u} deformation fundamentals, respectively, only the inactive torsion and the Raman-active vibrations need be considered in order to complete the assignment.

The polarization measurements of Nielsen, Claassen, and Smith leave no doubt as to the correctness of their assignment of 394, 778, and 1872 cm^{-1} to the totally symmetric (a_g) vibrations. Moreover, their interpretation of the 503–517 cm^{-1} doublet as the b_{2g} fundamental, and their deduction of a frequency around 550 cm^{-1} for the lower of the b_{1g} vibrations is supported by the work of Monfils and Duchesne [9] on the Raman spectrum of liquid TFE. Although the latter workers originally questioned [9] the assignment by Nielsen, Claassen, and Smith of a very feeble line at about 1340 cm^{-1} to b_{1g}, they appear now [10] to have accepted this interpretation. The present analysis also favors 1340 cm^{-1} for the higher b_{1g} vibration. Only the inactive torsion frequency remains unassigned.

3.2. Torsion Frequency of Tetrafluoroethylene

In order to obtain a rough estimate of the torsion frequency, the assumption was made that the force constant for the twisting motion in TFE is the same as that obtained by Arnett and Crawford [11] for ethylene, $H_2C{:}CH_2$.[5] In units of 10^{-11} erg/radian^2 the constant obtained by Arnett and Crawford is $F_\tau = 0.269$. With the distances and angles appropriate to TFE [13], this leads to a value of 199 cm^{-1} for the torsion frequency. Hence, the interesting possibility exists that one of the peaks around 205 cm^{-1} in the infrared spectrum of TFE may arise from the torsion vibration made active by Coriolis interaction with the neighboring b_{2u} fundamental at 218 cm^{-1}. Attempts to determine the torsion frequency directly from the observed combination bands tend to support a value in the range 190 to 200 cm^{-1}. Fortunately, the entropy of TFE has been determined very recently [2] and provides valuable evidence in favor of the complete assignment, while placing the torsion frequency at 190 cm^{-1}. Small inaccuracies in the fundamental frequencies, together with the experimental uncertainties in the entropy value, may account for the slight discrepancy. Because of the lack of stronger evidence favoring the higher value, 190 cm^{-1} was adopted for the torsion frequency. The corresponding force constant then becomes $F_\tau = 0.245$. The final and complete assignment is given in table 3.

[5] For brief mention of this point, see the paper by Torkington on TCE [12].

3.3. Spectra of Tetrachloroethylene

The infrared spectrum of liquid TCE was first studied by Coblentz [14]. Bonino examined a small portion of its spectrum in 1925 [15], and Spence and Easley observed the region between 0.8 and 3μ but found no bands [16]. Another early study of its near infrared spectrum was made by Freymann [17]. In 1934 Wu reported four bands, 755(m), 782(s), 802(s), 913(s), for gaseous TCE [18]. A few years later Duchesne and Parodi reported infrared bands at 332 and 387 cm^{-1} [19]. Bernstein has observed the spectrum of TCE from 2.5 to 25μ [7], and Plyler has extended the range to about 40 μ [6]. In the present work the entire region 3 to 52 μ has been investigated.[6]

The Raman spectrum of liquid TCE has been extensively investigated [20 to 31]. With the exception of the recent work of Sanyal [31], the available data have been considerably augmented and carefully reviewed by Wittek [29]. Summaries have also been given by Kohlrausch [32], Wu [33], and Herzberg [34]. The frequencies, relative intensities, and depolarization factors [7] given by Wittek are: 218(00,–), 235(10,0.62), 347(4,0.83), 447(15,0.14), 464(½,–), 512(4,0.77), 574(0,–), 631(00,–), 726(00,–), 784(00,–), 1000(00,–), 1025(1,p), 1441(0?,–), 1571-(10,0.36), 1819(0,–), 1998(½,–). Sanyal [31] reported for liquid TCE 238(7,dp), 346(4,dp), 382(Ob,–), 450-(9,p), 516(3,dp), 1572(10,dp); and for the solid at −150° C, he found 242(2,–), 346(1,–), 380(0,–), 454(1,–), 1576(58,–). The line at 382 cm^{-1} found by Sanyal was also reported by Wu [27] but was shown by Wittek to be spurious. Moreover, the depolarized character ascribed by Sanyal to the 1572 cm^{-1} line is in disagreement with all prior polarization measurements [25 to 27, 29]. Wittek's results are used in this paper.

The infrared spectrum of liquid TCE is shown in figure 2. The wave numbers and relative intensities of the observed bands, together with Wittek's Raman data and the present interpretation, are given in table 1.

3.4. Interpretation of the Vibrational Spectra Tetrachloroethylene

The Raman data for TCE clearly prescribe the three a_{1g} fundamentals: 235, 447, and 1571 cm^{-1}. These correspond approximately to the totally symmetric CCl_2 deformation (δ-CCl_2), CCl stretching (ν-CCl), and CC stretching (ν-CC), respectively.[8]

[6] After the work described in this paper was completed a private communication was received from K. S. Pitzer stating that the infrared spectrum of TCE had been observed in his laboratory down to about 135 cm^{-1}. Outside of the range used in the present investigation, two bands, a strong one at 176 cm^{-1} and a somewhat weaker one at 152 cm^{-1}, were observed.

[7] The depolarization factors are averages of the results given by Wittek for four separate determinations. For the 1025 cm^{-1} line, the data are too few to justify averaging but suffice to indicate its character.

[8] See [4] for a description of the notation used here to represent the various modes.

There remain three Raman-active fundamentals: a CCl stretching and CCl_2 rocking (ρ-CCl_2) in b_{1g}, and the out-of-plane CCl_2 wagging (β-CCl_2) in b_{2g}. Apart from the lines already assigned to a_{1g} vibrations, only 347 and 512 have appreciable intensity. As they are depolarized they cannot be overtones, nor, indeed, is it reasonable to suppose they arise from sum bands. In fact, the weak polarized line at 1025 cm^{-1} is most readily interpreted as 2×512. As fundamentals, they must be assigned in some manner to the b_{1g} and b_{2g} species. Analogy with TFE suggests that the b_{1g} stretching frequency in TCE is high, on a par with the infrared-active stretchings at 777 and 908 cm^{-1}, and that it would appear only feebly in the Raman spectrum. Hence, 347 and 512 may be assigned to the b_{1g} rocking and b_{2g} wagging modes, though it is not yet clear in what order. For the b_{1g} stretching one of the very weak lines at 726, 784, or 1000 cm^{-1} may be chosen. The repeated occurrence of the latter in combinations and its usefulness in explaining the line at 1998 as 2×1000 lends considerable support to its interpretation as a fundamental.

It is now convenient to consider the infrared-active vibrations. The very strong bands at 777 and 908 cm^{-1} may at once be assigned to the CCl stretchings in b_{2u} and b_{3u}, but in the absence of characteristic envelopes, it is not possible to determine uniquely their correspondence with the species. The infrared spectrum of TFE suggests that the b_{1u} wagging and the remaining b_{2u} and b_{3u} modes of TCE give rise to moderately strong bands. Figure 2 shows that between the intense cluster around 777 cm^{-1} and the lower limit of the present range of observation, 190 cm^{-1}, there appear only two relatively strong bands, viz., those at 288 and 224 cm^{-1}. It will be recalled that the b_{2u}, b_{1u}, and b_{2u} angular modes in TFE occur at 558, 406, and 218 cm^{-1}. This suggests that the TCE rocking frequency occurs well below the 224 cm^{-1} band. At the same time, however, this analogy with TFE requires the assignment of 288 cm^{-1} to the b_{3u} deformation and 224 cm^{-1} to the b_{1u} wagging motion. The attempt to infer the frequency of the b_{1u} rocking from the observed combination bands leads to a value around 170 cm^{-1}.[9]

Although it seems clear that aside from the torsion vibration all the fundamental frequencies are now known, it is still necessary to determine unequivocally the species to which the pairs 347, 512 and 777, 908 belong. An analysis of the force constants for the b_{1g} block leads to the conclusion that the frequency 512 cm^{-1} is far too high to be ascribed to the rocking mode. It must, therefore, correspond to the b_{2g} wagging, whereas 347 may be satisfactorily interpreted as the b_{1g} rocking frequency. Contrary to the objections raised by Torkington [12], this assignment leads to reasonable force constants for the out-of-plane bending modes. In table 2 are given the principal and interaction constants for the wagging motions in ethylene, TFE, and TCE. As was to be expected both H and h are much larger for TFE than for ethylene. For TCE, on the other hand, the principal constant H shows a marked decrease from its value for TFE, approaching, in fact, that for ethylene. Most interesting, however, is the zero interaction constant for TCE. Indeed, it may be anticipated that h also vanishes for the next higher member of the series, viz., tetrabromoethylene (TBE). Moreover, it is reasonable to expect that for TBE the constant H will be close to its value for TCE, being perhaps slightly smaller. If, then, the TCE constants are transferred to TBE, the b_{1u} and b_{2g} frequencies for the latter are found to be 200 and 489 cm^{-1}, respectively. The Raman data given for TBE by Kohlrausch [32] include a weak line at 463 cm^{-1}, which he has assigned to the b_{2g} wagging mode. If this interpretation of the 463 cm^{-1} is correct and h is taken to be zero, then H becomes 0.238, which is to be compared with 0.266 for TCE. It is, moreover, now possible to predict the value of the b_{1u} wagging frequency in TBE. With $H=0.238$, $h=0$, this vibration is calculated to occur at 189 cm^{-1}.

TABLE 2. *Frequencies and force constants for wagging modes of* $H_2C{:}CH_2$, $F_2C{:}CF_2$, *and* $Cl_2C{:}CCl_2$

Constants	$H_2C{:}CH_2$[a]	$F_2C{:}CF_2$	$Cl_2C{:}CCl_2$
$\nu_7(b_{1u})$	949.2	406	224
$\nu_8(b_{2g})$	943	508	512
[b] H	0.230	0.326	0.266
[b] h	.033	.127	.000

[a] The data for ethylene are taken from the paper by Arnett and Crawford [11].
[b] The principal constant H and the interaction constant h are given here in units of 10^{-11} erg/radian^2. The actual symmetrized constant for the b_{1u} motion is $(H+h)$, and that for b_{1g} is $(H-h)$.

The correlation of the 777 and 908 cm^{-1} bands with the species b_{2u} and b_{3u} is hindered by the absence of the usual aids to assignment. Analogy with TFE suggests that 908 cm^{-1} refers to the b_{2u} stretching mode and 777 cm^{-1} to that in b_{3u}. Because the remainder of the assignment is fairly well established, a force-constant calculation is justified. As yet unpublished results obtained by D. E. Mann for TCE, with the aid of a Urey-Bradley type of potential function [35], indicate that the suggested analogy with the TFE assignment is probably correct.[10]

All that is needed now to complete the assignment is a value for the torsion frequency. If we use for TCE the torsion constant previously determined for TFE, the frequency is calculated to be 106 cm^{-1}. This provides a plausible explanation for the very weak Raman line at 218 cm^{-1} as the overtone of the torsion fundamental. To avoid imputing too much significance to this calculation, the value of the frequency has been rounded to 110 cm^{-1}. The final assignment is given in table 3.

[9] The results quoted in footnote 6 provide encouraging support for this prediction.

[10] It is worth pointing out, however, that some modification of the simple Urey-Bradley field [35] is needed. In particular, the addition of a constant that describes the effect of the interaction of the CCl_2 groups in the rocking modes seems desirable.

TABLE 3. *Fundamental vibration frequencies for $F_2C{:}CF_2$ and $Cl_2C{:}CCl_2$*

Species (V_h)	Number	Designation	$F_2C{:}CF_2$	$Cl_2C{:}CCl_2$
			cm^{-1}	cm^{-1}
a_g	1	ν-CC	1872	1571
	2	ν-CX	778	447
	3	δ-CX_2	394	235
a_u	4	τ	190	110
b_{1g}	5	ν-CX	1340	1000
	6	ρ-CX_2	551	347
b_{1u}	7	β-CX_2	406	224
b_{2g}	8	β-CX_2	508	512
b_{2u}	9	ν-CX	1337	998
	10	ρ-CX_2	218	[a]176
b_{3u}	11	ν-CX	1186	777
	12	δ-CX_2	558	288

[a] See footnote 6.

4. Thermodynamic Functions

The thermodynamic functions to the rigid-rotator, harmonic-oscillator approximation were computed for TFE and TCE in their ideal gaseous state. The molecular constants used were taken from [13] and [36], but the assignments were those given in table 3. The results given in tables 4 and 5 are taken from the more complete tables calculated with the aid of SEAC.

TABLE 4. *Calculated thermodynamic functions in dimensionless units for $F_2C{:}CF_2$ as an ideal gas*

T	C_p°/R	$(H^\circ-E_0^\circ)/RT$	$-(F^\circ-E_0^\circ)/RT$	S°/R
°K				
197.53	7.787	5.467	27.013	32.480
300	9.707	6.607	29.526	36.133
400	11.054	7.559	31.561	39.120
500	12.073	8.364	33.336	41.701
600	12.849	9.050	34.924	43.974
700	13.441	9.637	36.364	46.001
800	13.895	10.142	37.685	47.827
900	14.247	10.580	38.905	49.485
1,000	14.523	10.961	40.040	51.001
1,100	14.741	11.295	41.101	52.395
1,200	14.917	11.590	42.096	53.686
1,300	15.059	11.851	43.034	54.886
1,400	15.176	12.085	43.921	56.006
1,500	15.273	12.294	44.762	57.056

TABLE 5. *Calculated thermodynamic functions in dimensionless units for $Cl_2C{:}CCl_2$ as an ideal gas* [a]

T	C_p°/R	$(H^\circ-E_0^\circ)/RT$	$-(F^\circ-E_0^\circ)/RT$	S°/R
°K				
300	11.519	8.054	33.292	41.346
[b]394.18	12.623	9.021	35.622	44.643
400	12.679	9.074	35.755	44.829
500	13.479	9.880	37.869	47.750
600	14.043	10.530	39.730	50.260
700	14.449	11.062	41.395	52.457
800	14.747	11.505	42.902	54.407
900	14.971	11.878	44.279	56.157
1,000	15.142	12.196	45.547	57.744
1,100	15.275	12.471	46.723	59.193
1,200	15.380	12.709	47.818	60.527
1,300	15.464	12.918	48.844	61.762
1,400	15.533	13.102	49.808	62.910
1,500	15.590	13.266	50.718	63.984

[a] The entries in this table have been corrected for the change of μ_{15} from 170 to 176 cm^{-1}.

[b] The boiling point of TCE at 1 atmosphere is given by Dreisbach and Shrader as 121.02° C [37]. The ice point, as well as the other basic constants needed for the computation of these tables, are taken from [38].

The authors are indebted to Prof. K. S. Pitzer for communicating to them the infrared spectrum of TCE below 190 cm^{-1}, and also acknowledge several helpful discussions with Dr. Takehiko Shimanouchi.

5. References

[1] Earle K. Plyler and Nicolo Acquista, J. Opt. Soc. Am. **43,** 212 (1953).
[2] G. T. Furukawa, R. E. McCoskey, and M. L. Reilly, J. Research NBS **51,** 69 (1953) RP2423.
[3] E. K. Plyler, R. Stair, and C. J. Humphreys, J. Research NBS **38,** 211 (1947) RP1769.
[4] D. E. Mann, N. Acquista, and Earle K. Plyler, J. Chem. Phys. **21,** 1949 (1953).
[5] J. R. Nielsen, H. H. Claassen, and D. C. Smith, J. Chem. Phys. **18,** 812 (1950).
[6] E. K. Plyler, J. Chem. Phys. **16,** 1008 (1948).
[7] H. J. Bernstein, J. Chem. Phys. **18,** 478 (1950).
[8] P. Torkington and H. W. Thompson, Trans. Faraday Soc. **41,** 236 (1945).
[9] A. Monfils and J. Duchesne, J. Chem. Phys. **18,** 1415 (1950).
[10] A. Monfils and J. Duchesne, Compt. rend. **236,** 685 (1953).
[11] R. L. Arnett and B. L. Crawford, Jr., J. Chem. Phys. **18,** 118 (1950).
[12] P. Torkington, Trans. Faraday Soc. **45,** 445 (1949).
[13] I. L. Karle and J. Karle, J. Chem. Phys. **18,** 963 (1950).
[14] W. W. Coblentz, Investigations of infrared spectra (Publ. Carnegie Inst. of Wash., D. C. No. 35, Part I (1905)).
[15] G. B. Bonino, Gazz. chim. ital. **55,** 335 (1925).
[16] B. J. Spence and M. A. Easley, Phys. Rev. **34,** 730 (1929).
[17] R. Freymann, Compt. rend. **194,** 1471 (1932).
[18] T-Y. Wu, Phys. Rev. **46,** 465 (1934).
[19] J. Duchesne and M. Parodi, Nature **144,** 382 (1939).
[20] P. Pringsheim and B. Rosen, Z. Physik, **50,** 741 (1928).
[21] A. Dadieu and K. W. F. Kohlrausch, Sitz. ber. Akad. Wiss. Wien, Math.-naturw. Kl. [II] **138,** 635 (1929).
[22] A. Dadieu and K. W. F. Kohlrausch, Monatsh. Chem. **55,** 58 (1930).
[23] V. N. Thatte and S. M. Shahane, Indian J. Phys. **6,** 155 (1931).
[24] C. S. Morris, Phys. Rev. **38,** 141 (1931).
[25] L. Simons, Soc. Sci. Fennica, Commentationes Phys.-Math. **6,** No. 13 (1932).
[26] F. Heidenreich, Z. Physik **97,** 277 (1935).
[27] T-Y. Wu, J. Chinese Chem. Soc. **4,** 402 (1936).
[28] M. Kowalewska, Acta Phys. Polon. **7,** 279 (1938).
[29] H. Wittek, Z. physik. Chem. B **48,** 1 (1940).
[30] D. H. Rank, N. Sheppard, and G. J. Szasz, J. Chem. Phys. **16,** 698 (1948).
[31] S. B. Sanyal, Indian J. Phys. **24,** 151 (1950).
[32] K. W. F. Kohlrausch, Ramanspektren (Becker and Esler, Leipzig, 1943).
[33] T-Y. Wu, Vibrational spectra and structure of polyatomic molecules (J. W. Edwards, Ann Arbor, Mich., 1946).
[34] G. Herzberg, Infrared and Raman spectra of polyatomic molecules (D. van Nostrand Co., Inc., New York, N. Y., 1945).
[35] Y. Morino, K. Kuchitsu, and T. Shimanouchi, J. Chem. Phys. **20,** 726 (1952).
[36] I. L. Karle and J. Karle, J. Chem Phys. **20,** 63 (1952).
[37] R. R. Dreisbach and S. A. Shrader, Ind. Eng. Chem. **41,** 2879 (1949).
[38] F. D. Rossini, F. T. Gucker, Jr., H. L. Johnston, Linus Pauling, and G. W. Vinal, J. Am. Chem. Soc. **74,** 2699 (1952).

WASHINGTON, October 2, 1953.

Journal of Research of the National Bureau of Standards Vol. 52, No. 2, February 1954 Research Paper 2475

Preparation of Nickel Chloride of High Purity

W. Stanley Clabaugh, John W. Donovan, and Raleigh Gilchrist

A method is described for the preparation of cobalt-free nickel chloride, which consists in the repeated precipitation by hydrogen chloride of nickel chloride dihydrate from a mixture of a saturated aqueous solution of nickel chloride with acetone. Methods are also given for determining cobalt, aluminum, iron, copper, and combined phosphorus and silicon in nickel salts.

Introduction

In developing methods of testing nickel salts used as analytical reagent-grade chemicals, it became necessary to prepare nickel compounds that were free of cobalt. Most reagent-grade nickel salts contain approximately 0.2 percent of cobalt, although a special low-cobalt nickel sulfate, containing 0.002 to 0.005 percent of cobalt, is available.

The literature revealed no reliable process for preparing nickel salts free of cobalt. However, three papers did have a bearing on the subject. Garwin and Hixson,[1] in a study of the separation of cobalt from nickel by extraction from aqueous solution, found that anhydrous cobalt chloride was soluble in organic solvents, such as certain aliphatic alcohols, ketones, esters, and acids. They state that the addition of an electrolyte, hydrogen chloride in particular, greatly increases the efficiency of the extractive separation.

Tillu [2] developed an analytical separation of cobalt from nickel, based on the solubility of anhydrous cobalt chloride in acetone.

Katzin and Ferraro [3] studied the systems, cobaltous nitrate-water-acetone and cobaltous nitrate-water-*t*-butyl alcohol, with respect to types of compounds formed to gain information to account for the high solubility of inorganic salts in certain types of organic solvents.

The following procedure embraces the general principles involved in the above-mentioned papers. In addition to eliminating cobalt, the procedure also reduces or eliminates other impurities, such as aluminum, copper, iron, etc.

2. Procedure for Removing Cobalt from Nickel Chloride

Prepare a nearly saturated solution of nickel chloride in water at room temperature. Add a volume of acetone equal to approximately four times the volume of the aqueous nickel solution. The two liquids are only very slightly miscible under these conditions.

Warm the mixture on the steam bath to a temperature just below the boiling point of the acetone. Pass a rapid stream of hydrogen-chloride gas into the lower aqueous layer until the nickel chloride precipitates as a dihydrate and the two liquid phases become one. Decant most of the supernatant liquid, collect the nickel salt on a suction filter, and wash it with acetone.

If the operation is performed at a temperature just below the boiling point of the acetone, the nickel salt separates in a fine crystalline form that is very easy to filter and to wash. The product formed at room temperature appears to consist of a mixture of hydrates that separate in large aggregates of moist crystals. This type of precipitate has a tendency to cohere into one solid mass at the bottom of the container. Precipitation at the higher temperature increases the yield of nickel salt, furnishes a product that is easy to handle, but does not significantly affect the efficiency of the separation.

3. Purification of Nickel Chloride

One kilogram of nickel chloride hexahydrate, which contained 0.17 percent of cobalt, was subjected to four successive precipitations in the manner described above. The over-all yield of high-purity nickel salt was approximately 85 percent. Because of the great solubility of nickel chloride, the volumes of the solutions were relatively small, so that the precipitating operation could be performed in a 4-liter beaker.

The original material taken, when calculated as the dihydrate, contained 2,400 parts of cobalt per million. The first precipitation reduced the cobalt content to 130 ppm; the second, to 6.4 ppm; the third, to about 0.2 or 0.3 ppm. Cobalt was not detected in the fourth precipitate either chemically, by the method described later, or spectrochemically.

In addition to removing the cobalt, it was found that the aluminum content dropped from 4 to 1 ppm; copper, from 16 to 0.4 ppm; and iron, from 1 to less than 0.1 ppm. These values, determined chemically, were confirmed by independent spectrochemical analysis. Spectrochemical test showed that calcium and magnesium each was present in the final product to the extent of from 1 to 10 ppm. The combined phosphorus and silicon content in the final product was found chemically to be less than 1 ppm, calculated as silicon.

The nickel, chlorine, and water contents of the purified product were found to be 35.4, 42.4, and 21.0 percent, respectively, as compared with the calculated values of 35.4, 42.8, and 21.7 percent for $NiCl_2 \cdot 2H_2O$.

[1] L. Garwin and A. Hixson, Ind. Eng. Chem. **41**, 2298, 2303 (1949).
[2] M. M. Tillu, J. Indian Chem. Soc. **20**, 139 (1943).
[3] I. Katzin and J. R. Ferraro, J. Am. Chem. Soc. **72**, 5451 (1950).

4. Methods of Determining Impurities

4.1. Determination of Cobalt

Cobalt was determined by means of a potentiometric titration in which bivalent cobalt is oxidized to tervalent cobalt by potassium ferricyanide. The method used was an adaptation of that developed by Tomicek and Freiberger.[4]

Any manganese present will be titrated and reported as cobalt.[5]

Tomicek was able to estimate as little as 15 μg of cobalt in the presence of 0.2 g of nickel.[6] The present authors were able to determine as little as 2 μg of cobalt in the presence of 2 g of nickel. The accuracy of the determination for amounts of cobalt less than 20 μg appeared to be ± 0.5 μg.

In adapting the method of Tomicek to this work, the present authors found that the potential at the end point of the titration depends on the concentration of ammonia and ammonium chloride. Large amounts of ammonia lower the potential, whereas ammonium chloride increases it. Ammonium chloride tends to stabilize the potential, especially during stirring of the solution. If the proper concentrations of ammonia and ammonium chloride are established, the end point of the titration may be taken as that point at which the potential of the solution is zero when compared to the potential of a saturated calomel electrode. Although this method of determining the end point may introduce a small error, usually less than 10 μg of cobalt, it does serve as a rapid routine method for determining fairly small amounts. For the accurate determination of very small amounts of cobalt, the values of the potentials must be plotted and the exact end point determined graphically. In the present work, measurements of the voltage were made with a high-impedance input vacuum-tube voltmeter.

Because the presence of even small amounts of oxygen interferes with the titration, all the solutions must be prepared with oxygen-free water and protected during the titration. A suitable titration assembly consists of a 100-ml beaker with a close-fitting rubber stopper, through which are holes for inserting the calomel and platinum electrodes, buret tip, and a tube for passing in inert gas. The amount of ferricyanide added can be easily controlled if the buret is connected by means of a short piece of transparent tubing to a glass tube that is drawn to a fine tip. It is this latter tip that should be inserted through the rubber stopper. The above arrangement will allow the solution to be stirred by swirling the contents of the beaker.

In determining microgram quantities of cobalt, a 0.001-*M* solution of ferricyanide is used, whereas for larger quantities a 0.02-*M* concentration is satisfactory. The nickel salt may be either the chloride, nitrate, sulfate, or acetate, etc., provided sufficient ammonia is added to convert all the nickel to the cation $[Ni(NH_3)_6]^{++}$ and to provide a final concentration of ammonia of about 4 *N*.

In the determination of cobalt in the nickel chloride dihydrate, 2 g of the salt was dissolved in 10 ml of water in the 100-ml titration beaker. After inserting the rubber stopper containing the electrodes, etc., carbon dioxide was passed through the solution for 10 to 20 min, after which 20 ml of an ammonia-ammonium chloride solution, made by dissolving 6 g of NH_4Cl in 100 ml of 6 *N* NH_4OH (10 percent of NH_3), was added. The flow of carbon dioxide was stopped and the cobalt titrated with ferricyanide.

To ascertain whether known quantities of cobalt, when added to the cobalt-free nickel chloride, could be accounted for, 2.0, 3.0, 5.0, and 10.0 μg of cobalt each added to 2 g of the dihydrate gave 1.7, 2.8, 5.0, and 10.0 μg, respectively.

4.2. Determination of Other Impurities

Aluminum was determined according to the general method of Gentry and Sherrington,[7] which consists in complexing the nickel with cyanide in ammoniacal solution, and extracting the aluminum with a 1-percent solution of 8-hydroxyquinoline in chloroform. The amount of aluminum was ascertained by measuring the absorbancy of the chloroform extract at 395 mμ. The value so obtained was corrected for a small amount of iron, which was also extracted, by measuring the absorbancy of the same extract at 580 mμ.[8]

Iron was determined by measuring the absorbancy of the isoamyl alcohol extract of the thiocyanate complex.

Copper was determined by extracting with a 0.002-percent solution of dithizone in carbon tetrachloride, from a solution containing 0.05 *N* acid, to eliminate any interference by nickel, and by measuring the absorbancy of the extract.

The combined phosphorus and silicon content was determined by measuring the absorbancy of the "molybdenum blue" that was produced. The heteropolycomplex with molybdenum was formed in ammoniacal solution. The solution was then acidified and filtered to remove any nickel ammonium sulfate. The combined heteropolycomplexes were extracted with isoamyl alcohol and reduced to molybdenum blue by stannous chloride. The color produced was compared with those of known amounts of silicon, as silicate, treated in the same manner as the sample.

[4] O. Tomicek and F. Freiberger, J. Am. Chem. Soc. **57**, 801 (1935).
[5] O. Tomicek and J. Kalny, J. Am. Chem. Soc. **57**, 1209 (1935).
[6] O. Tomicek, Chem. Listy **36**, 44 (1942).
[7] C. H. R. Gentry and L. G. Sherrington, The Analyst **71**, 432 (1946).
[8] T. Moeller, Ind. Eng. Chem., Anal. Ed. **15**, 346 (1943).

WASHINGTON, July 16, 1953.

Journal of Research of the National Bureau of Standards Vol. 52, No. 2, February 1954 Research Paper 2476

The System of Lime, Alumina, and Water from 50° to 250° C

Richard B. Peppler and Lansing S. Wells

The system CaO-Al_2O_3-H_2O has been investigated over the range 50° to 250° C. At equilibrium, only two stable ternary compounds exist in the system, namely, $3CaO \cdot Al_2O_3 \cdot 6H_2O$ up to 215° C and $4CaO \cdot 3Al_2O_3 \cdot 3H_2O$ from 215° to 250° C. Hexagonal hydrated calcium aluminates occur as metastable phases with decreasing stability with increasing temperature until at temperatures over 100° C they exist only momentarily. There are only two stable alumina hydrates, namely, gibbsite ($Al_2O_3 \cdot 3H_2O$) up to 150° C, and boehmite ($Al_2O_3 \cdot H_2O$) thereafter. A stable phase throughout the temperature range is $Ca(OH)_2$. The equilibria curves of these solid phases maintain the same general relationships to each other throughout. As the temperature increases to 250° C, the solubility fields are compressed into the water apex of the diagram.

1. Introduction

Numerous investigations of the system CaO-Al_2O_3-H_2O have been reported in the literature [1, 2, 3, 4, 5],[1] and present knowledge of the system has been ably summarized by Steinour [6]. The importance and applications of studies of this system have been stressed by these authors.

Although calcium hydroaluminates have been prepared hydrothermally [7, 8, 9, 10], the ternary system as such has not been studied at elevated temperatures and pressures. The present paper is a study of this system from 50° to 250° C and from 1- to approximately 39-atm pressure. The system, in turn, will be compared with that previously studied at 21° C and 90° C [5].

At higher temperatures, such difficulties as the low solubility of the compounds and interference of carbon dioxide, become magnified, and superimposed on these difficulties are those inherent in hydrothermal investigations.

The system was investigated at one intermediate temperature, namely, 50° C, and then at 120°, 150°, 200°, and 250° C. Thus it is possible to describe the system over the range 21° to 250° C. This probably includes the entire range over which useful information may be obtained because the solubilities of the various compounds in this system become immeasurably small above 250° C.

A study of this system at elevated temperatures may provide some information about the mechanism of the reactions that occur in the steam curing of portland cement. It should also have a bearing on reactions that take place if high-alumina cements (which are composed largely of anhydrous calcium aluminates) are heated to elevated temperatures and pressures. The system from 21° to 250° C may also have applications in the fields of geology, soil equilibria, water purification, and in the formation of boiler scale.

2. Apparatus and Procedure

In the investigation at 50° C, the apparatus and techniques were essentially the same as those used by Wells, Clarke, and McMurdie [5], who studied this system at 21° and 90° C. The method is described in detail by these authors.

In the present investigation polyethylene bottles of ½-liter capacity were used. They were filled with lime water of varying concentrations, and 1 g of an appropriate solid phase was added to each. The bottles were then tightly stoppered and stored in an electric oven maintained at 50° C for periods up to 200 days.

They were shaken manually at least once a day, and from time to time, portions of each were filtered. Aliquots of these filtrates were analyzed gravimetrically for lime and alumina. The alumina was determined by the method of Blum [11], and the lime was precipitated as the oxalate and ignited to the oxide.

The corresponding solid phases in the precipitate were identified by the petrographic microscope, and, in case of any doubt as to their identities, By X-ray diffraction patterns also.

It is not known to what extent the solubilities of the compounds in this system are affected by pressure, but it is assumed that the effect is small. The investigation was carried out with sealed bombs in which both the vapor and liquid coexisted at equilibrium. Because the amount of dissolved material was generally small, the pressures corresponding to the various temperatures are approximately the equilibrium vapor pressures of water at those temperatures. The system is throughout considered to be condensed.

The metastable equilibria in this system at 50° C were determined by an approach from supersaturation. In this case also, the method of Wells, Clarke, and McMurdie was used [5]. Briefly, a series of initially metastable solutions was prepared from the filtrate of high-alumina cement shaken with water, and from calcium hydroxide solutions. Precipitation of metastable solid phases began immediately upon mixing the alumina-cement filtrate and the lime water in all cases except those of lowest alumina concentrations. There were precipitates in all cases at the end of 3 days, however. Again, aliquots of filtrates of these metastable solutions were analyzed gravimetrically and the solid phases identified petrographically and with X-ray diffraction patterns.

[1] Figures in brackets indicate the literature references at the end of this paper.

For the investigations above 100° C, three stainless-steel pressure bombs were used. These bombs are described in detail in a previous publication [12]. Briefly, these bombs consisted of two vessels, each of ½- to 1-liter capacity, separated by a stainless-steel disk containing a Munroe filter crucible. The liquid and solid phases were placed in one of these vessels, which was then covered by the center disk, and the other vessel, and the whole was bolted together.

The filter crucible was coated with platinum sponge made by reducing an alcoholic paste of ammonium chloroplatinate. It was held in place in the center disk by means of a threaded nut, with an annealed silver washer placed on the top and the bottom of the flange of the filter crucible. Copper gaskets made the seals between the center disk and the two vessels.

When assembled, the bombs were placed in electric ovens maintained at the desired temperature for periods of time up to 7 days. Tests made at 120° C indicated that equilibrium had been attained in this time.

The bombs were shaken manually at least once a day, and at the end of 5 or 7 days were removed from the ovens. Filtration was accomplished by inverting the bombs and plunging into cold running water the vessel that did not contain the solid and liquid phases. The lowering of the pressure in this vessel resulting from vapor condensation caused the liquid in the other vessel to be pushed through the filter crucible by its own vapor pressure.

The bombs were then removed from the cold water, further cooled, and disassembled. Aliquots of the filtrate were analyzed gravimetrically for lime and alumina as before.

The calcium oxide used in this investigation was prepared by heating calcium carbonate of reagent quality overnight in an electric furnace at 950° C. The calcium hydroxide solutions were prepared with the addition of distilled water to this calcium oxide and stored in a large tightly stoppered bottle. Whenever some of the solution was withdrawn from the stock bottle for use in a series of experiments, it was filtered and analyzed gravimetrically for CaO.

The gibbsite ($Al_2O_3 \cdot 3H_2O$) used in these experiments was homogeneous when examined under the microscope. It contained 0.02 percent of total alkalies as Na_2O, as determined by the flame photometer.

Boehmite ($Al_2O_3 \cdot H_2O$) was prepared from this gibbsite by heating it in a pressure bomb with excess water for 5 days at 250° C. It appeared homogeneous when examined by the microscope, and its X-ray powder pattern was identical with published patterns of artificial boehmite (see table 1).

TABLE 1. *X-ray pattern of synthetic boehmite: interplanar spacing, d, and relative intensity, I*

[S, strong; M, medium; W, weak; VW, very weak]

d	*I*	*d*	*I*
7.21	S	27.63	W
7.77	VW	30.28	VW
14.08	M	32.05	W
19.18	M	32.52	VW
22.90	VW	33.85	VW
24.48	M	35.98	W
24.61	M	36.08	W
25.82	VW		

The isometric $3CaO \cdot Al_2O_3 \cdot 6H_2O$ was prepared as follows: An aqueous slurry prepared from CaO and gibbsite, with CaO in slight excess of the stoichiometric ratio, was placed in a platinum dish in a pressure bomb containing excess water. The bomb was heated at 170° C for 5 days. The resulting compound was filtered from the excess water, and washed with water to remove the calcium hydroxide, after which it was washed by alcohol and ether. This product appeared homogeneous when examined under the microscope and had an index of 1.605. In all such preparations, there were small amounts of birefringent inclusions. A gravimetric analysis of one preparation gave a formula of $3.0\ CaO \cdot 1.0\ Al_2O_3 \cdot 6.2\ H_2O$.

The hydrated calcium aluminate, $4CaO \cdot 3Al_2O_3 \cdot 3H_2O$, was prepared by heating a lime-alumina clinker with a 4 to 3 molar ratio of CaO to Al_2O_3 with water for 7 days at 278° C. The resulting product was found to be homogeneous when examined microscopically. It consisted of rectangular plates having low birefringence with indices very close to 1.627.

Several difficulties and sources of error were encountered. At temperatures under 150° C, the filtrations in the pressure bombs were slow, taking approximately 10 minutes. It is estimated that the temperature of the vessel containing the solid and liquid phases changed 15 deg in this time, when taken from an oven at 150° C. In an effort to minimize this temperature change, the portion of the bomb that was not being cooled was covered with an asbestos glove during the filtration. The magnitude of the error is not known, because it depends in each case on how rapidly the liquid phase changes composition with temperature.

Above 150° C the filtrations were much more rapid, because of the greater pressure differential. In these cases, however, the spongy platinum on the Munroe-filter crucibles became perforated, allowing some solid to get into the filtrate. To overcome this difficulty, additional layers of spongy platinum had to be put on the filters. At 200° C and above, the liquid phase would go around the annealed silver gaskets above and below the flanges of the filter crucible, and this, too, would permit solid to get into the filtrate. Asbestos paper and Garlock gaskets were tried with no success. This problem was eventually solved by extending the layer of spongy platinum to cover the joints between the filter crucible and the silver gaskets.

It was found that distilled water alone, even at 120° C, attacked the bombs. With lime solutions the attack was more severe until a protective coating had been built up on the inner surface of the bombs. Then, at 120° C, the iron in the filtrate was reduced to about 1 part per million and the soluble chromate to a few parts per million.

When it became necessary to change the solid phase in the bombs, great care was taken to

remove every trace of the preceding solid phase.

The attack on the bomb became increasingly severe as the temperature increased. At the same time, above 120° C, the solubilities of the compounds were decreasing. Accordingly, a platinum lining was fabricated for one of the bombs, and the system at 200° and 250° C was worked out by using this bomb.

The chromium extracted from the bombs was apparently all in the oxidized state as chromate and so did not interfere with the gravimetric determinations of lime and alumina. Most of the iron extracted from the bombs appeared to be in the form of insoluble flakes.

The necessity of excluding carbon dioxide from these determinations has been frequently pointed out by other investigators. The present authors, however, found that even when the most elaborate precautions were taken, it was impossible to exclude carbon dioxide completely. After each determination a trace of calcite was evident in the solid phases.

The constancy of oven temperature was about 1 percent at 120° C and 2 percent at 200° C.

3. Review of the System CaO-Al_2O_3-H_2O at 21° and 90° C

The investigation by Wells, Clarke, and McMurdie [5] has been mentioned earlier. They found that gibbsite is the only stable alumina hydrate in this system at both 21° and 90° C. Amorphous hydrated alumina exists metastably with respect to this gibbsite at 21° C, but no attempt was made to work out its solubility curve. Phase-equilibria diagrams are presented for this system at these two temperatures (see figs. 1 and 2). From these two diagrams, which, for convenience, are reproduced here (see figs. 1 and 2), one sees that at 21° C gibbsite is the stable hydrate of alumina from 0 to 0.33 g/liter of CaO and that it exists metastably to a concentration of about 0.7 g/liter of CaO. The maximum alumina hydrate in stable solution is about 0.02 g/liter at 0.33 g/liter of CaO, and the maximum alumina hydrate in metastable solution is about 0.06 g/liter at 0.7 g/liter of CaO. At 90° C, the stable gibbsite curve has rotated counterclockwise about the origin, and so lies above and has a steeper slope than the corresponding curve at 21° C. Gibbsite is seen to be the stable alumina hydrate from 0 to 0.33 g/liter of CaO and to have a much shorter metastable prolongation thereafter. The maximum ascertained stable solubility of alumina hydrate at 90° may be seen to be about 0.11 g/liter at 0.33 g/liter of CaO. The maximum stable solubility of the gibbsite at each of these temperatures corresponds to an invariant point with isometric $3CaO$-Al_2O_3-$6H_2O$.

One might suppose from the equilibria diagrams at these two temperatures (as the authors suggest) that there exists a family of stable equilibria curves for gibbsite at various intermediate temperatures, starting at the origin and being more or less straight lines with increasing slope as the temperature increases. It might also be supposed that since the gibbsite-isometric $3CaO$-Al_2O_3-$6H_2O$ invariant points at these two temperatures lie directly above each

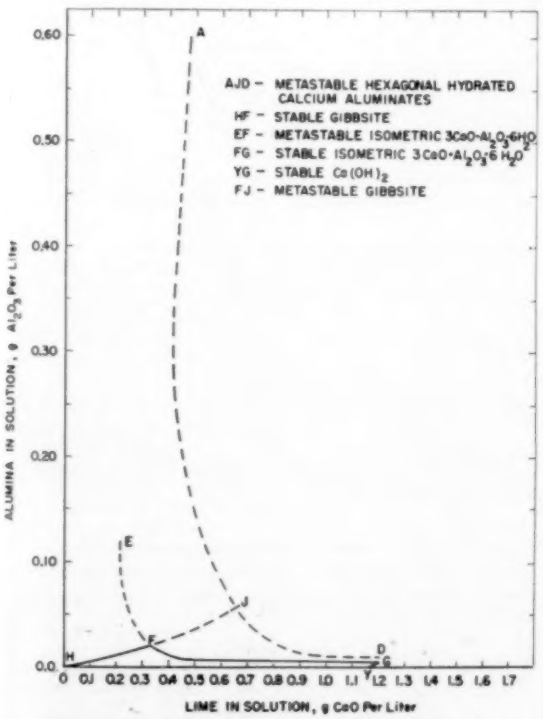

FIGURE 1. *The system* CaO-Al_2O_3-H_2O *at 21° C.*

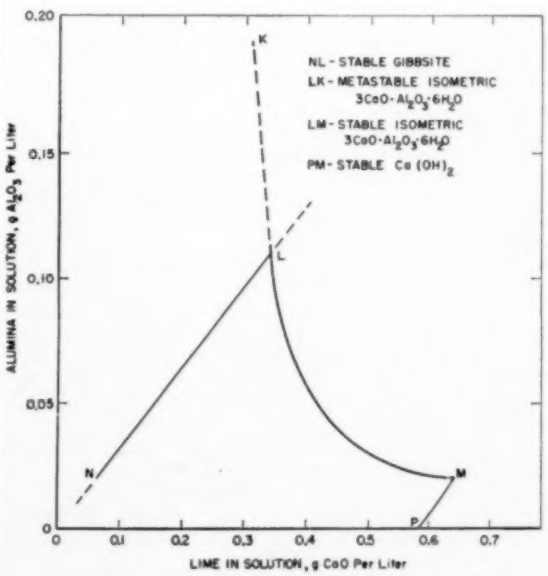

FIGURE 2. *The system* CaO-Al_2O_3-H_2O *at 90° C.*

other, the corresponding invariant points of the intermediate family of curves would lie on the straight line joining them.

Referring to figures 1 and 2, one sees that the authors found that the solubility of $Ca(OH)_2$ in water alone to be 1.17 g/liter at 21° C and about 0.58 g/liter at 90° C. The stable equilibria curves of $Ca(OH)_2$ were taken to be the straight line joining the points representing its solubility in water alone to the points where it coexists at equilibrium with isometric $3CaO{\cdot}Al_2O_3{\cdot}6H_2O$. In going from 21° to 90° C, this equilibrium curve lengthened and moved toward the origin. As it is known that the solubility of $Ca(OH)_2$ decreases with increasing temperature [13], it is assumed that at temperatures between 21° and 90° C there exists in this system a family of stable $Ca(OH)_2$ equilibria curves, lengthening and moving toward the origin as the temperature increases.

Wells, Clarke, and McMurdie [5] found three ternary compounds in this system at 21° C, namely, stable isometric $3CaO{\cdot}Al_2O_3{\cdot}6H_2O$ and two metastable hexagonal calcium aluminate hydrates, $2CaO{\cdot}Al_2O_3{\cdot}8H_2O$ and $4CaO{\cdot}Al_2O_3{\cdot}13H_2O$.

To establish the metastable solubility curve of the hexagonal hydrates by approach from supersaturation, they prepared large quantities of metastable solutions by shaking alkali-free calcium-aluminate cements with distilled water. These mixtures were filtered, analyzed, and mixed with known amounts of lime water. They were put in stoppered bottles, stored at 21° C, and examined microscopically and aliquots analyzed from time to time. The same metastable equilibria as defined by final compositions of these solutions was approached also from undersaturation by mixing $2CaO{\cdot}Al_2O_3{\cdot}8H_2O$ and $4CaO{\cdot}Al_2O_3{\cdot}13H_2O$ with known varying concentrations of lime water. In this fashion these authors [5] were able to establish a metastable curve for the hexagonal phases lying above and to the right of the stable isometric hydrate curve. This curve is reproduced in fig. 1. From the molar CaO to Al_2O_3 ratios of the resulting solutions and the solid phases, these authors concluded that their metastable hexagonal hydrates curve actually corresponds to two intersecting metastable equilibria curves, one for $4CaO{\cdot}Al_2O_3{\cdot}13H_2O$ and one for $2CaO{\cdot}Al_2O_3{\cdot}8H_2O$. From these molar ratios, the shift in refractive index, and from X-ray diffraction data, they also concluded that so-called hexagonal tricalcium aluminate hydrate is actually a mixture of $4CaO{\cdot}Al_2O_313H_2O$ and $2CaO{\cdot}Al_2O_38H_2O$ intercrystallized in equimolecular proportions. This problem was not investigated further and for simplicity only the one metastable hexagonal calcium aluminate hydrate curve is reproduced here.

These same authors permitted a series of these metastable solutions containing hexagonal phases to stand at 21° C until the hexagonal phases were partially transformed to the stable isometric $3CaO{\cdot}Al_2O_3{\cdot}6H_2O$, and the stable isometric hydrate equilibrium curve was approached.

The only stable ternary compound in this system at 21° C was found to be the isometric $3CaO{\cdot}Al_2O_3{\cdot}6H_2O$. Its equilibrium curve was established by approach from undersaturation by letting the isometric $3CaO{\cdot}Al_2O_3{\cdot}6H_2O$ stand in contact with lime solutions of varying concentrations. The isometric hydrate was found to dissolve congruently (went into solution parallel to the $3CaO{:}Al_2O_3$ composition line) at all concentrations up to the stable invariant point between $Ca(OH)_2$ and isometric $3CaO{\cdot}Al_2O_3{\cdot}6H_2O$, which in this case lies very close to the point representing the solubility of $Ca(OH)_2$ in water at 21° C (fig. 1).

It was assumed that the hexagonal phases would be so extremely metastable at 90° C and would have such a transitory existence before converting to the stable isometric hydrate that their equilibria relationships were not investigated by these authors.

In the present investigation, however, the undiluted filtrate of a high-alumina cement, representing a metastable solution of approximately 1.2 g/liter of CaO and 1.9 g/liter of Al_2O_3, was allowed to stand at 90° C. Precipitation of solid phases began almost immediately. At the end of 1 hour, these solid phases were metastable hexagonal aluminate hydrates only. At 4 hours, there were approximately equal amounts of isometric and hexagonal phases, and, at the end of 22 hours, although the isometric phases greatly predominated, the hexagonal phases were still present. Accordingly, a series of preparations of metastable solutions, whose Al_2O_3 contents varied from 0.1 to 0.6 g/liter, were held at 90° C for 1 hour and filtered. The solid phases were examined microscopically and the filtrates analyzed gravimetrically for lime and alumina. In all cases there was isometric $3CaO{\cdot}Al_2O_3{\cdot}6H_2O$ as well as the hexagonal hydrates in the solid phases, though the isometric hydrate was of relatively small particle size. The initial and final compositions are shown in table 2 and figure 3. The curve so defined is considered to represent a metastable region rather than to define a metastable equilibrium. The metastable hexagonal hydrate equilibrium curve would lie above this curve and to the right of it. Experiments were performed that indicated that the solutions would have to be analyzed after only 5 minutes in order to define this curve. As one cannot expect to obtain consistent data in so short a time, this was not done. Wells, Clarke, and McMurdie found a metastable extension of their stable isometric curve to the left and above the stable gibbsite-isometric $3CaO{\cdot}Al_2O_3{\cdot}3H_2O$ invariant. This metastable extension would presumably intersect the metastable hexagonal calcium aluminate hydrate curve at some point, as was the case at 21° C.

TABLE 2. *Metastable hexagonal phases at 90° C*

Experiment	Initial CaO	Initial Al_2O_3	Time	Final Al_2O_3	Final CaO	Final solid phases
	g/liter	*g/liter*	*Hours*	*g/liter*	*g/liter*	
1	1.20	0.60	1	0.640	0.585	Hexagonal phases predominate over isometric, with Al_2O_3 gel, in all cases.
2	1.20	.40	1	.252	.440	
3	1.20	.30	1	.118	.488	
4	1.20	.20	1	.055	.626	
5	1.20	.10	1	.026	.834	

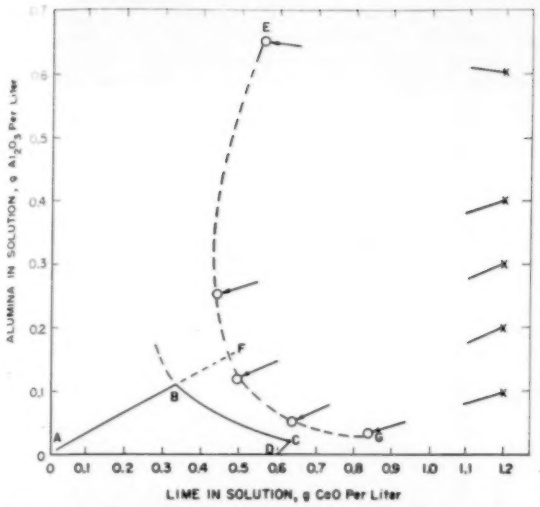

FIGURE 3. *Metastable hexagonal calcium aluminate hydrates in the system* $CaO\text{-}Al_2O_3\text{-}H_2O$ *at 90° after one hour.*

Composition of initial metastable solutions are indicated by an X; compositions of these solutions at the end of one hour by an O. The dashed line, EFG, defines the region of metastability of the hexagonal calcium aluminate hydrates. The stable solubility fields in the system $CaO\text{-}Al_2O_3\text{-}H_2O$ at 90° C are indicated by the area ABCD.

Presumably there exists also in this system at 21° C a metastable amorphous hydrated alumina solubility curve lying above the stable solubility curve of gibbsite. There should be an invariant between this curve and the metastable part of the isometric hydrate curve, as well as an invariant between the metastable alumina hydrate and the metastable hexagonal hydrate curve. This was not investigated by the present authors. If one takes Bessey's curve [3] for the solubility of Al_2O_3Aq and superimpose it on the diagram of the system at 21° C (fig. 1), the invariant with the metastable isometric would be at about 0.17 g/liter of Al_2O_3 and 0.20 g/liter of CaO, and the invariant with the metastable hexagonal phases would be at about 0.32 g/liter of Al_2O_3 and 0.4 g/liter at CaO. Unfortunately, Bessey gave no details about how he prepared and determined the solubility of Al_2O_3Aq, and, indeed, the practical difficulties of doing so are very great. More will be said about this in another portion of this paper.

The equilibrium curve for isometric $3CaO\text{-}Al_2O_3\text{-}6H_2O$ in this system at 90° C, as found by Wells, Clarke, McMurdie [5] is also reproduced here for convenience (see fig. 2). Referring to it one sees that this curve has the same shape as that at 21° C, lies above it, and has a shorter metastable extension. This curve was established by a perfectly analogous procedure, and again it was found that the isometric hydrate dissolves congruently in lime water of all concentrations up to that of the $Ca(OH)_2$-isometric $3CaO\text{-}Al_2O_3\text{-}6H_2O$ invariant. As the above authors point out, it is reasonable to expect that a family of such curves exist between these two curves corresponding to temperatures between 21° and 90° C. The system was accordingly investigated at 50° C.

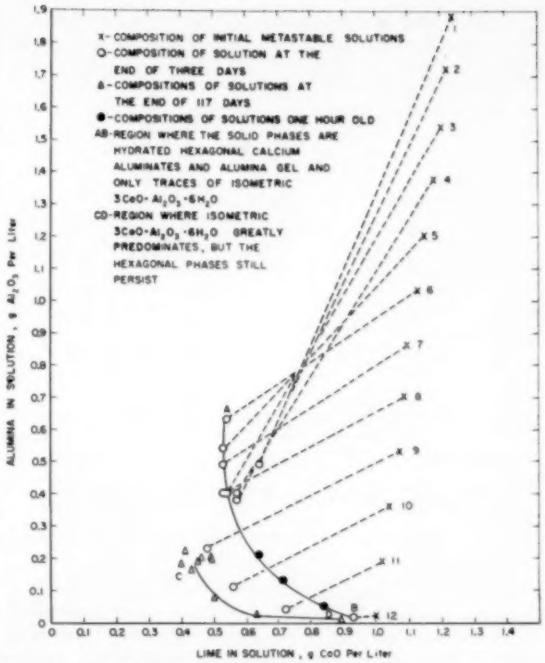
X- COMPOSITION OF INITIAL METASTABLE SOLUTIONS
O- COMPOSITION OF SOLUTION AT THE END OF THREE DAYS
Δ- COMPOSITIONS OF SOLUTIONS AT THE END OF 117 DAYS
●- COMPOSITIONS OF SOLUTIONS ONE HOUR OLD
AB- REGION WHERE THE SOLID PHASES ARE HYDRATED HEXAGONAL CALCIUM ALUMINATES AND ALUMINA GEL AND ONLY TRACES OF ISOMETRIC $3CaO\text{-}Al_2O_3\text{-}6H_2O$
CD- REGION WHERE ISOMETRIC $3CaO\text{-}Al_2O_3\text{-}6H_2O$ GREATLY PREDOMINATES, BUT THE HEXAGONAL PHASES STILL PERSIST
ALUMINA IN SOLUTION, g Al_2O_3 Per Liter
LIME IN SOLUTION, g CaO Per Liter

FIGURE 4. *Metastable hexagonal calcium aluminate hydrates in the system* $CaO\text{-}Al_2O_3\text{-}H_2O$ *at 50° C.*

4. Discussion

4.1. The System $CaO\text{-}Al_2O_3\text{-}H_2O$ at 50° C

The role of the hexagonal phases in the system $CaO\text{-}Al_2O_3\text{-}H_2O$ at 50° C was investigated, using techniques similar to those used in the investigation at 21° C mentioned earlier.

A series of initially metastable solutions were prepared from the filtrate of high-alumina cement shaken with water plus additions of $Ca(OH)_2$ solutions. Precipitation began immediately upon mixing the alumina cement filtrate and the lime water in all cases except those of lowest alumina concentration. There was precipitation in all cases at the end of 3 days, however. Points representing these initial compositions are shown in figure 4. Referring to this figure, one sees that those initial mixes of highest alumina content were least stable. At the end of 3 days these mixtures had precipitated hexagonal phases and approached a relatively small area representing the alumina hydrate hexagonal calcium aluminate hydrate invariant point. Data on the solubility of the hexagonal calcium aluminate hydrates in the system $CaO\text{-}Al_2O_3\text{-}H_2O$ at 50° C are presented in table 3. A total of 70 points was determined, but in the interests of simplicity, only the initial and final data are presented.

The behavior of composition 12, figure 4, is of special interest. The first precipitate, at the end

TABLE 3. *Solubility of the hexagonal calcium aluminate hydrates in the system* $CaO\text{-}Al_2O_3\text{-}H_2O$ *at 50° C*

	Time	Initial Al_2O_3	Initial CaO	Final Al_2O_3	Final CaO	Final solid phases
		g/liter	*g/liter*	*g/liter*	*g/liter*	
1	3 days	1.88	1.24	0.487	0.635	Al_2O_3 gel, hexagonal, and isometric with hexagonal phases predominating.
2	do	1.72	1.22	.377	.566	Do.
3	do	1.54	1.20	.404	.545	Do.
4	do	1.37	1.18	.402	.568	Do.
5	do	1.20	1.15	.542	.539	Do.
6	do	1.03	1.13	.630	.545	Do.
7	do	.86	1.11	.488	.532	Do.
8	do	.70	1.09	.397	.527	Do.
9	1 hour	.30	1.20	.208	.639	Al_2O_3 gel and hexagonal phases.
10	do	.20	1.20	.132	.710	Do.
11	do	.10	1.20	.050	.836	Do.
12	3 days	.019	1.00	.013	.930	Do.
13	117 days	1.54	1.20	.200	.490	Hexagonal and isometric with hexagonal phases predominating.
14	do	1.37	1.18	.200	.462	Do.
15	do	1.20	1.15	.193	.494	Do.
16	do	1.03	1.13	.161	.430	Do.
17	do	.86	1.11	.189	.445	Do.
18	do	.70	1.09	.217	.414	Do.
19	do	.53	1.07	.185	.400	Hexagonal and isometric with isometric phases predominating.
20	do	.36	1.04	.076	.495	Do.
21	do	.188	1.02	.022	.630	Do.
22	do	.019	1.00	.002	.894	Hexagonal and isometric with hexagonal phases predominating.

of 3 days, was a mixture of isometric $3CaO\cdot Al_2O_3\cdot 6H_2O$ and the hexagonal phases. When measured again at 10 days, however, the proportions of these two phases were reversed, with the hexagonal phases predominating. When the resulting composition of mixture 12 was measured at 35 days, hexagonal phases greatly predominated over the isometric phase, and after 90 days, the isometric phase had disappeared completely. At 117 days, $Ca(OH)_2$ crystals were observed, together with the hexagonal calcium aluminate hydrates, and the composition of the liquid in contact with these solid phases defined a point below the stable isometric $3CaO\cdot Al_2O_3\cdot 6H_2O$ curve.

It has been speculated by others [3, 15] that at high calcium hydroxide concentrations, the hexagonal rather than the isometric calcium aluminate hydrates are stable. As the behavior of the mixture represented by composition 12 tended to support this view, two new preparations, whose initial compositions lay between those of compositions 11 and 12 in figure 13, were prepared. These new preparations, however, precipitated both isometric and hexagonal phases. One of them defined a point on the metastable hexagonal hydrate equilibrium curve and the other a point between the hexagonal hydrate curve and the stable isometric curve at 0.95 g/liter of CaO. The distance between the two curves at this point is equivalent to only 0.05 g/liter of Al_2O_3. If one assumes that this point represents a hexagonal hydrate-isometric hydrate invariant point, and that composition 12 at the end of 117 days represents a hexagonal hydrate-$Ca(OH)_2$ invariant point, it might be concluded that the metastable curve of the hexagonal phases extends downward, intersecting both the stable isometric $3CaO\cdot Al_2O_3\cdot 6H_2O$ and the stable $Ca(OH)_2$ equilibria curves. The authors feel that the evidence is entirely too slight to warrant this assumption. Moreover, the triangular area that would be thus defined is considerably smaller than the area of experimental uncertainty, so that the problem could not be resolved.

The path of precipitation of compositions 1 to 5, inclusive, (fig. 4) was extremely steep downward, and there was little difficulty in identifying Al_2O_3 gel in the solid phases. There was also in these compositions at the end of 3 days very small amounts of the isometric $3CaO\cdot Al_2O_3\cdot 6H_2O$, though the hexagonal phases greatly predominated. Between 3 and 10 days, the hexagonal phases continued to predominate greatly, and the cluster of points representing the compositions of the solutions coalesced and moved vertically downward as Al_2O_3 gel precipitated. For simplicity, only the initial paths of precipitation are shown in figure 4. At the end of 90 days, the hexagonal phases still predominated in all compositions except number 1.

The compositions of preparations 6 to 11 all alter in a path downward and parallel to each other but not exactly parallel to either the $3CaO{:}Al_2O_3$ or the $4CaO{:}Al_2O_3$ composition lines. The compositions of preparations 6 to 8 defined the cluster of points representing the Al_2O_3Aq-hexagonal calcium aluminate hydrate invariant (the point approached by the points representing the compositions of preparations 1 to 6) and had only traces of the isometric $3CaO\cdot Al_2O_3\cdot 6H_2O$ in them at the end of 3 days. Preparations whose compositions are indicated by 9 to 11 at the end of 3 days had a large proportion of isometric phase in the solid phases and no hydrated alumina detectable either with the petrographic microscope or X-ray patterns. The metastable curve of the hexagonal phases at 50° C (see fig. 4) was drawn through all points representing the compositions at the end of 3 days, except in the case of

compositions 9 through 11. In these cases it is drawn through the points representing the compositions at the end of 1 hour of preparations, originally at approximately the same place as preparations 9, 10, and 11, and not shown in figure 4. The solid phases in compositions 9, 10, 11, even at 22 hours, had a large proportion of isometric $3CaO \cdot Al_2O_3 \cdot 6H_2O$, and this proportion increased with increasing time until at 90 days, although the hexagonal phases still existed, their proportion was very small.

The X-ray diffraction patterns of the hexagonal phases obtained in this investigation agree fairly well with those published by Wells, Clarke, and McMurdie [5], as seen in table 4. It could not be decided whether they more nearly represented those of $4CaO \cdot Al_2O_3 \cdot 13H_2O$ or $2CaO \cdot Al_2O_3 \cdot 8H_2O$, the patterns of which are themselves very similar.

Although the conversion of the hexagonal phases to the isometric phase is more rapid at 50° C than at 21° C, it is too slow to try to define the position of the stable isometric $3CaO \cdot Al_2O_3 \cdot 6H_2O$ curve from supersaturation. The closest approach to this curve is shown in figure 4, at the end of 117 days.

The stable equilibrium curve of isometric $3CaO \cdot Al_2O_3 \cdot 6H_2O$ in this system at 50° C was established by approach from undersaturation, using the same technique as was used in the investigation at 21° and 90° C. Stoppered polyethylene bottles were used instead of glass. Quantities of solid isometric hydrate in the proportion of 2 g/liter of solid were mixed with different lime solutions of known concentrations.

TABLE 4. *X-ray patterns of the hexagonal phases interplanar spacings, d; relative intensities, I*

[S, strong; M, medium; W, weak]

This investigation at 50° C		Investigation of Wells, Clarke, and McMurdie [5] at 21° C for $2CaO \cdot Al_2O_3 \cdot 8H_2O$	
d	*I*	*d*	*I*
7.557	S	10.6	S
5.15	S	5.3	S
3.767	S	3.55	M
2.864	S	2.87	S
2.576	W	2.69	W
		2.54	W
2.482	M	2.48	M
2.144	W	2.11	W
2.039	M	1.955	W
1.680	S	1.835	W
1.664	M		
		1.667	M
		1.591	W
1.596	W	1.443	M

It was observed that, as in the case of the investigation at 21° C, the isometric hydrate went into solution congruently in all concentrations of lime water up to that corresponding to the $Ca(OH)_2$-isometric $3CaO \cdot Al_2O_3 \cdot 6H_2O$ invariant point.

Limitations of sample caused some of the determinations to be ended much sooner than corresponding ones that established the position of the gibbsite equilibrium curve at 50° C. However, the isometric hydrate approached equilibrium much faster at 50° C than does gibbsite.

In shape, the isometric hydrate curve is completely analogous to those at 21° and 90° C and lies between them. It is one of a family of such curves predicted by Wells, Clarke, and McMurdie [5]. The isometric calcium aluminate hydrate equilibrium curve at 50° C is presented in figure 5 and the corresponding data in table 5. It may be observed that the solubility of the isometric tricalcium aluminate hydrate, both in water and in lime solutions, is higher than at 21° C. The invariant point, C, with $Ca(OH)_2$ is taken as the average of the cluster of points in that area, where $Ca(OH)_2$ and the isometric $3CaO \cdot Al_2O_3 \cdot 6H_2O$ coexist at equilibrium. This invariant point is located at 0.961 g/liter of CaO and 0.005 g/liter of Al_2O_3.

TABLE 5. *Solubility of isometric* $3CaO \cdot Al_2O_3 \cdot 6H_2O$ *in the system* $CaO\text{-}Al_2O_3\text{-}H_2O$ *at 50° C*

Experiment	Concentration of lime solution	Time	Final Al_2O_3	Final CaO	Final solid phases
	g/liter	*Days*	*g/liter*	*g/liter*	
1	0	14	0.133	0.223	Isometric $3CaO \cdot Al_2O_3 \cdot 6H_2O$.
2	0.10	15	.089	.317	Do.
3	.10	40	.055	.254	Do.
4	.10	170	.095	.233	Do.
5	.20	15	.060	.386	Do.
6	.20	40	.036	.232	Do.
7	.30	14	.021	.332	Do.
8	.30	18	.019	.325	Do.
9	.30	38	.013	.319	Do.
10	.40	14	.007	.408	Do.
11	.40	18	.006	.404	Do.
12	.40	38	.007	.416	Do.
13	.50	15	.007	.552	Do.
14	.50	30	.008	.559	Do.
15	.60	14	.010	.678	Do.
16	.60	30	.007	.671	Do.
17	.70	14	.003	.747	Isometric; some birefringent occlusions.
18	.70	30	.005	.737	Do.
19	.80	15	.006	.805	Do.
20	.80	40	.004	.717	Do.
21	.90	16	.002	.887	Isometric with birefringent occlusions.
22	1.00	8	.003	.968	Isometric+$Ca(OH)_2$.
23	1.00	36	.003	.956	Do.
24	1.10	54	.005	.930	Do.
25	1.10	100	.007	.980	Do.
26	(a)	49	.002	.924	Do.
27	(a)	100	.006	.947	Do.
Experiments in which which both isometric $3CaO \cdot Al_2O_3 \cdot 6H_2O$ and gibbsite were the initial solid phases					
28	0	49	0.130	0.301	
29	0	100	.153	.258	
30	0	220	.182	.271	

[a] Saturation.

It is probable that Al_2O_3 gel has a metastable existence in the system at 50° C, lying above the stable gibbsite ($Al_2O_3 \cdot 3H_2O$) curve and intersecting and the metastable prolongation of the isometric $3CaO \cdot Al_2O_3 \cdot 6H_2O$ curve and the metastable hexagonal calcium aluminate hydrate curve.

In an attempt to determine the solubility of alumina gel, a quantity of it was prepared by double decomposition between $AlCl_3$ and NH_4OH. The resulting gelatinous hydrated alumina had occluded

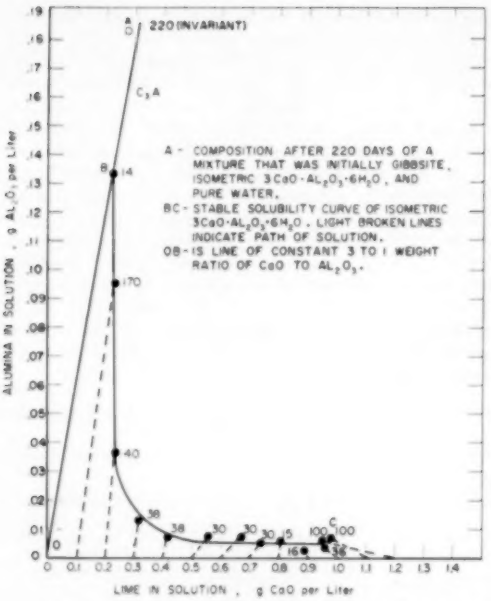

FIGURE 5. *Solubility of isometric* $3CaO \cdot Al_2O_3 \cdot 6H_2O$ *in the system* $CaO\text{-}Al_2O_3\text{-}H_2O$ *at 50° C.*

much of the NH_4Cl formed by this reaction. An attempt was made to remove this occluded NH_4Cl by ordinary dialysis. At the end of 5 days, however, the gelatinous hydrated alumina still had retained enough electrolyte to suppress its solubility to 0.001 g/liter, or less. Moreover, X-ray diffraction patterns of the gel indicated that at the end of 3 days the hydrated alumina had already gone over to the gibbsite structure. Accordingly, attempts to measure the solubility of alumina gel were abandoned.

The solubility of alumina hydrate in this system at 50° C was found to be somewhat higher than that at 21° C. Again, gibbsite was found to be the stable hydrated phase of alumina, and its equilibrium curve and invariant point with isometric $3CaO \cdot Al_2O_3 \cdot 6H_2O$ had the relation to those at 21° and 90° C that were earlier predicted.

Referring to figure 6 and table 6, one sees that the gibbsite apparently absorbs lime even at concentrations of lime less than that at the isometric hydrate-gibbsite invariant point. This is caused mainly by the fact that in the long periods of time involved carbon dioxide from the air was able to leak through the rubber stoppers and thus reduce the lime concentration by formation of calcite. The amount of calcite increased with increasing time, and the solubility of the gibbsite was essentially congruent until it had been formed. The fact that examination of the final solid phases showed nothing but gibbsite (other than a small amount of calcite) indicates that the reduction in lime concentration was not caused by chemical reaction between lime water and gibbsite.

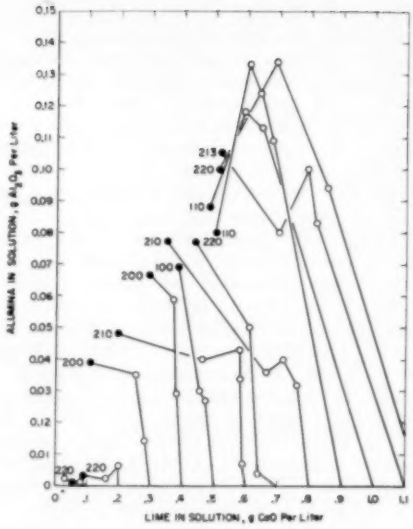

FIGURE 6. *Solubility of gibbsite in the system* $CaO\text{-}Al_2O_3\text{-}H_2O$ *at 50° C.*

Closed circles indicate the composition of liquids in contact with gibbsite at the termination of the experiments. The corresponding ages in days are indicated by the accompanying numbers.

At concentrations of lime greater than that at the invariant point, however, once the gibbsite had reached its maximum metastable solubility, the reduction in lime concentration was much greater. The variation in the composition of the liquid phase occurred consistently in one path, and the final solid phases were gibbsite and hexagonal calcium aluminate hydrates. Accordingly, this is interpreted to mean that the gibbsite in supersaturated solution reacted with the lime water and points representing the composition of the liquid phase moved from the metastable hexagonal calcium aluminate hydrate-gibbsite invariant point toward the stable isometric $3CaO \cdot Al_2O_3 \cdot 6H_2O$-gibbsite invariant point. The behavior at 50° C is thus analogous to the behavior observed at 21° C.

The maximum metastable solubility of gibbsite at 50° C is seen by reference to figure 6 to be 0.13 g/liter as Al_2O_3, and is therefore considerably greater than that observed at 21° C.

The stable and metastable solubility curves of gibbsite are defined by the heavy black dots in figure 6; those taken at longest periods of time from the initial mixture of gibbsite and lime solutions. In most cases, these times were over 200 days. It is recognized that in no case was final equilibrium attained. This was due mainly to limitations of sample. The extreme sluggishness of approach to equilibrium at this temperature was somewhat unexpected.

Taking these final points as the best or nearest approach to equilibrium, it was thought that the

TABLE 6. *Solubility of gibbsite in the system* $CaO\text{-}Al_2O_3\text{-}H_2O$ *at 50° C*

Experiment	Concentration of lime solution	Time	Final Al_2O_3	Final CaO	Final solid phases
	g/liter	*Days*	*g/liter*	*g/liter*	
1	0.10	45	[a] 0.001	0.077	Gibbsite.
2	.10	100	.002	.031	Do.
3	.10	220	.001	.053	Do.
4	.20	30	.006	.197	Do.
5	.20	48	[a] .002	.171	Do.
6	.20	220	.003	.088	Do.
7	.30	45	.014	.276	Do.
8	.30	100	.035	.250	Do.
9	.30	200	.039	.106	Do.
10	.40	48	.029	.379	Do.
11	.40	100	.059	.368	Do.
12	.40	200	.067	.286	Do.
13	.50	30	.030	.447	Do.
14	.50	50	.027	.467	Do.
15	.50	100	.069	.385	Do.
16	.60	14	.007	.587	Do.
17	.60	39	.034	.580	Do.
18	.60	56	.043	.584	Do.
19	.60	110	.040	.460	Do.
20	.60	210	.047	.197	Do.
21	.70	50	[a] .004	.641	Gibbsite+C_2Aaq.
22	.70	100	.050	.609	Do.
23	.70	200	.077	.436	Do.
24	.80	20	.032	.761	Gibbsite.
25	.80	39	.040	.712	Do.
26	.80	56	.036	.660	Do.
27	.80	110	[a] .02	.60	Do.
28	.80	210	.077	.352	Do.
29	.90	20	.109	.678	Do.
30	.90	39	.124	.642	Do.
31	.90	55	.133	.606	Do.
32	.90	110	.080	.500	Do.
33	1.00	20	.082	.675	Do.
34	1.00	39	.113	.641	Do.
35	1.00	55	.118	.590	Do.
36	1.00	110	.088	.48	Do.
37	1.10	45	.083	.820	Do.
38	1.10	55	.100	.787	Do.
39	1.10	110	[a] .08	.70	Do.
40	1.10	213	.105	.520	Do.
41	[b]	48	.094	.846	Do.
42	[b]	100	.134	.696	Do.
43	[b]	220	.100	.507	Do.

[a] The value of the Al_2O_3 is uncertain because a very small sample was taken for analysis.
[b] Saturation.

equilibrium curve could best be represented by a straight line. Accordingly, a straight line was fitted to these data by the method of least squares.

The invariant point of gibbsite-isometric hydrate was taken as the intersection of the stable gibbsite and stable isometric hydrate equilibria curves.

An attempt was made to find this invariant point directly by adding gibbsite and isometric $3CaO\cdot Al_2O_3\cdot 6H_2O$ to water and analyzing the resulting solutions from time to time. However, the stable invariant point was not approached closely even after 220 days, and attempts to define it in this fashion were abandoned.

The over-all diagram of the system at 50° C is presented in figure 7. It is analogous to the corresponding diagram of the system at 21° C (fig. 1).

The metastable invariant point between the metastable hexagonal phases and the metastable prolongation of the stable gibbsite solubility curve was found to be at 0.13 g/liter of Al_2O3 and 0.63 g/liter of CaO. Referring to figure 7, one sees that

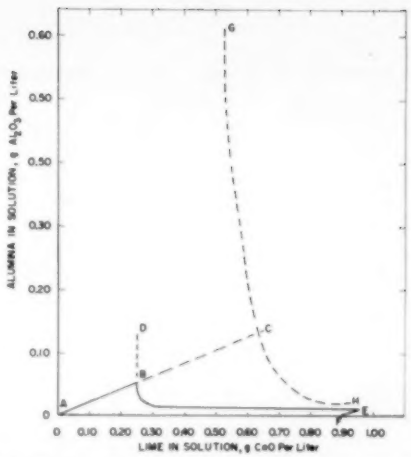

FIGURE 7. *The system* $CaO\text{-}Al_2O_3\text{-}H_2O$ *at 50° C.*

The solid line AB indicates the stable gibbsite equilibrium curve; BE, the stable isometric $3CaO\text{-}Al_2O_3\text{-}6H_2O$ curve; EF, stable $Ca(OH)_2$; the dashed line BC, metastable gibbsite; DB, metastable isometric $3CaO\text{-}Al_2O_3\text{-}6H_2O$; GCH, metastable hexagonal calcium aluminate hydrates.

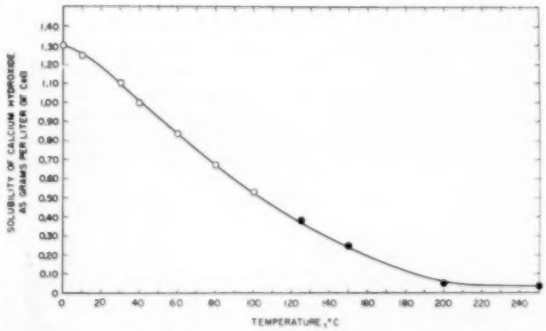

FIGURE 8. *The solubility of* $Ca(OH)_2$ *at various temperatures.*

The data of Bassett [13] is indicated by open circles; that of this investigation by closed circles.

this metastable invariant has the relationship to the corresponding invariant at 21° C that might be expected.

The solubility of $Ca(OH)_2$ in this system at 50° C was taken from a graph of Basset's data [13], reproduced here in figure 8. It is seen, as was predicted, that the solubility curve of $Ca(OH)_2$ has lengthened and moved toward the origin, and is intermediate between that at 21° and that at 90° C.

4.2. The System $CaO\text{-}Al_2O_3\text{-}H_2O$ at 120° C

In investigating the solubility of alumina hydrate in this system at 120° C, it was found that gibbsite again was the stable phase, that its solubility curve was again a straight line, and that it dissolved congruently in all concentrations of lime water up to the invariant point with isometric $3CaO\cdot Al_2O_3\cdot 6H_2O$.

TABLE 7. *Solubility of gibbsite in the system* $CaO-Al_2O_3-H_2O$ *at 120° C*

Experiment	Concentration of lime solution	Time	Final CaO	Final Al_2O_3	Final solid phases	Remarks
	g/liter	*Days*	*g/liter*	*g/liter*		
1	0.10	5	0.085	0.070	Gibbsite	
2	.20	5	.195	.176	do	
3	.30	13	.337	.323	do	
4	.40	5	.320	.294	do	Index raised.
5	.50	5	.336	.293	do	Do.
6	.60	5	.315	.308	Gibbsite, isometric $3CaO \cdot Al_2O_3 \cdot 6H_2O$	Index of gibbsite raised.
7	.70	5	.323	.316	Gibbsite	Do.
8	.80	5	.320	.320	do	Do.
9	.90	5	.347	.266	do	Do.
10	1.00	5	.296	.293	do	Index raised.
11	1.10	5	.332	.338	Gibbsite, isometric $3CaO \cdot Al_2O_3 \cdot 6H_2O$.	
12	[a] 1.17	5	.330	.300	do	

[a] Saturation.

Thereafter it lowered the concentrations of the lime of the initial solutions by reacting chemically to form isometric $3CaO \cdot Al_2O_3 \cdot 6H_2O$. The final compositions of the solutions were those of the stable isometric $3CaO \cdot Al_2O_3 \cdot 6H_2O$-gibbsite invariant, which was found to lie directly above this invariant at lower temperatures. In the system at 120°, however, there was virtually no metastable prolongation of the gibbsite equilibrium curve, and, of course, no invariant between this metastable curve and that of the hexagonal phases (see table 7 and fig. 9).

The pressure at 120° C, the equilibrium vapor pressure of water at this temperature, has approximately doubled, but the system, as discussed earlier, is still to be considered as a condensed system. The equilibrium curve of gibbsite at 120° C is then comparable to those at lower temperatures. It is a member of the same family of curves starting near the origin and having increasing slope with increasing temperature. The sudden pressure change, however, is accompanied by a change in the rate at which the slope of these curves have been increasing with temperature (see fig. 10 and table 8).

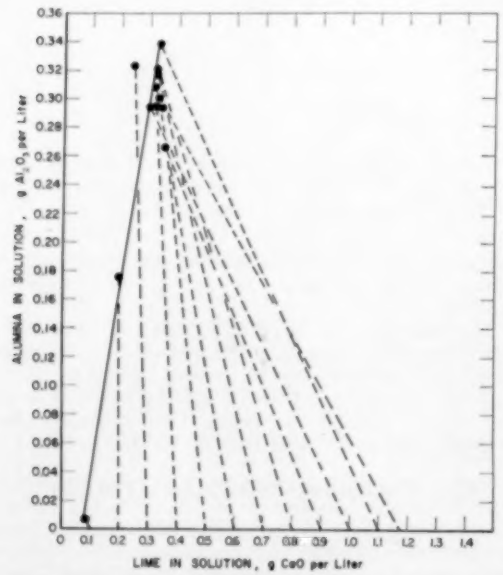

FIGURE 9. *Solubility of gibbsite in the system* $CaO-Al_2O_3-H_2O$ *at 120° C.*

Equilibrium approached from under-saturation. Dotted lines indicate change in composition of the liquids in contact with solid gibbsite.

TABLE 8. *Slope of the gibbsite equilibria curves as a function of temperature*

Temperature	Average slope [1]
°C	
21	0.054
50	.184
90	.336
120	.909

[1] Average slope is the average ratio of Al_2O_3 to CaO for all experimental points at lesser lime concentrations than that corresponding to the gibbsite-isometric $3CaO \cdot Al_2O_3 \cdot 6H_2O$ invariant point.

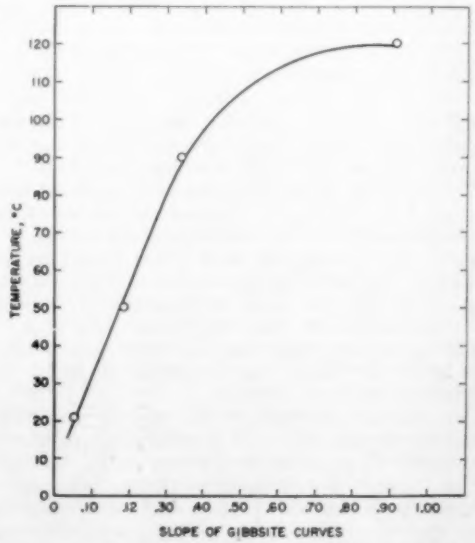

FIGURE 10. *Slope of the gibbsite equilibria curves in the system* $CaO-Al_2O_3-H_2O$ *as a function of temperature.*

Values for the solubility of $Ca(OH)_2$ in water at 125°, 150°, 200°, and 250° C (see table 9) were determined with the apparatus and technique used in the phase equilibria investigations. A solution of $Ca(OH)_2$ saturated at room temperature was placed in one vessel of the pressure bomb, which was heated to the desired temperature for 5 days. It was then removed from the oven and filtration accomplished as described earlier. The liquid in each case was in equilibrium with large, well-developed crystals of $Ca(OH)_2$. It was analyzed for CaO by the usual gravimetric determination of oxalate and ignition to the oxide. These values of the solubility of $Ca(OH)_2$ in water were added to those obtained by Bassett [13], and a composite graph was constructed (fig. 8). The solubility of $Ca(OH)_2$ in water at 120° C was taken from this graph.

TABLE 9. *Solubility of calcium hydroxide in water at various temperatures*

Experiment	Temperature	Time	Solubility	Remarks
	°C	Days	g/liter as CaO	
1	30	9	0.87	
2	30	10	.90	
3	30	11	.91	
4	30	14	.93	
5	30	16	.96	
6	30	18	.97	
7	30	21	.99	
8	30	23	1.00	
9	30	25	1.03	Constant thereafter.
10	125	5	0.380	
11	150	2	.266	Equilibrium with small crystals.
12	150	10	.270	Do.
13	150	2	.240	Equilibrium with large crystals.
14	150	5	.247	Do.
15	200	5	.047	
16	200	7	.05	
17	200	5	.05	
18	250	7	.037	

The invariant point of calcium hydroxide and isometric $3CaO \cdot Al_2O_3 \cdot 6H_2O$ was determined in the course of an investigation of the solubility of $3CaO \cdot Al_2O_3 \cdot 6H_2O$ in this system at 120° C. It was found to lie at 0.42 g/liter of CaO and 0.042 g/liter of Al_2O_3. Accordingly, a straight line between this invariant point and the point on the CaO concentration axis representing the solubility of CaO in water alone is taken to represent the stable equilibrium curve of $Ca(OH)_2$ in the ternary system at 120°. It is evident that this line is also a member of the family o. $Ca(OH)_2$ equilibria lines that lengthen and approach the origin as the temperature increases.

Possible metastable existence of the hexagonal calcium aluminate hydrates phases was not investigated, but none was found in any of the experiments made. The equilibrium curve of isometric $3CaO \cdot Al_2O_3 \cdot 6H_2O$ was established by an approach from undersaturation, by heating isometric $3CaO \cdot Al_2O_3 \cdot 6H_2O$ with lime water of varying strengths for 5 to 7 days.

The equilibrium curve of $3CaO \cdot Al_2O_3 \cdot 6H_2O$ in the system at 120° C is shown in figure 11 and the corresponding data in table 10. It may be seen that the equilibrium line is a nearly vertical straight line, having no horizontal section as had the corresponding equilibria curves at lower temperatures. The isometric $3CaO \cdot Al_2O_3 \cdot 6H_2O$ still dissolves congruently, however, at all lime concentrations under that of the invariant with $Ca(OH)_2$.

TABLE 10. *Solubility of isometric* $3CaO \cdot Al_2O_3 \cdot 6H_2O$ *in the system* $CaO \cdot Al_2O_3 \cdot H_2O$ *at 120° C*

Experiment	Time	Concentration of lime solution	Final CaO	Final Al_2O_3	Final solid phases
	Days	g/liter	g/liter	g/liter	
1	5	0.00	0.300	0.170	Isometric $3CaO \cdot Al_2O_3 \cdot 6H_2O$
2	5	.10	.327	.132	Do.
3	5	.10	.335	.132	Do.
4	5	.20	.359	.115	Do.
5	5	.30	.432	.070	Isometric + $Ca(OH)_2$.
6	5	.40	.408	.050	Do.
7	5	.60	.428	.054	Do.
8	5	.70	.450	.040	Do.
9	5	.80	.415	.052	Do.
10	5	.90	.408	.038	Do.
11	5	1.10	.433	.038	Do.
12	5	[1] 1.204	.402	.043	Do.
Invariant, initial phases being gibbsite and isometric.					
13	6	0.00	0.273	0.252	Gibbsite + isometric $3CaO \cdot Al_2O_3 \cdot 6H_2O$. Gibbsite, with index raised.

[1] Saturated.

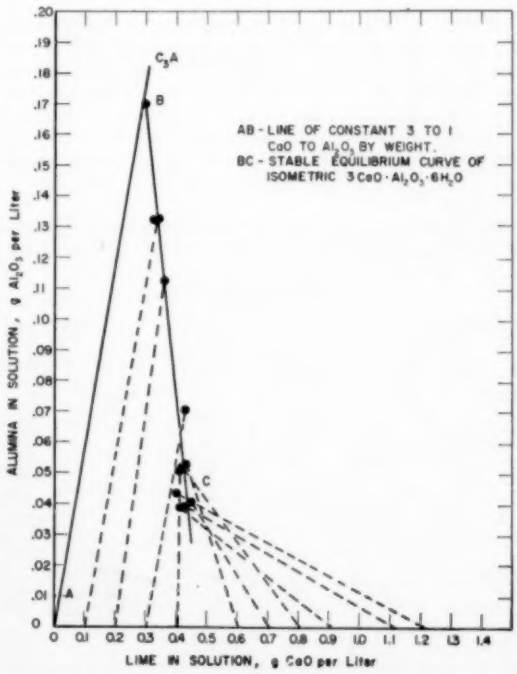

FIGURE 11. *Solubility of isometric* $3CaO \cdot Al_2O_3 \cdot 6H_2O$ *in the system* $CaO \cdot Al_2O_3 \cdot H_2O$ *at 120° C.*

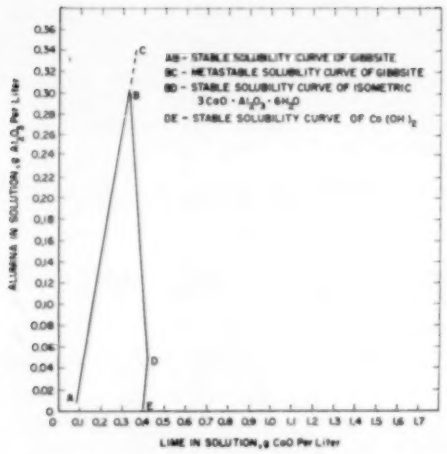
AB – STABLE SOLUBILITY CURVE OF GIBBSITE
BC – METASTABLE SOLUBILITY CURVE OF GIBBSITE
BD – STABLE SOLUBILITY CURVE OF ISOMETRIC 3CaO · Al2O3 · 6H2O
DE – STABLE SOLUBILITY CURVE OF Ca(OH)2
ALUMINA IN SOLUTION, g Al2O3 Per Liter
LIME IN SOLUTION, g CaO Per Liter

FIGURE 12. *The system* $CaO\text{-}Al_2O_3\text{-}H_2O$ *at 120° C.*

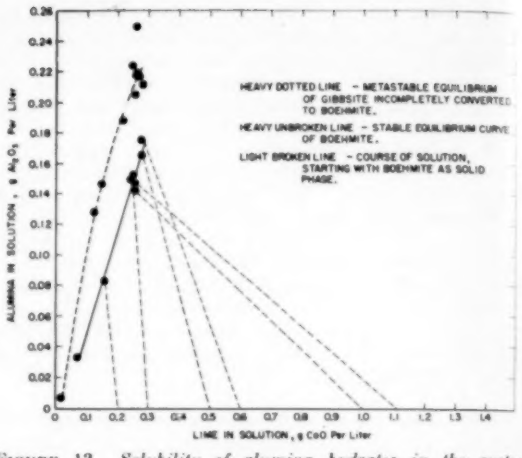
HEAVY DOTTED LINE – METASTABLE EQUILIBRIUM OF GIBBSITE INCOMPLETELY CONVERTED TO BOEHMITE.
HEAVY UNBROKEN LINE – STABLE EQUILIBRIUM CURVE OF BOEHMITE.
LIGHT BROKEN LINE – COURSE OF SOLUTION, STARTING WITH BOEHMITE AS SOLID PHASE.
ALUMINA IN SOLUTION, g Al2O3 Per Liter
LIME IN SOLUTION, g CaO Per Liter

FIGURE 13. *Solubility of alumina hydrates in the system* $CaO\text{-}Al_2O_3\text{-}H_2O$ *at 150° C.*

The over-all system at 120° C is presented in figure 12. The solubility of alumina has reached a maximum, and the solubility fields are compressed toward the alumina-concentration axis. It may be observed that the metastable prolongation of the alumina hydrate curve still persists at this temperature, to a maximum of 0.34 g/liter of Al_2O_3.

4.3. The System $CaO\text{-}Al_2O_3\text{-}H_2O$ at 150° C

At 150° C it was found that gibbsite ($Al_2O_3 \cdot 3H_2O$) was no longer the stable alumina hydrate, but converted to boehmite ($Al_2O_3 \cdot H_2O$). The transformation was sufficiently slow at this temperature, because it is very close to the gibbsite-boehmite transition temperature in water alone as reported in the literature [14], that it was possible to work out a metastable solubility curve for gibbsite at 150° C (see fig. 13 and table 11).

When gibbsite was the initial solid phase, the final solid phase at the end of 5 days was not gibbsite, but a mixture of gibbsite and boehmite. The "metastable equilibrium curve" of gibbsite in figure 13 is then an arbitrarily chosen one, the one which represents the particular degree of conversion to boehmite that obtains at the end of 5 days. It is intended that this curve represents only a region of metastability.

The stable boehmite curve was established in the same manner as before, using boehmite as the initial solid phase and placing it in varying concentrations of lime water (see fig. 13 and table 12).

Again the points representing the composition of the liquids in equilibrium with boehmite define a straight line starting near the origin. It may be noted that the slope of this line is less than that of the gibbsite at 120° C.

The positions, lengths, and slopes of the various equilibria curves at 150° C no longer show a direct proportionality to the temperature. The pressures are increasing, and the solubilities are decreasing at an accelerated rate. It was found that the departure

TABLE 11. *Solubility of gibbsite in the system* $CaO\text{-}Al_2O_3\text{-}H_2O$ *at 150° C*

Experiment	Concentration of lime solution	Time	Final CaO	Final Al_2O_3	Final solid phases	Remarks
	g/liter	*Days*	*g/liter*	*g/liter*		
1	0.05	7	0.020	0.008	Boehmite [1]	Some gibbsite, index of boehmite is lowered.
2	.10	5	.127	.128	do	Do.
3	.20	5	.248	.200	do [2]	Do.
4	.20	5	.276	.212	do	Do.
5	.30	5	.153	.147	do	Do.
6	.40	5	.217	.189	do	Index varies between boehmite and gibbsite.
7	.50	5	.247	.224	Boehmite+isometric $3CaO\text{-}Al_2O_3\text{-}6H_2O$.	Some gibbsite.
8	.60	5	.259	.219	do	Do.
9	.70	5	.255	.250	do	Do.
10	.80	5	.258	.218	do	Do.
11	.90	5	.262	.205	do	Do.
12	[3] 1.11	5	.273	.217	do	Do.

[1] Boehmite predominated in all cases, but gibbsite was incompletely converted.
[2] Filtration imperfect.
[3] Saturation.

from the behavior below 120° C could be correlated with pressure, but as pressure is not an independent variable here but a function of temperature, only the effect of temperature on solubility will be discussed.

It may be observed from figure 13 that the boehmite-isometric $3CaO \cdot Al_2O_3 \cdot 6H_2O$ invariant point has shifted from 0.33 g/liter of CaO to 0.25 g/liter in going from 120° to 150° C. No metastable prolongation of the boehmite equilibrium curve was found beyond this invariant point. When mixes of boehmite with lime water of concentrations greater than 0.25 g/liter were held at 150° C for 5 days, the final compositions of the liquids fell in a small area, the average of which was taken as the invariant point. This indicated that the boehmite behaved in the same manner as the gibbsite, combining with CaO of the solution to form the isometric $3CaO \cdot Al_2O_3 \cdot 6H_2O$. The solid phases in equilibrium at this invariant point were again identified both petrographically and by X-ray diffraction patterns.

The solubility of CaO in water at 150° C was taken from the graph mentioned earlier. The $Ca(OH)_2$ equilibrium curve in this system at 150° C has again lengthened and moved to the left, continuing the trend previously established.

The equilibrium curve of the isometric $3CaO \cdot Al_2O_3 \cdot 6H_2O$ in the system at 150° C is shown in figure 14, and the corresponding data are presented in table 13. It is analogous in all respects to the corresponding curve at 120° C, but it is shorter and closer to the alumina concentration axis.

The over-all system at 150° C is shown in figure 15. The solubility fields have been compressed

TABLE 12. *Solubility of boehmite in the system* $CaO\text{-}Al_2O_3\text{-}H_2O$ *at 150° C*

Experiment	Concentration of lime solution	Time	Final CaO	Final Al_2O_3	Final solid phases
	g/liter	*Days*	*g/liter*	*g/liter*	
1	0.10	7	0.072	0.034	Boehmite.
2	.20	7	.160	.084	Do.
3	.30	7	.240	.150	Do.
4	.40	7	.250	.153	Boehmite+isometric $3CaO \cdot Al_2O_3 \cdot 6H_2O$.
5	.50	7	.277	.166	Do.
6	.60	7	.281	.176	Do.
7	.70	7	[1].210	.116	Do.
8	1.00	5	.259	.142	Do.
9	[2] 1.112	5	.261	.147	Do.

[1] Filtration imperfect.
[2] Saturation.

TABLE 13. *Solubility of isometric* $3CaO \cdot Al_2O_3 \cdot 6H_2O$ *in the system* $CaO\text{-}Al_2O_3\text{-}H_2O$ *at 150° C*

Experiment	Concentration of lime solution	Time	Final CaO	Final Al_2O_3	Final solid phases
	g/liter	*Days*	*g/liter*	*g/liter*	
1	0.00	7	0.256	0.208	Isometric $3CaO \cdot Al_2O_3 \cdot 6H_2O$.
2	.00	6	.235	.204	Do.
3	.10	7	.270	.130	Do.
4	.20	7	.300	.090	Do.
5	.30	7	.290	.070	Do.
6	.60	7	.340	.046	Isometric $3CaO \cdot Al_2O_3 \cdot 6H_2O + Ca(OH)_2$.
7	.70	7	.342	.050	Do.
8	.80	7	.345	.054	Do.
9	.90	7	.324	.060	Do.
10	1.00	7	.342	.061	Isometric $3CaA \cdot Al_2O_3 \cdot 6H_2O + Ca(OH)_2$.
11	Satin	7	.331	.042	Do.
12 [1]	0.00	5	.267	.154	
13 [2]	.00	5	.256	.194	
14 [1]	.00	5	.226	.200	

[1] Isometric $3CaO \cdot Al_2O_3 \cdot 6H_2O$ and gibbsite initially.
[2] Isometric $3CaO \cdot Al_2O_3 \cdot 6H_2O$ and boehmite initially.

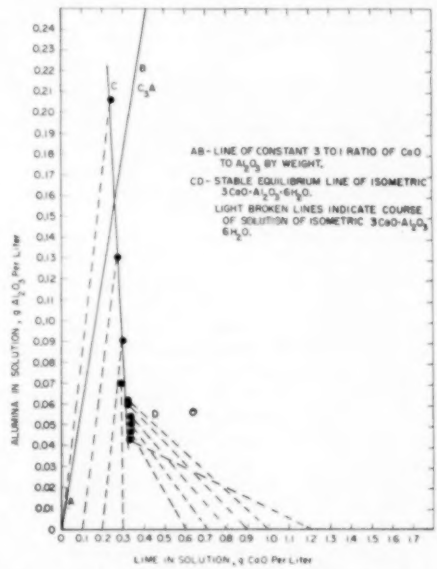
AB - LINE OF CONSTANT 3 TO 1 RATIO OF CaO TO Al_2O_3 BY WEIGHT.
CD - STABLE EQUILIBRIUM LINE OF ISOMETRIC $3CaO \cdot Al_2O_3 \cdot 6H_2O$.
LIGHT BROKEN LINES INDICATE COURSE OF SOLUTION OF ISOMETRIC $3CaO \cdot Al_2O_3 \cdot 6H_2O$.
B
C_3A
C
D
A
ALUMINA IN SOLUTION, g Al_2O_3 Per Liter
LIME IN SOLUTION, g CaO Per Liter

FIGURE 14. *Solubility of isometric* $3CaO \cdot Al_2O_3 \cdot 6H_2O$ *in the system* $CaO\text{-}Al_2O_3\text{-}H_2O$ *at 150° C.*

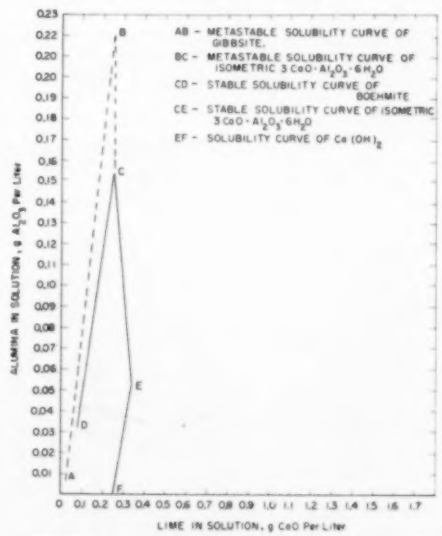
AB - METASTABLE SOLUBILITY CURVE OF GIBBSITE.
BC - METASTABLE SOLUBILITY CURVE OF ISOMETRIC $3CaO \cdot Al_2O_3 \cdot 6H_2O$
CD - STABLE SOLUBILITY CURVE OF BOEHMITE
CE - STABLE SOLUBILITY CURVE OF ISOMETRIC $3CaO \cdot Al_2O_3 \cdot 6H_2O$
EF - SOLUBILITY CURVE OF $Ca(OH)_2$
B
C
D
E
A
F
ALUMINA IN SOLUTION, g Al_2O_3 Per Liter
LIME IN SOLUTION, g CaO Per Liter

FIGURE 15. *The system* $CaO\text{-}Al_2O_3\text{-}H_2O$ *at 150° C.*

toward the water apex. The maximum stable solubility of alumina has become 0.15 g/liter, and nowhere does the solubility of $Ca(OH)_2$ exceed 0.33 g/liter. The metastable prolongation of the isometric $3CaO \cdot Al_2O_3 \cdot 6H_2O$ equilibrium curve, which meets the metastable gibbsite curve, was not determined experimentally. Indeed, as this portion of the isometric $3CaO \cdot Al_2O_3 \cdot 6H_2O$ curve lies above the $3CaO:Al_2O_3$ composition line, and the $3CaO \cdot Al_2O_3 \cdot 6H_2O$ dissolves congruently, it could not be directly determined. Although it might be established indirectly, its length is too short to justify the work involved.

4.4. The System CaO-Al_2O_3-H_2O at 200° C

At 200° C, when gibbsite is the initial phase and is placed in varying concentrations of lime water, it converts completely to boehmite. After 5 days, and perhaps much earlier, gibbsite does not exist even metastably in the system at 200° C.

At this temperature, attack on the bomb is very severe, and boehmite absorbs CaO from the lime solutions. When boehmite was placed in contact with lime solutions up to 0.10 g/liter, it absorbed as much as 5 percent by weight of CaO from the solution, causing marked reduction in lime concentrations and making it impossible to work out the boehmite equilibrium curve in the same fashion as before. What was actually obtained was a small cluster of points in the area between 0 and 0.03 g/liter of CaO and 0 and 0.007 g/liter of Al_2O_3.

When gibbsite or boehmite were held in contact with saturated lime water for 5 days, however, the composition of the final solutions was the isometric $3CaO \cdot Al_2O_3 \cdot 6H_2O$-boehmite invariant at 0.085 g/liter of Al_2O_3 and 0.11 g/liter of CaO. Accordingly, a straight line from the average value of the cluster of points near the origin to this invariant was taken to represent the stable equilibrium curve of boehmite, even though, because of experimental difficulties, intermediate points could not be obtained (see table 14 and fig. 16). This line is shorter than the corresponding one at 150° C, and its maximum is somewhat lower, but the alope has again increased.

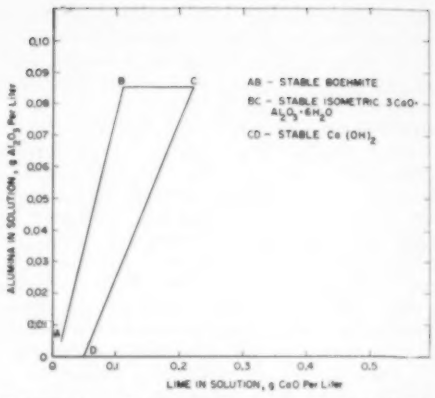

FIGURE 16. *The system* CaO-Al_2O_3-H_2O *at 200° C.*

The solubility of $Ca(OH)_2$ in the system at 200° C was found to be of the order of 0.05 g/liter as CaO, and mixtures of isometric $3CaO \cdot Al_2O_3 \cdot 6H_2O$ and saturated lime water gave equilibrium mixtures of the two solid phases in contact with a solution whose composition was 0.085 g/liter of Al_2O_3 0.22 g/liter of CaO. The point thus defined is the $Ca(OH)_2$- isometric $3CaO \cdot Al_2O_3 \cdot 6H_2O$ invariant point. A straight line joining this point with the point representing the solubility of $Ca(OH)_2$ in water alone is, as before, taken to be the stable equilibrium curve of $Ca(OH)_2$ in the system at 200° C. It follows the trend of and belongs to the family of curves for $Ca(OH)_2$ at lower temperatures.

The phase diagram for the system CaO-Al_2O_3-H_2O at 200° C is presented in figure 16 and the corresponding data in table 14. The equilibrium curve of the isometric $3CaO \cdot Al_2O_3 \cdot 6H_2O$ is analogous to that at 150° C, but again has shortened and moved toward the alumina concentration axis.

TABLE 14. *Equilibrium compositions in the system* CaO-Al_2O_3-H_2O *at 200° C*

Experiment	Initial solid phase	Initial CaO	Time	Final Al_2O_3	Final CaO	Final solid phases
		g/liter	*Days*	*g/liter*	*g/liter*	
1	Boehmite	0.025	7	0.001	0.022	Boehmite
2	Gibbsite	.025	7	.001	.003	Do.
3	Boehmite	.050	7	.004	.023	Do.
4	do	.200	7	.002	.018	Do.
5	Gibbsite	.200	7	.002	.020	Do.
6	Gibbsite+isometric $3CaO \cdot Al_2O_3 \cdot 6H_2O$	0.00	7	.064	.093	Boehmite+isometric $3CaO \cdot Al_2O_3 \cdot 6H_2O$.
7	Boehmite	1.20	5	.051	.100	Do.
8	do	1.20	5	.080	.112	Do.
9	do	1.20	5			
10	Isometric $3CaO \cdot Al_2O_3 \cdot 6H_2O$	1.20	7	.091	.200	Isometric $3CaO \cdot Al_2O_3 \cdot 6H_2O$+$Ca(OH)_2$.
11	do	1.20	7	.080	.225	Do.
12	do	1.20	7	.080	.258	Do.
13	do	1.20	7	.091	.200	Do.
14	Isometric $3CaO \cdot Al_2O_3 \cdot 6H_2O$	0.00	7	.148	.175	Isometric $3CaO \cdot Al_2O_3 \cdot 6H_2O$.
15		1.20	5		.047	$Ca(OH)_2$
16		1.20	7		.050	Do.
17		1.20	5		.050	Do.

When the compound $4CaO{\cdot}3Al_2O_3{\cdot}3H_2O$ is added to saturated lime water at 200° C, the isometric hydrate and boehmite are found to be the final phases, and when the isometric hydrate is the initial phase it is also the final solid phase. There is some difficulty, however, in that the proportion of birefringent inclusions of the isometric hydrate, never absent, increases with temperature, until at 200° C, the occlusions are definitely prominent. A series of determinations was made between 200° C and 250° C, at 10-deg intervals to locate more accurately the isometric $3CaO{\cdot}Al_2O_3{\cdot}6H_2O$-$4CaO{\cdot}3Al_2O_3{\cdot}3H_2O$ transition temperature. The temperature at which microscopically detectable amounts of the 4:3:3 hydroaluminate were first evident was found to be between 210° and 220° C. At times under 4 days, however, the isometric $3CaO{\cdot}Al_2O_3{\cdot}6H_2O$ persisted metastably up to 250° C.

Above 120° C, a maximum solubility of the alumina hydrate has been reached, and the invariants between the alumina hydrate and the stable ternary compound descend with temperature after 120° C. The lengths of the isometric hydrate equilibria curves continue to decrease and are defined by straight lines as the solubility fields compress with increasing temperature to the H_2O apex.

4.5. The System $CaO{\cdot}Al_2O_3{\cdot}H_2O$ at 250° C

When the isometric $3CaO{\cdot}Al_2O_3{\cdot}6H_2O$ is used as the initial solid phase at 250° C, it is quantitatively converted to the 4:3:3 hydroaluminate at initial concentrations of lime water from 0.1 g/liter to saturation. A photomicrograph of this compound is shown in figure 17. The $Ca(OH)_2$–$4CaO{\cdot}3Al_2O_3{\cdot}3H_2O$ invariant at this temperature was determined by heating $4CaO{\cdot}3Al_2O_3{\cdot}3H_2O$ with saturated lime water. Similar experiments, starting with boehmite as the initial solid phase, established the $4CaO{\cdot}3Al_2O_3{\cdot}3H_2O$-boehmite invariant. The $4CaO{\cdot}3Al_2O_3{\cdot}3H_2O$-$Ca(OH)_2$ invariant is at 0.02 g/liter of Al_2O_3 and 0.065 g/liter of CaO; that of $4CaO{\cdot}3Al_2O_3 3H_2O$-boehmite, at 0.034 g/liter of Al_2O_3 and 0.063 g/liter of CaO (see table 15). These two invariants are so close together and so close to a point representing the solubility of $Ca(OH)_2$ in water alone that the phase diagram at 250° C was constructed simply by connecting these points by straight lines (see fig. 18).

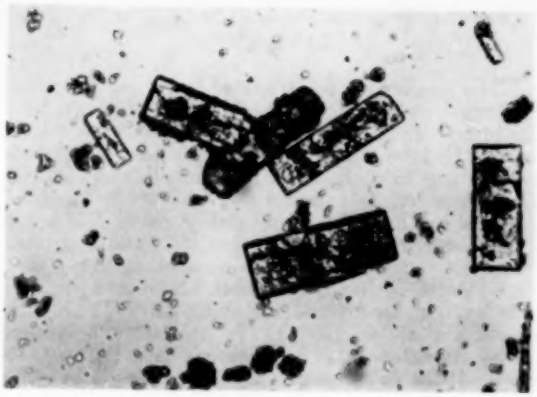

FIGURE 17. *Synthetic* $4CaO{\cdot}3Al_2O_3{\cdot}3H_2O$.
Magnification, X 180.

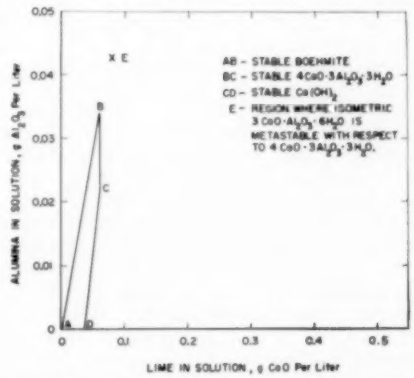

FIGURE 18. *The system* $CaO{\cdot}Al_2O_3{\cdot}H_2O$ *at 250° C.*

The region where the isometric $3CaO{\cdot}Al_2O_3{\cdot}6H_2O$ exists metastably with respect to $4CaO{\cdot}3Al_2O_3{\cdot}3H_2O$ is indicated in this figure by a cross, E.

The entire solubility fields have been compressed severely into the water apex. It may be seen that the diagram at 250° C is similar to that at 200° C, differing mainly in that the solubility of the alumina hydrate at 250° C is much smaller.

TABLE 15. *Equilibrium compositions in the system* $CaO{\cdot}Al_2O_3{\cdot}H_2O$ *at 250° C*

Experiment	Initial solid phase	Initial CaO	Time	Final CaO	Final Al_2O_3	Final solid phase
		g/liter	*Days*	*g/liter*	*g/liter*	
1		1.20	5	0.037		$Ca(OH)_2$.
2	Boehmite	1.20	4	.078	0.045	Boehmite+$4CaO{\cdot}3Al_2O_3{\cdot}3H_2O$.[1]
3	do	1.20	5	.039	.022	Do.
4	do	1.20	6	.072	.036	Do.
5	$4CaO{\cdot}3Al_2O_3{\cdot}3H_2O$	1.20	5	.065	.018	$Ca(OH)_2$+$CaO{\cdot}3Al_2O_3{\cdot}3H_2O$.
6	do	0.10	5	.057	.025	Do.

[1] Contains trace of isometric $3CaO{\cdot}Al_2O_3{\cdot}6H_2O$.

4.6. The System CaO-Al_2O_3-H_2O Over the Range 21° to 250° C

The metastable equilibria of hydrated amorphous alumina, which presumably exist only at lower temperature in the system, have not been worked out. Its invariant with metastable hexagonal phases at 21° and 50° C has been determined, and a straight line between this point and the origin probably represents the Al_2O_3Aq solubility curve fairly well. The experimental difficulties in obtaining these solubility curves have been discussed earlier.

Gibbsite is the only stable alumina hydrate in the system, up to and including 150° C. At temperatures up to 100° C, its solubility is directly proportional to the temperature (see fig. 10), the slope of the equilibrium curve increasing 0.04 g/liter of Al_2O_3 for every 10-deg C increase in the temperature.

Gibbsite persists in the system at 150° C, but it is metastable with respect to boehmite, and at 200° C, gibbsite does not exist in the system, and boehmite is the stable alumina phase.

It is seen from figure 20 that the equilibria curves for alumina are a family of straight lines from the vicinity of the origin. Above 120° C these curves shorten and have greater slopes. At some temperature above 250° C the solubility of Al_2O_3 would presumably become negligibly small.

The maximum Al_2O_3 concentration values, which are those of the alumina hydrate-isometric hydrate invariant point versus temperature, may be seen in figure 10. It may be observed that the corresponding concentration of CaO remains almost constant throughout. (0.30 $\pm$0.05 g/liter.) There is a sharp maximum at 120° C of 0.30 g/liter of Al_2O_3. This is presumably the maximum Al_2O_3 that can exist in stable solution in this system at any temperature.

The solubility of $Ca(OH)_2$ in water alone decreases rapidly as the temperature increases (see fig. 9). In the temperature range investigated in varies from 1.15 g/liter at 21° C to 0.037 g/liter as CaO at 250° C. At all temperarures, the $Ca(OH)_2$ equilibria curves slope slightly to the right (with the possible exception of that at 21° C, where the $Ca(OH)_2$ equilibrium curve is so short as to be very difficult to define). The slope of the $Ca(CH)_2$ equilibrium curve, like that of alumina hydrate, is directly proportional to the temperature up to 120°, where it goes through a sharp maximum. From figure 20 it can be seen that the $Ca(OH)_2$ equilibria curves are a family, lengthening and moving to the left as the temperature increases. A line through the extremities of these curves represents the maximum solubility of $Ca(OH)_2$ in the system as a function of temperature.

The equilibria curves of the isometric $3CaO{\cdot}Al_2O_3{\cdot}6H_2O$ in this system at various temperatures are of two types (fig. 20). Those at 120° C and below have sharp curves, from a nearby vertical to a nearly horizontal direction. Above 150° C the curves are straight lines, with negative slopes, moving to the left and becoming shorter as the temperature increases. The effect of the rapidly diminishing solubility of $Ca(OH)_2$ with increasing temperature on the slope and position of these curves has already been mentioned.

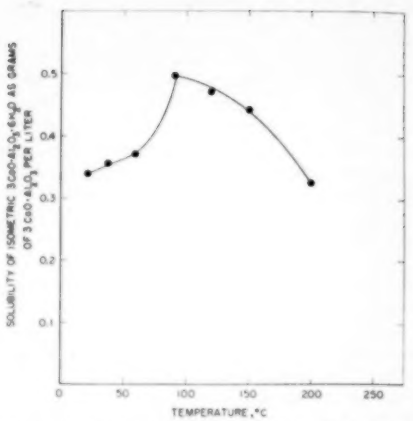

FIGURE 19. *Solubility of isometric* $3CaO{\cdot}Al_2O_3{\cdot}6H_2O$ *in water at various temperatures.*

TABLE 16. *Solubility of isometric* $3CaO{\cdot}Al_2O_3{\cdot}6H_2O$ *in water as a function of temperature*

Temperature	Final composition of solution		$CaO+Al_2O_3$	Weight ratio CaO/Al_2O_3
	CaO	Al_2O_3		
°C	*g/liter*	*g/liter*	*g/liter*	
21	0.208	0.131	0.339	1.59
50	.223	.133	.356	1.68
60[1]	.246	.123	.369	2.00
90	.306	.190	.496	1.61
120	.300	.170	.470	1.76
150	.235	.204	.439	1.51
200	.175	.148	.323	1.19

[1] For 17 days.

Table 16 gives values of the solubility of the isometric $3CaO{\cdot}Al_2O_3{\cdot}6H_2O$ in water at various temperatures, and these values are plotted in figure 19. One observes that the solubility increases rapidly with the temperature to the neighborhood of the boiling point of water and thereafter falls off rapidly. It follows that the maximum stable solubility of isometric $3CaO{\cdot}Al_2O_3{\cdot}6H_2O$ is 0.49 g/liter as $3CaO{\cdot}Al_2O_3$, corresponding to 0.685 g/liter as $3CaO{\cdot}Al_2O_3{\cdot}6H_2O$. There is a great deal of variation in the literature values of the solubility of isometric hydrate near room temperature. These are discussed in detail in the investigation of Wells, Clarke, and McMurdie, [5], whose value is plotted in figure 19.

An over-all picture of the system CaO-Al_2O_3-H_2O from 21° to 250° C is seen in figure 20. It is assumed that at temperatures above 250°C, the solubility fields will become immeasurably small and vanish into the water apex of the diagram.

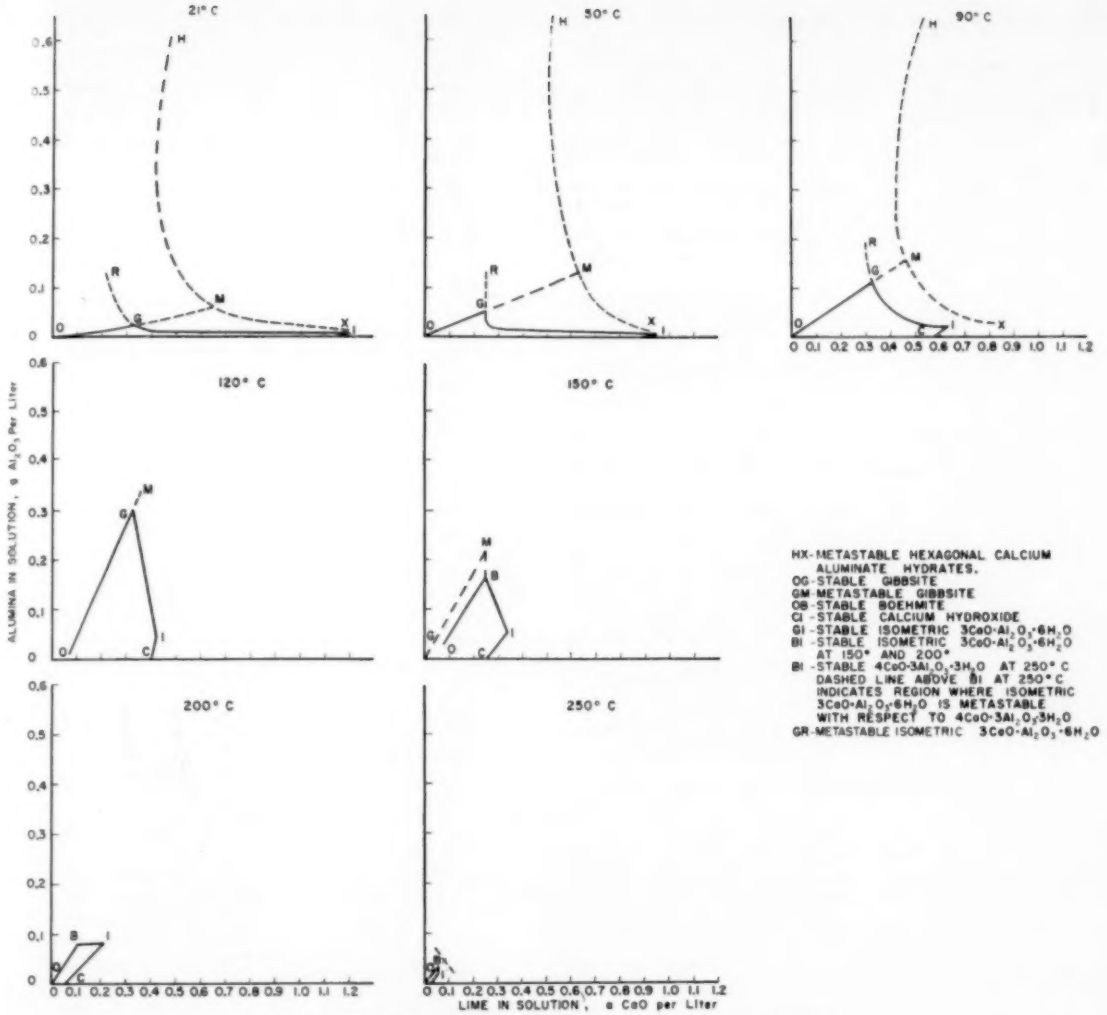
21° C
50° C
90° C
120° C
150° C
200° C
250° C
ALUMINA IN SOLUTION, g Al_2O_3 Per Liter
LIME IN SOLUTION, g CaO per Liter
HX-METASTABLE HEXAGONAL CALCIUM ALUMINATE HYDRATES.
OG-STABLE GIBBSITE
GM-METASTABLE GIBBSITE
OB-STABLE BOEHMITE
CI-STABLE CALCIUM HYDROXIDE
GI-STABLE ISOMETRIC $3CaO·Al_2O_3·6H_2O$
BI-STABLE ISOMETRIC $3CaO·Al_2O_3·6H_2O$ AT 150° AND 200°
BI-STABLE $4CaO·3Al_2O_3·3H_2O$ AT 250° C
DASHED LINE ABOVE BI AT 250° C INDICATES REGION WHERE ISOMETRIC $3CaO·Al_2O_3·6H_2O$ IS METASTABLE WITH RESPECT TO $4CaO·3Al_2O_3·3H_2O$
GR-METASTABLE ISOMETRIC $3CaO·Al_2O_3·6H_2O$

FIGURE 20. *The system* CaO-Al_2O_3-H_2O *at various temperatures.*

5. Summary

The system CaO-Al_2O_3-H_2O has been investigated over the range 50° to 250° C.

It was found that gibbsite was the stable alumina hydrate under 150° C, and that above this temperature boehmite was the stable alumina phase. Isometric $3CaO·Al_2O_3·6H_2O$ is the only stable ternary compound in the system up to and including approximately 215° C, and the metastable hexagonal calcium aluminate hydrates persist up to and including 90° C. At 250° C, the stable ternary compound is $4CaO·3Al_2O_3·3H_2O$.

With increasing temperature, the $Ca(OH)_2$ equilibria curves lengthen and move toward the origin in a rectangular plot, the isometric $3CaO·Al_2O_3·6H_2O$ curves become shorter and more vertical, and move toward the origin; the alumina curves rotate counterclockwise about the origin to a maximum at 120° C and thereafter shorten and rotate clockwise. The over-all effect is to compress all the equilibria curves against the Al_2O_3-concentration axis and into the water apex of the diagram.

283819—54——4

6. References

[1] Lansing S. Wells, Reaction of water on calcium aluminates, BS J. Research **1,** 951–1009 (1928) RP34.

[2] Sunnar Assarsson, The conditions of formation of the hydrated compounds in the system CaO-Al_2O_3-H_2O (solutions) and the hydration of the anhydrous calcium aluminates, Sveriges Geol. Undersökn, Arsbok (1936) **30,** C No. 399, 8–202.

[3] G. E. Bessey, The calcium aluminate and silicate hydrates, Proc. Symposium on Chem. of Cements, p. 178–230 (Stockholm, 1938).

[4] F. E. Jones, The quaternary system CaO-Al_2O_3-$CaSO_4$-H_2O at 25° C, Trans. Faraday Soc. **35,** 1484–1510 (1939).

[5] Lansing S. Wells, W. F. Clarke, and H. F. McMurdie, Study of the System CaO-Al_2O_3-H_2O at temperatures of 21° and 90° C, J. Research NBS **30,** 367–409 (1943) RP1539.

[6] Harold H. Steinour, Aqueous cementitious systems containing lime and alumina, Bul. 34, Research and Development Division, Portland Cement Association (February 1951).

[7] W. G. Schneider and T. Thorvaldson, The hydration of the aluminates of calcium, III. The hydration of the 5:3, 1:1, and 3:5 calcium aluminates, Can. J. Research [B] **21,** 34–42 (1943).

[8] G. M. Harris, W. S. Schneider, and T. Thorvaldson, The hydration of the aluminates of calcium IV. Hydrothermal reactions of tricalcium aluminate and its hydrates, Can. J. Research [B] **21,** 65–72 (1943).

[9] Herbert Johnson and Thorbergur Thorvaldson, The hydration of the aluminates of calcium V. The hydrothermal decomposition products of tricalcium aluminate at 350° C, Can. J. Research [B] **21,** 236–246 (1943).

[10] Friedel, Bul. soc. franç. minéral **26,** 121 (1903).

[11] W. Blum, Determination of aluminum as oxide, Bul. BS **13,** 515–34 (1916–17) S286.

[12] Elinar P. Flint, Howard F. McMurdie, and Lansing S. Wells, Formation of hydrated calcium silicates at elevated temperatures and pressures, J. Research NBS **21,** 617–638 (1938) RP1147.

[13] Henry Bassett, Notes on the system lime-water, and on the determination of calcium, J. Chem. Soc., part II, 1270–5 (1934).

[14] A. W. Laubengayer and R. S. Weiss, A hydrothermal study of equilibria in the system Al_2O_3-H_2O, J. Am. Chem. Soc. **65,** 247–250 (1943).

[15] H. Kuhl, F. Thilo, and A. Chi Yu, Zement **23,** 249–56 p. 13, 26, 30 (1934).

WASHINGTON, September 30, 1953.

Journal of Research of the National Bureau of Standards Vol. 52, No. 2, February 1954 Research Paper 2477

Absolute Calibration of the NBS Standard Thermal Neutron Density

James A. De Juren and Hyman Rosenwasser

A moderating geometry providing a constant thermal neutron flux from two radium-beryllium (α,n) sources has been constructed. The flux at the center of the geometry has been calibrated by absolute alpha counting from boron films exposed in pulse ionization chambers. The boron capture cross section has been obtained by comparison of the NBS boron with the Argonne "standard" boron, and a value of $n\hat{v}=3918$ (± 2 percent) n/cm^2 sec has been determined for the flux.

1. Introduction

The NBS standard thermal neutron flux was designed to provide a uniform flux in a region suitable for the absolute calibration of foils, small neutron detectors, and dosimeters. This flux is obtained by the moderation of neutrons in paraffin and carbon from two radium-beryllium (α,n) sources and does not have a precise Maxwellian velocity distribution. If a thin foil having a thermal neutron-capture cross section varying as $1/v$ is placed in the flux, the rate of neutron capture is $C=\Sigma_i n_i v_i \sigma_i N$, where n_i, is the neutron density, σ_i is the capture cross section at velocity v_i and N is the number of nuclei in the foil. As $v_i\sigma_i$ is a constant independent of velocity,

$$C=nNK=nN(\hat{\sigma}\hat{v}). \quad (1)$$

Thermal-capture cross sections, $\hat{\sigma}$, are usually listed [1][1] at the most probable Maxwellian velocity at room temperature, $\hat{v}=2.2\times10^5$ cm/sec.

Measurement of the absolute capture rate by a thin foil thus yields the thermal neutron density unambiguously. This density is usually multiplied by $\hat{v}$, and $n\hat{v}$ represents a flux density of monoergic neutrons that is equivalent to the original flux for foil activation of $1/v$ absorbers. For a flux with a Maxwellian-velocity distribution, $\Sigma_i n_i v_i = n\bar{v}=1.128\ n\hat{v}$. In this work $n\hat{v}$ has been used to represent the flux, which has been standardized by the absolute counting rates obtained from boron films exposed in pulse ionization chambers.

2. Description of Geometry

The geometry providing the NBS thermal neutron flux (fig. 1) consists of two 1-curie radium-beryllium (α,n) sources imbedded in lead cylinders 8½ inches in diameter. Two inches of paraffin and 4 inches of carbon are between the lead cylinders and the exposure slot. Carbon surrounds the exposure slot so that the depression in neutron density [2] caused by absorbing foils will be small. The effect would be much greater if paraffin alone were used for moderation. At the center of the slot the neutron flux should be nearly isotropic, and from symmetry considerations the gradient of the neutron density should be zero. Therefore, a pure scatterer placed at the center will not alter the flux.

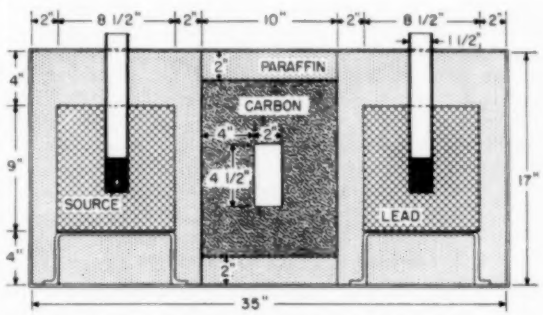

FIGURE 1. *Standard neutron flux geometry.*

3. Description of Pulse Ionization Chambers

An aluminum chamber of pillbox design, 2¾ in. in internal diameter and 1¼ in. deep, having a boron film clamped to the cover plate, was used for the measurements [3]. Either an aluminum parallel plate mounted on Teflon insulators 1.4 cm from the film or a 1.14-mm carbon-steel wire (1.7 cm distant) was used for electron collection. A mixture of 5 percent of carbon dioxide and 95 percent of argon was used as the filling gas.

Boron films were deposited by vacuum evaporation of natural boron from carbon crucibles over an area 2.0 by 3.4 cm^2 on Pt-coated 0.015-in. quartz wafers or on Pt foils.

[1] Figures in brackets indicate literature references at the end of this paper.

An aluminum holder that slides into the exposure slot contains the pulse chamber and cathode follower. The holder exterior has been milled for the snug fit of a 0.020-in. cadmium cover.

Pulses from the chamber were amplified by a Bell-Jordan preamplifier and amplifier system and fed into a three (integral) channel discriminator unit. Most of the measurements were made with a 2-μsec differentiating time constant; a few were repeated with a 20-μsec time constant.

4. Analysis of Data

Measurements were made with and without cadmium, and the cadmium-difference counting rate was determined as a function of discriminator setting for three different boron films. This procedure almost entirely eliminates spurious counts from the data and the cadmium-difference counting rate is confined to captures of neutrons of energy less than 0.3 ev. To avoid multiple- and back-scattering corrections the alpha-particle counting rate was determined at a discriminator level two-thirds or three-fourths that of the maximum pulse height of the 1.473-Mev alpha-particle ionization from the main branch of the reaction:

$$n+B^{10}\begin{cases}\rightarrow Li^{*7}+He^4 \text{ (93.5 percent)}\\ \rightarrow Li^7+He^4 \text{ (6.5 percent)}.\end{cases}$$

Li^{*7} refers to the 0.48-Mev excited state. The particles from the reaction proceeding directly to the ground state have 20.7 percent more kinetic energy than those from the main branch.

A correction must be made for the alpha particles that are degraded below the bias level by ionization losses in the film. For 1.5-Mev alphas it is safe to assume that the energy of a particle emerging from a plane film is given by $E=E_0(1-x/R\cos\theta)$ where x is the perpendicular distance from the origin of the particle to the surface of the film, θ is the angle of the particle direction with respect to the normal, and R is the particle range in the film material. If $2N_0$ alphas are produced per second in the film of thickness T, the energy distribution of the emerging particles becomes

$$\frac{dN}{dE}=\frac{N_0R}{2E_0T} \quad \text{for} \quad E_0>E>E_0\left(1-\frac{T}{R}\right) \tag{2}$$

$$=\left(\frac{dN}{dE}\right)_{max} \text{ a constant independent of } E, \text{ and}$$

$$\frac{dN}{dE}=\frac{N_0T}{2E_0R\left(1-\frac{E}{E_0}\right)^2} \quad \text{for} \quad E<E_0\left(1-\frac{T}{R}\right). \tag{3}$$

The number of particles with energy greater than E is given by

$$N_E=N_0\left[1-\frac{T}{2R\left(1-\frac{E}{E_0}\right)}\right] \quad \text{for} \quad E<E_0\left(1-\frac{T}{R}\right). \tag{4}$$

Combining (2) and (4)

$$\frac{T}{R}=\frac{N_E}{1-\frac{T}{2R\left(1-\frac{E}{E_0}\right)}}\frac{1}{2E_0\left(\frac{dN}{dE}\right)_{max}}.$$

At $E=\frac{3}{4}E_0$,

$$\frac{T}{R}\left(1-\frac{2T}{R}\right)=\frac{N_{3/4}E_0}{2E_0\left(\frac{dN}{dE}\right)_{max}}. \tag{5}$$

For thick films eq (5) was used to determine T/R, but for thin films eq (3) must be used because the amplifier noise causes a deviation in dN/dE near the maximum energy, E_0.

The path of the ionizing particle in the gas distorts the energy spectrum because the pulse height at the collecting electrode is proportional to the mean voltage of the ionization electrons divided by the total voltage drop between electrodes. With wire collection this effect is minimized, and T/R may be extracted without too much difficulty.

All three films were counted with parallel-plate collection in the aluminum chamber. Film 2 was counted with a collecting wire in the aluminum chamber, and T/R was determined for film 3 in a similar brass chamber (fig. 2). Another film, which had a smaller thickness correction than the others, was measured with wire collection in the aluminum chamber, but the film was unfortunately spoiled before analysis. All parallel-plate measurements were made with a filling of 95 percent of argon and 5 percent of carbon dioxide at 4 atmos-

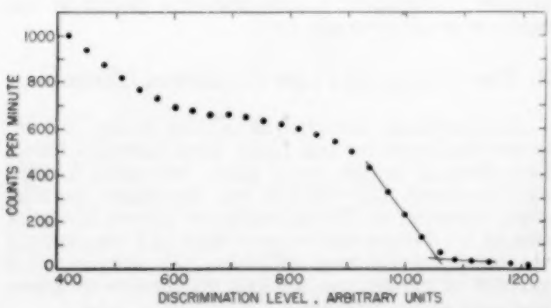

FIGURE 2. *Film 3 pulse-height distribution.*

Brass chamber; 1– atm A-CO_2; 1,500 volts; wire collection.

plates, and measurements of T/R with wire collection were made at a variety of pressures. As the alphas are counted with 2π geometry, the neutron capture rate is twice the corrected alpha counting rate.

Carbon was also deposited during the boron evaporation, obviating a boron mass determination by weighing. A technique for determination of the boron content of the films was developed by microchemical modification of the fixed pH titration method of Foote [4]. After analysis each film backing was replaced in the chamber, which was reinserted in the flux as a check of the efficiency of the boron removal. The counting rates at the alpha-plateau discrimination level were 2 to 3 counts per minute, the normal background for the boron-free chamber.

There is considerable evidence indicating a slight variation of the boron isotopic ratio with geographic origin [5] (or processing). The boron evaporated for use in the chambers was obtained by the thermal decomposition of diborane supplied by the Naval Research Laboratory. From the diborane a sample of boric-acid solution was prepared for comparison with a solution of the standard boric oxide of the Argonne National Laboratory by the danger-coefficient method in the Argonne low-energy pile. The boron cross section of this standard has been accurately measured as 755 ± 3 barns [6] and verified by the Brookhaven National Laboratory's result of 753 ± 3 [7]. The Argonne comparison gave a value of 746 ± 7 barns for the NBS boron. Dibeler and Mohler [8] have measured the B^{10}/B^{11} isotopic ratio for the NRL diborane and obtained a value of 0.251 as compared with 0.253 for a sample from the University of Southern California (both the USC and Argonne boron are presumably of California origin), which is in line with the Argonne comparison.

Table 1 summarizes the boron-film data. I_b has a weighted average of 1.761×10^6 disintegrations per mole of boron in the NBS flux.

TABLE 1. *Boron-film data*

Film	Boron content	T/R	N_b, corrected counting rate	I_b, Twice counting rate per mole of boron
	Moles		*Counts/sec*	*Disintegration /sec mole*
1	1.416×10^{-3}	0.050	12.57	1.775×10^6
2	1.012	.0505	8.84 (parallel plate)	1.747
			8.93 (wire)	1.764
3	1.751	.102	15.29	1.753

$I_b=n\hat{v}\hat{\sigma}L=1.761\times10^6$ where $\hat{\sigma}=746$ barns, and $L=6.025\times10^{23}$ atoms/mole. Finally, $n\hat{v}=3{,}918$ neutrons/cm^2 sec.

5. Sources of Error

It is somewhat difficult to estimate the errors precisely in this experiment. For each film the alpha plateau counting rate was determined with a statistical accuracy of at least 0.7 percent. For the thickest film, the thickness correction was 18 percent at $E/E_0=2/3$, but since T/R is probably good to 5 percent this introduces an error of only 0.9 percent in the corrected counting rate. The boron cross section should be accurate within 1 percent. Repeated analyses of standard solutions of boric acid containing 100 to 300 micrograms of boron had a standard error within 1.5 percent. Effects such as the neutron density depression and shielding by the platinum backing (including the boron) are each less than 0.15 percent.

When parallel plate collection is used a slight correction must be made to formula (4) because of the path of the particles in the gas. For the thickest film this correction is less than 0.4 percent at $E/E_0=3/4$.

Film 1 did not have a precise measurement of T/R and was analyzed, using a 10-ml buret for the NaOH titrant before the technique was refined with the use of a Gilmont ultramicroburet-pipet of 1-ml capacity subdivided into 1,000 divisions. This film has been assigned an error of 3.3 percent. Films 2 and 3 yielded measurements of $n\hat{v}$ good to 2.2 percent. The weighted average should be accurate to 1.5 percent (standard error).

Systematic errors may be present, e. g., isotopic enrichment during evaporation or loss of boric acid by volatilization during solution of the boron film in warm nitric acid. Assuming the systematic errors to be of the same order of magnitude as the statistical errors, then $n\hat{v}$ equals 3,918 neutrons/cm^2 sec (±2-percent standard error).

6. Comparison with Oak Ridge National Laboratory

Ritchie and Klema of the Oak Ridge National Laboratory have measured the thermal neutron flux in slot 11 of their standard graphite pile by beta-gamma coincidence measurements of activated gold foils. They obtained a value for $n\hat{v}\hat{\sigma}_{Au}$ of 5.905×10^4, and assuming $\hat{\sigma}_{Au}$ is 95 barns, $n\hat{v}$ equals 622 (±5 percent) neutrons/cm^2 sec. Identical gold foils were simultaneously exposed to the ORNL and NBS fluxes. The Oak Ridge foil was flown to the Bureau and alternately counted with the NBS foil under the same end-window beta counter. Exposures were made with and without cadmium, and the ratio of the cadmium difference counting rate is

$$\frac{A_{NBS}}{A_{ORNL}}=\frac{(n\hat{v})_{NBS}}{(n\hat{v})_{ORNL}}=6.42\ (\pm2.5\text{ percent}).$$

The ratio of the independently calibrated fluxes is

$$\frac{(n\hat{v})_{NBS}}{(n\hat{v})_{ORNL}}=\frac{3918}{623}=6.29,$$

which agrees with the gold-foil ratio within the experimental error.

7. References

[1] AECU report 2040.

[2] C. W. Tittle, Nucleonics **9**, 60 (1951).

[3] James A. De Juren and Hyman Rosenwasser, Phys. Rev. (Feb. 1954).

[4] Foote, Ind. Eng. Chem., Anal. Ed., **4**, 39 (1932).

[5] Thode, MacNamara, Lossing, and Collins, J. Am. Chem Soc. **70**, 3008 (1948).

[6] Hamermesh, Ringo, and Wexler, Phys. Rev. **90**, 603 (1953).

[7] Carter, Palevsky, and Myers, Phys. Rev. **91**, 450 (1953).

[8] V. Dibeler and F. Mohler, J. Am. Chem. Soc. **70**, 987 (1948).

WASHINGTON, September 3, 1953.

Journal of Research of the National Bureau of Standards Vol. 52, No. 2, February 1954 Research Paper 2478

Electron-Optical Shadow Method of Magnetic-Field Mapping [1]

L. Marton, J. Arol Simpson, and S. H. Lachenbruch

The essential features of the electron-optical shadow method for the quantitative mapping of magnetic fields are presented in unified form. The processes of obtaining and analyzing the shadowgrams are given in some detail. Iterative procedures of analysis, which have proved successful in practice, are illustrated by the mapping of an otherwise inaccessible ferromagnetic domain field. Sections 5 and 6 give an analytical method, involving inversion of integral operators. The method, although it has not yet been applied to the analysis of shadowgrams, is given because of its generality and applicability to the equivalent problem of interpretation of fluid dynamic interferograms.

I. Introduction

A technique was introduced about 3 years ago [2, 3] for quantitative mapping by means of an electron-optical system, of electric- and magnetic-field distributions, which, because of their small dimensions extending to below 1 micron or because they would appreciably be affected by the presence of a probe, are not capable of satisfactory measurement by conventional probe methods. Since that time, both experimental and theoretical studies of this "shadow method" have been made. The purpose of this paper is to summarize briefly in unified form the essential features of the method, as modified and broadened through subsequent published and unpublished studies and experiments.

The shadow method may be considered as consisting of the following three main basic steps: [to be discussed separately]:

Step 1 (Experimental). The field to be studied is placed in the path of an electron beam in the object space of an electron-optical lens system whose image space contains an opaque object, such as a wire grid, and the distortion of the shadow of this object due to the presence of the unknown field is measured as a function of position. When the field does not have axial symmetry, additional experimental data of value may be obtained by repeating the experiment with different orientations of the field and/or varying beam energies. Figure 1 shows the arrangement of one such nonsymmetrical sample and a representative shadow graph.

Step 2 (Geometrical). From this shadow distortion, and from known geometrical parameters of the electron-optical system, the angular deflections of different rays by the given field are calculated.

Step 3 (Analytical). The field distribution is calculated from this deflection function and from any known or assumed qualitative properties of the unknown field.

2. Step 1 (Experimental)

Figure 2 is a schematic diagram of the electron-optical arrangement used. The main components of the system are:

(a) an objective-lens system, characterized by the principal planes, P, P', and the focal length, f;

(b) the unknown field, placed in object space with its center at a distance s', from the first principal

[1] This paper is a summary of 3 years work in the Electron Physics Section of the National Bureau of Standards. Many members, past and present, have contributed to the work described. The bulk of the mathematical development, part of which appears as sections 5 and 6, is due to S. H. Lachenbruch. In the experimental part, much is due to the work of A. Van Bronkhorst, G. Ford, J. Suddeth, and T. McCraw.

[2] L. Marton and S. H. Lachenbruch, J. Research NBS **43** 409 (1949) RP2033.

[3] L. Marton and S. H. Lachenbruch, J. Appl. Phys. **20**, 1171 (1949).

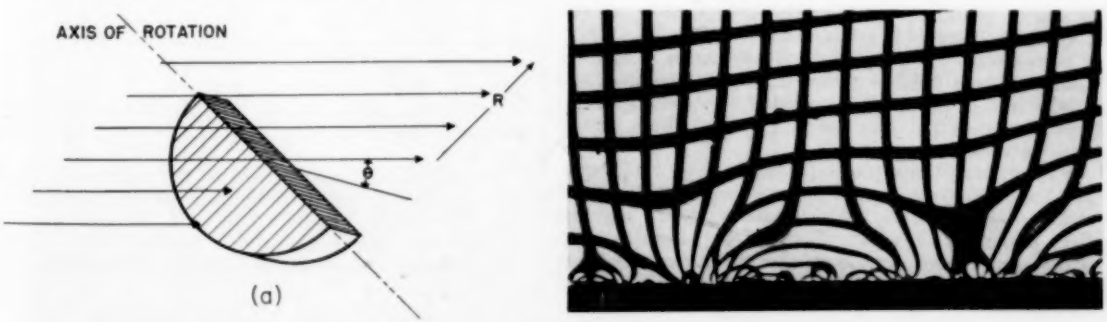

FIGURE 1.

(a) Typical arrangement for obtaining the shadowgraphs of a nonsymmetrical object. (b) Typical distorted mesh shadows.

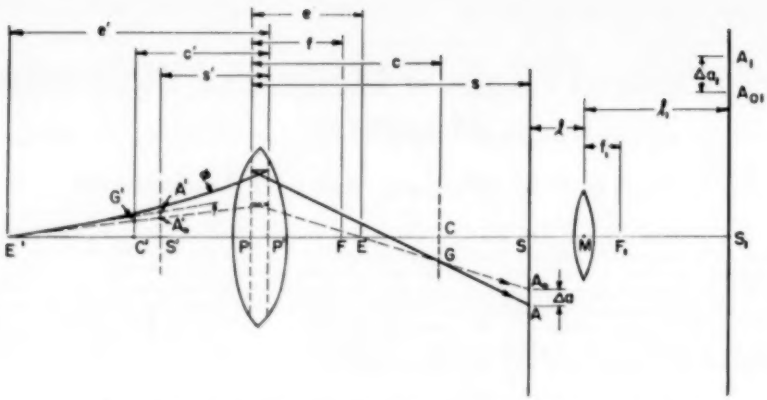

FIGURE 2. *Schematic drawings of the optics of the shadow method.*

plane (this determines the conjugate distance s);

(c) a point source, E', of electrons, at an "object distance" e', (usually $e'=\infty$), which determines a crossover point, E, at a distance e (usually $e=f$) in the absence of the unknown field;

(d) a wire mesh or other shadow-casting obstruction, placed in image space at a distance c, thereby determining the conjugate distance c';

(e) an optional projector lens, M, for magnifying the shadow image, characterized by the lens separation, $s+l$, and the focal length, f_1;

(f) a fluorescent screen or photographic plate in the final image plane (S or S_1) conjugate to the plane containing the center of the field.

Most of the work at the Bureau has been done with a modified [4] electron microscope, which provides the above components in a convenient form.

As the following conditions are to be assumed in the calculations, it is necessary that they be satisfied experimentally:

Assumption 1. The trajectories within the field lie entirely in one plane (the plane of fig. 2).

Assumption 2. All lateral distances and angles, measured from the optical axis, are sufficiently small to make geometrical aberrations negligible, so the Gaussian dioptrics is applicable.

Assumption 3. The distance between deflecting field and lens field is sufficiently great so that the interaction between the two fields may be neglected.

Assumption 4. The electron energy, V, is in the nonrelativistic range.

The assumptions place limitations on the form, position, orientation, and order of magnitude of the electromagnetic field. Thus, assumption 1 requires that planes exist in which the field produces only plane deflections, and assumption 2 requires that these deflections be small. No restriction is placed on the time variation of the field which may be static or varying.[5]

The solid ray in figure 2 represents a typical electron trajectory, deflected by an angle ϕ by the unknown field before entering the lens system, and casting, on the final screen S_1, a shadow A_1 of the point G of the opaque obstruction. The broken ray represents the trajectory, which, in the absence of the deflecting field, would pass through this same point G, the corresponding shadow being at A_{01}. The distance between these two points, which represents the displacement of the shadow of G due to the presence of the field, may be measured for each point G, whose shadow can be identified and then be plotted as a function of the distance $a(\overline{S_1A_1})$, which is approximately proportional to the coordinate $a'(\overline{S'A'})$ in the deflecting field.

Practically, the distances Δa can be measured (1) directly on a plate on which two exposures with and without deflecting field are superimposed; (2) if only one exposure with deflecting field is taken and there exists an undistorted region of the shadow pattern, the straight line corresponding to this part of the plot $(a-a_0)$ versus a can be extrapolated, and the distances between the actually observed portions of the shadow and their extrapolated line can be measured; (3) if no undistorted part of the shadow pattern exists, a second mesh can be introduced between the electron gun (or condensor lens) and the deflecting field providing a reference mesh-wire system.[6]

Tests with the known field in the equatorial plane of a Helmholtz coil as deflecting object have shown that the errors introduced in this $(a-a_0)$ versus a plot by the aberration of the lens and the experimental uncertainties are smaller than 2 percent.

[4] J. A. Simpson and A. Van Bronkhurst, Rev. Sci. Instr. **21**, 669 (1950).

[5] L. Marton and D. L. Reverdin, J. Appl. Phys. **6**, 617 (1950).

[6] D. L. Reverdin J. Appl. Phys. **22**, 257 (1951).

3. Step 2 (Geometrical)

Assumption 2 above implies the existence of a linear relation between Δa_1, a measurement in the final image plane, and the angle ϕ, through which the unknown field deflects the ray that passes through the typical point A' of the field. This relation may be expressed as

$$\phi = K\Delta a_1 \tag{1}$$

where K is a known function of the magnifications and other fixed geometrical parameters of the system. From the geometry of figure 2, it is easy to show that K may be expressed as

$$K = \frac{1}{f\mu_1(\nu-1)(1-\epsilon/\mu)}, \tag{2}$$

where

$\mu_1 = l_1/l = \Delta a_1/\Delta a$ = magnification of projector system;

$\mu = s/s' = \Delta a/\Delta a'$ = magnification of magnetic object on screen S;

$\nu = (s-e)/(c-e)$ = magnification of opaque object C as determined by its shadow on screen S in absence of deflecting field;

$\epsilon = e/e'$ which vanishes when incident beam is parallel.

Whereas in step 1 the deflecting effect of the field was magnified, by means of a lens system and shadow-casting object, in order to facilitate the measurement of that effect, in step 2 this magnified effect, represented by the measurement Δa_1, is converted back to angular deflection in object space.

The problem of experimentally determining K by measuring the quantities on the right-hand side of eq (2) is somewhat complicated by the distortion introduced by the projector lens. This distortion makes the precise determination of the magnifications difficult. A series of tests [7] on the known field of a small Helmholtz coil shows that with care the errors introduced in the determination of K can be less than 5 percent.

4. Step 3 (Analytical)

The discussion of this step will be limited, for simplicity, to magnetic fields, which have been studied in considerable detail.

We note first that assumption 1 above confines the analysis of magnetic fields to planes (such as the equatorial plane) that intersect all magnetic lines of force orthogonally. All electrons initially moving in such a plane will remain therein because their deflection by the field is everywhere normal to both the path and the lines of force. The plane of figure 2 must therefore have this property.

[7] J. A. Simpson, Proceedings of the NBS Semicentennial Symposium on Electron Physics, NBS Circular 527 (1954).

Figure 3, which lies in one such plane, summarizes the theoretical problem of step 3. The polar coordinate system (r, θ) is attached to the magnetic field $H(r, \theta)$, which is directed normal to the plane of the figure. The relative orientation of field and optical system may be varied experimentally. The curve L represents a typical electron trajectory through the field in this plane. It may be considered as approximately straight because assumption 2 implies that the deflection angle ϕ is necessarily small—otherwise the method, which involved geometrical optics, would not have been applicable. Moreover, this assumption eliminates the variation of beam energy as an added parameter for investigation of nonsymmetrical fields.

In steps 1 and 2 a lens system has served the purpose of measuring, by magnifying its effect, the deflection angle, ϕ, corresponding to each of a certain set of directed lines, L, in the plane of figure 3. Now, each such line is identified uniquely by a pair of coordinates (p,β) as shown, where the angle β may be varied experimentally by arbitrary plane rotations of the field relative to the lens system, and p is the classical impact parameter, and in the case of parallel illumination is equal to a_0/μ. Having served its purposes, therefore, the lens system may now be disregarded, and the problem remaining may be stated as follows: For each of a certain set of directed lines $L = L(p,\beta)$ in the plane of figure 2, each identified by coordinates (p,β), we have an experimentally determined deflection angle $\phi = \phi(p,\beta)$, and hence, by the well-known relation (giving the deflection of a charged particle in motion through a magnetic field), the value of

$$I(p,\beta) = \int_{L(p,\beta)} H(r,\theta)\,ds = \sqrt{\frac{2mV}{e}}\,\phi(p,\beta), \tag{3}$$

the integral of H along that line. (Here e, m, and V are the charge, mass, and potential of the electrons.) We wish to derive from this the magnitude

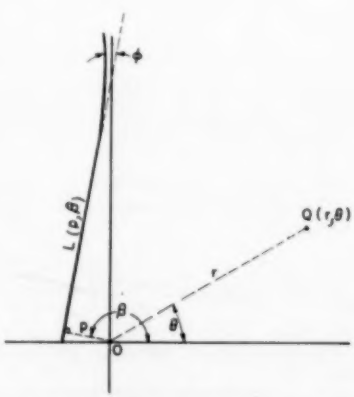

FIGURE 3. *Coordinates used in the analysis of shadowgraphs.*

and sign of the unknown H at an arbitrary point Q with polar coordinates (r,θ). It is in this step—that of obtaining the unknown function H (r,θ) from its integral $I(p,\beta)$—that a number of procedures have been proposed, and several tried. These methods are summarized below.

▸ It is worth noting that the problem is essentially the same one that arises in the interpretation of interferograms taken of air flow, and any of the methods used in that field apply. Recently, it has been shown that the problem may be programmed for a large-scale computer.[8] If such a computer is available, this represents the ideal method of analysis of shadowgrams.

▸ For the case where the field is known to have axial symmetry about some axis normal to the plane of figure 3, we can choose the origin as the intersection of the axis with the plane. Then $H=H(r)$ is independent of θ, and also $I=I(p)$ is independent of β, so the problem is greatly simplified. Some of the methods about to be described are limited to this case, which, due to the difficulties of the more general case, is the only one that has been investigated in detail up until this time.

4.1. Method (a). Fitting of parameters

In the method first used, the unknown field $H(r,\theta)$ is assumed to have a specific analytical form, usually selected from known or predicted physical properties of the field and field-producing object, and involving one or more unknown parameters $(a_1,a_2, \ldots)$ to be determined

$$H(r,\theta)=F(r,\theta,a_1,a_2 \ldots a_n), \tag{4}$$

where F is a preassigned function of r and θ, periodic in θ.

Integrating the specified function F in advance gives a predicted analytical form for I, as a known function G of $(n+2)$ quantities

$$I(p,\beta)=\int_{L(p,\beta)} F(r,\theta,a_1,a_2 \ldots a_n)ds=G(p,\beta,a_1 \ldots a_n) \tag{5}$$

We wish to solve for the n quantities a_i by matching this G-function against the values of the I-function obtained experimentally for different values of p and β.

One way to do this is statistical—by applying least squares to the experimental results, starting with an equation of the form

$$\sum_{k=1}^{m}[I_k-G(p_k,\beta_k,a_1 \ldots a_n)]^2=\text{minimum}, \tag{6}$$

m being the number of electron paths for which experimental data have been obtained. Here the closeness of fit can usually be used as a partial check on the validity of the functional form F chosen. But how good a check is not known until we consider the question of uniqueness, mentioned at the conclusion of section 6.

An example of the method of fitting of parameters is described in detail in an earlier paper (see footnote 3). The field of a magnetized wire, in its equatorial plane, was evaluated on the hypothesis that its form approximated that of the field between two equal and opposite point poles of unknown magnetic moment, a^1, separated by an unknown distance, $2a_2$. For this case, the function F of eq (4) is

$$H(r)=F(r,a_1,a_2)=a_1(r^2+a_2^2)^{-3/2}. \tag{8}$$

The corresponding function G is found from eq (5) to be

$$G(p,a_1,a_2)=2a_1/(p^2+a_2^2). \tag{9}$$

The moment a_1 and pole separation, $2a_2$, and hence the field $H(r)$, were obtained by a least-squares method of fitting the function G to an experimental scatter diagram derived from deflection measurements.

4.2. Method (b). Evaluation by step-function approximation

In a second method, the field is assumed to exist only in a finite portion of the plane of figure 3, and this portion subdivided into n regions R_k of chosen shape and size, and the field calculated as if it were a step-function constant within each such region

$$H(r,\theta)\equiv a_k \tag{10}$$

where $(r,\theta)\epsilon R_k, k=1,2 \ldots n$. By integration we obtain

$$I(p,\beta)=\sum_{k=1}^{n} a_k\lambda_k(p,\beta), \tag{11}$$

where $\lambda_k(p,\beta)$ is defined to be the length of the segment of intersection of the line $L(p,\beta)$ and the region R_k.

If, then, I (p,β) is known experimentally for n different electron paths $L(p,\beta)$, there result n simultaneous linear equations in the n constant values a_k of H. These equations may, in general, be solved for the a_k,although the labor may be great in many cases. Moreover, it is not possible generally to choose a grid and a set of rays that insure that the set of equations is linearly independent. This proves to be a very serious difficulty.

The technique to be described avoids both difficulties. Figure 4 shows the grid used to study the field about a corner of the cobalt crystal of figure 1. This is merely an illustration, and a number of other grids have been developed for specific problems, but all use the same technique. The rays are so

[8] F. D. Bennett et al. Interferometric analysis of airflow about projectiles in free flight, Ballistic Research Laboratories, Aberdeen Proving Ground, Report No. 797 (March 1952).

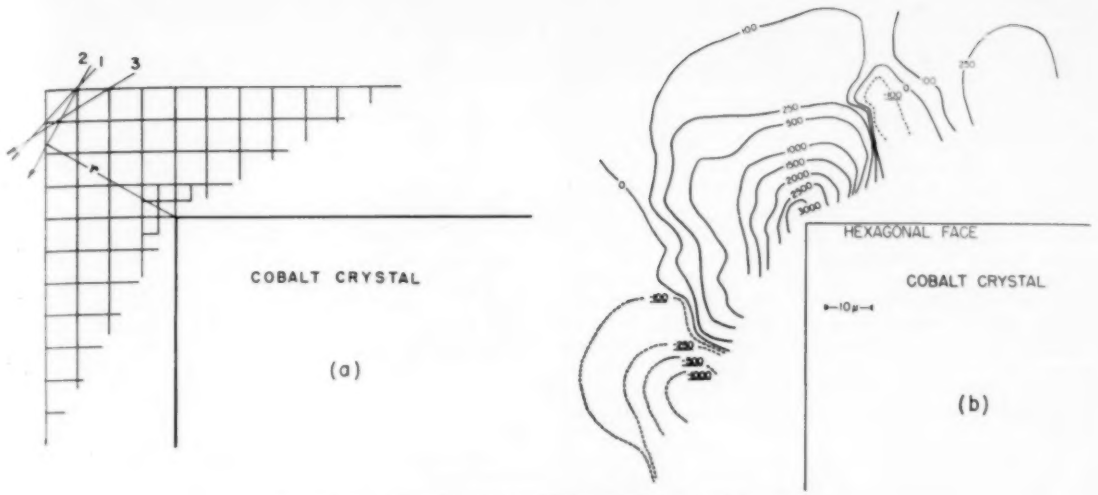

FIGURE 4. *Analysis of magnetic fringe field of a cobalt crystal.*

(a) Grid used in evaluation of fields about the corner of the sample by means of the step-function approximation. (b) Results of this method on the fringe field of a single cobalt crystal.

chosen that each ray passes through only one square for which a_k has not previously been determined. The first three such rays are shown in figure 4. With such a system, the determinant is triangular and can be solved within a reasonable time. Unfortunately, with a given number of values of the angular parameter, only a limited number of grids may be used before it is impossible to draw a line that does not pass through two or more unknown grids. In the grid illustrated, this takes place after 47 squares have been evaluated, when there are shadowgraphs available for each 15° of revolution. Figure 4, b, shows the results of this method applied to the field of the cobalt crystal

The errors inherent in this procedure are complicated and large. In addition to any experimental errors involved, one has the error caused by replacing the integral with the rather crude sum. This error can be estimated by changing the number of the meshes up to the maximum possible and observing the change in values. A value for this error seems, in practice, to be as large as several hundred percent. The exact value depends on the magnitude of the gradient and also on the sensitivity of the original shadowgraph. (The field is considered to fall to zero outside the grid, which, in practice, is extended to the limit of the region in which there is a measurable deflection.)

Known properties of the field sometimes suggest a special choice of subdivision. For example, if the field is known to have rotational symmetry about some known point in the plane of figure 3, the most appropriate mode of subdivision would be into rings bounded by concentric circles about that point, inasmuch as the field is constant along any one of these circles.

The field surrounding a magnetized wire has been computed by this method and showed good agreement with the result obtained by method (a), in which the field was assumed to be that of a pair of point poles (see eq 8 and 9).

4.3. Method (c). Series expansion

A field that is known to have axial symmetry about a point at which it may reasonably be assumed to become infinite can, in general, be assumed expansible as a series in inverse powers of the distance r from that point, such a series being convergent for sufficiently large r

$$H(r)=\frac{a_2}{r^2}+\frac{a_3}{r^3}+\cdots \tag{12}$$

Physically, this expansion corresponds to assuming that the field is that of an n-pole, and hence no terms below that corresponding to a single pole (a_2) appears.

By integration of (12) along the horizontal line $L(p,\pi/2)$ whose equation is $r \sin\theta = p$, we obtain

$$\begin{aligned} I(p)&=\int_{L(p,\pi/2)} H(r)ds=\int_L H(r)d\left(\sqrt{r^2-p^2}\right)\\ &=2\int_p^\infty\left(\frac{a_2}{r}+\frac{a_3}{r^2}+\cdots\right)\frac{dr}{\sqrt{r^2-p^2}}\\ &=\frac{\pi a_2}{p}+\frac{2a_3}{p^2}+\cdots \end{aligned} \tag{13}$$

On matching this series expression for $I(p)$ against the function obtained experimentally, one is able to

evaluate numerically the coefficients $a_2, a_3, \ldots$, and hence deduce the series representation (12) for H.

Even when the condition of axial symmetry is not satisfied, it may sometimes be possible to find types of series appropriate for expansion of given field distributions. The numerical evaluation of the coefficients would then be obtained, as above, by matching the termwise integral of the series with the experimentally derived function $I(p,\beta)$. The restrictions, techniques, etc., would of course vary from case to case; thus, for example, if a Fourier series, or other series in orthogonal functions, is used, the unknown coefficients will generally be obtainable from an explicit formula involving definite integrals.

The series expansion method, although it has a certain amount of generality, must be used with some caution. On account of questions of convergence, for example, a series of form (12) could never be used in the neighborhood of the point $r=0$.

5. Direct Method of Inversion of Integral Operators

It is to be noted that in all three methods described above, the approach consists in assuming *a priori* some specific analytical form for H, involving one or more unknown parameters, which are then evaluated from experimental results. In this sense, they may all, in fact, be regarded as special cases of method (a). If, for example, the function F of (4) is taken to be the step function of (10), the result is essentially method (b); and if F is a series such as (12), one obtains method (c). Still other methods may be derived by choosing F as a function of still different form. Thus a generalization of method (b) is obtained by choosing F to be a linear or second-degree function, rather than a constant, in each region R_k.

An entirely different approach consists in interpreting (3) as an integral equation, and observing that it can, in general, be uniquely solved for the unknown function $H(r,\theta)$ in terms of the function $I(p,\beta)$ which may be obtained experimentally.

To date, no use has been made of the method in experimental work. However, because of its generality, preciseness, and application to the analysis of interferograms in fluid dynamics, it is given in detail.

5.1 Analytical solution for case of axial symmetry

For the following considerations, the integral equation (3) may be expressed in a more specific form by using the equation of $L(p,I)$ (see fig. 3).

$$P=r\cos(\theta-\beta). \tag{14}$$

By solving (14) for θ, we see that, on the line $L(p,\beta)$

$$\theta=\begin{cases}\beta+\cos^{-1}p/r & \text{on the one half-line}\\ \beta-\cos^{-1}p/r & \text{on the other half line}\end{cases} \tag{15}$$

Substituting (15) into (3), and expressing ds as a function of r, we obtain

$$I(p,\beta)=\int_p^\infty\left[H\left(r,\beta+\cos^{-1}\frac{p}{r}\right)+H\left(r,\beta-\cos^{-1}\frac{p}{r}\right)\right]\frac{rdr}{\sqrt{r^2-p^2}}. \tag{16}$$

We take first the important special case where the field is known to have axial symmetry about some axis normal to the plane P. We can choose as origin of coordinates the intersection of this axis with P. Then $H=H(r)$ is independent of θ, and also $I=I(p)$ is independent of β. Hence, (16) simplifies to the form

$$I(p)=2\int_p^\infty H(r)rdr/\sqrt{r^2-p^2}. \tag{17}$$

Now Abel's integral equation,

$$f(z)=\int_a^z g(y)dy/(z-y)^\lambda \quad (0<\lambda<1), \tag{18}$$

is known to have the unique continuous solution

$$g(y)=\frac{\sin\lambda\pi}{\pi}\frac{d}{dy}\int_a^y f(z)dz/(y-z)^{1-\lambda}, \tag{19}$$

provided $f(z)$ satisfies certain very general continuity conditions and $f(a)=0$. If in (18) one replaces z by $(-p^2)$, $f(z)$ by $I(p)$, a by $-\infty$, λ by $\frac{1}{2}$ by 2, y by $(-r^2)$, and $g(y)$ by $H(r)$, it is seen to reduce exactly to (17). By (19), therefore, the unique solution of integral eq (17) is

$$H(r)=\frac{\sin\pi/2}{\pi}\frac{d}{d(-r^2)}\int_{-\infty}^{-r^2}I(p)d(-p^2)/\sqrt{p^2-r^2},$$

which may be reduced to any of the following equivalent forms

$$\begin{aligned}H(r)&=\frac{-1}{\pi r}\frac{d}{dr}\int_r^\infty I(p)pdp/\sqrt{p^2-r^2}\\&=\frac{-1}{\pi r}\int_0^\infty\frac{\partial}{\partial r}[I(\sqrt{r^2+\mu^2})]d\mu\\&=-\frac{1}{\pi}\int_0^\infty I'(\sqrt{r^2+\mu^2})d\mu/\sqrt{r^2+\mu^2}\\&=-\frac{1}{\pi}\int_r^\infty I'(p)dp/\sqrt{p^2-r^2}.\end{aligned} \tag{20}$$

We have thus an explicit expression for the field $H(r)$ in terms of the empirically known function $I(p)$. If $I(p)$ is known at a sufficient number of experimental points so that a curve may be plotted, the value of $H(r)$ corresponding to each value of r may be calculated directly from (20) by some numerical integration procedure.

The integral eq (17) and its solution (20) may be abbreviated as

$$I(p)=T\{H(r)\};\quad H(r)=T^{-1}\{I(p)\}. \tag{21}$$

This form suggests a somewhat different way of viewing the problem: viz, as the problem of inverting a linear integral operator T in function-space.

It can also be considered as a problem in integral transforms. When miscellaneous elementary functions are substituted for $H(r)$, and the corresponding functions $I(p)$ are calculated from (17) and simplified, and then verified by substitution into (20), a table of transforms may be constructed, similar in form to a table of Fourier or Laplace transforms, and the linearity property may be used to derive the transforms of more complicated functions, including the field-distribution functions most frequently encountered.

The one-to-one correspondence implied by (21), or by (17) and (20), provides a conclusive answer, for the axially symmetric case, to the question of uniqueness of the result—a question not rigorously investigated previously. We can now state that if the shadow method is applied to a magnetic field known to have axial symmetry, and if a sufficient number of experimental measurements are made so that the empirical function $I(p)$ may be considered as a known continuous function of the continuous variable p, then there exists one and only one (continuous) function $H(r)$ satisfying (17), and it is given in terms of the known $I(p)$ by (20).

5.2. Analytical solution for fields of general form

Finally, we turn to the general case, removing the condition of axial symmetry. The general problem is that of solving (16) for the function $H(r,\theta)$ of two variables, when sufficient experimental data are available so that $I(p,\beta)$ may be treated as an experimentally known function of both variables.

We note first that for any fixed value of r, the field H must be a periodic function of θ, with period 2π, and so it must have a unique Fourier series expansion with functions of r as coefficients

$$H(r,\theta)=\sum_{n=-\infty}^{+\infty} H_n(r)\exp(in\theta). \tag{22}$$

Similarly, I has a unique Fourier expansion, with functions of p as coefficients

$$I(p,\beta)=\sum_{-\infty}^{+\infty} I_n(p)\exp(in\beta). \tag{23}$$

On substituting (22) and (23) into (16), and equating coefficients of like powers of $\exp(i\beta)$ on the two sides of the resulting equation, one obtains

$$I_n(p)=2\int_p^\infty H_n(r)\cos(n\cos^{-1}p/r)\frac{rdr}{\sqrt{r^2-p^2}},$$
$$(n=0,\pm1,\pm2,\ldots). \tag{24}$$

For each value of n, (24) is an integral equation for $H_n(r)$ in terms of $I_n(p)$.

A calculation carried out in the appendix shows that these integral equations have unique solutions for the H-coefficients in terms of the corresponding I-coefficients. If, then, one has sufficient experimental data to define the continuous function $I(p,\beta)$, the coefficients in its Fourier expansion (23) are uniquely determined from the formula

$$I_n(p)=\frac{1}{2\pi}\int_0^{2\pi} I(p,\beta)\exp(-in\beta)d\beta, \tag{25}$$

the coefficients $H_n(r)$ are then determined in turn as solutions of the integral eq (24), and so the desired function $H(r,\theta)$ will be obtained explicitly in the form of a Fourier series (22).

The fact that a Fourier series representation was used here as a tool to solve the general problem, and to investigate existence and uniqueness questions, may tend to obscure the basic nature of the result. By analogy with (21), we may abbreviate the integral eq (16) and its solution as

$$I(p,\beta)=T(H(r,\theta)),\quad\text{and}\quad H(r,\theta)=T^{-1}(I(p,\beta)). \tag{26}$$

This form again suggests that the problem may be viewed as that of inverting a linear integral operator T, this time in a space of functions of two variables. It is possible that more compact expressions and proofs might be possible when the problem is attacked from such a point of view.

The question of uniqueness is again seen to be conclusively answered as a by-product of this analysis—this time for the general (nonsymmetric) case. We can state that if, in applying the shadow method to a magnetic field that is not known to have axial symmetry, sufficient experimental data are obtained so that the function $I(p,\beta)$ may be considered as a known continuous function of the two continuous variables p and β, periodic in β (with period 2π), then there exists one and only one (continuous) function $H(r,\theta)$, periodic in θ (with period 2π), and satisfying (3). It is obvious that in order to satisfy the requirement of sufficient data in this general case, it will be necessary to determine the dependence of I on β by repeating the experimental measurements for different relative orientations of field and optical axis.

6. Appendix. Outline of a Procedure for the successive solution of the integral equations (24)

(a) When $n=0$, (24) becomes

$$I_0(p)=2\int_p^\infty H_0(r)dr/\sqrt{r^2-p^2}, \tag{27}$$

which has exactly the same form as (17), and, therefore, by (20), has the unique continuous solution

$$H_0(r)=-\frac{1}{\pi}\int_r^\infty I_0'(p)/\sqrt{p^2-r^2}. \tag{28}$$

(b) When $n=\pm 1$, (24) takes the form

$$I_{\pm 1}(p)=2p\int_p^\infty H_{\pm 1}(r)dr/\sqrt{r^2-p^2}$$

or

$$I_{\pm 1}(p)/p=2\int_p^\infty \frac{H_{\pm 1}(r)}{r}\frac{rdr}{\sqrt{r^2-p^2}}, \tag{29}$$

which is of the same form as (27) except that the functions $I_0(p)$ and $H_0(r)$ are replaced, respectively, by $I_\pm(p)/p$ and $H_{\pm 1}(r)/r$. The unique solution, obtained from (20), is therefore

$$H_{\pm 1}(r)=-\frac{r}{\pi}\int_r^\infty \frac{d}{dp}\left[\frac{I_{\pm 1}(p)}{p}\right]\frac{dp}{\sqrt{p^2-r^2}} \tag{30}$$

(c) The higher-order coefficients (for $|n|\geq 2$) are more difficult to evaluate. The following method of obtaining the coefficients for $n=\pm 2$ and $n=\pm 3$ appears capable of extension to coefficients of higher order.

Since

$$\cos[\pm 2\cos^{-1}k]$$

$$=2(k^2-1)+1;\quad \cos[\pm 3\cos^{-1}k]=4k(k^2-1)+k \tag{31}$$

(24) becomes, for $n=\pm 2$ or ± 3,

$$I_n(p)=2\int_p^\infty H_n(r)\left(\frac{p}{r}\right)^{|n|-2}\left\{A_n\left[\left(\frac{p}{r}\right)^2-1\right]+1\right\}\frac{rdr}{\sqrt{r^2-p^2}}, \tag{32}$$

where

$$A_2=A_{-2}=2,\ A_3=A_{-3}=4 \tag{33}$$

But (32) may be written as

$$\frac{I_n(p)}{p^{|n|-2}}=2\int_p^\infty \frac{H_n(r)rdr}{r^{|n|-2}\sqrt{r^2-p^2}}-2A_n\int_p^\infty \frac{Hn^{(r)}}{r^{|n|-1}}\sqrt{r^2-p^2}dr, \tag{34}$$

which becomes, on applying integration by parts to the last integral,

$$\frac{I_n(p)}{p^{|n|-2}}=2\int_p^\infty f_n(r)\frac{rdr}{\sqrt{r^2-p^2}} \tag{35}$$

where

$$f_n(r)=\frac{H_n(r)}{r^{|n|-2}}-A_n\int_r^\infty \frac{H_n(\mu)d\mu}{\mu^{|n|-1}}. \tag{36}$$

Equation (35) is again of the general form (17) with certain replacemen s, and hence, by (20)

$$f_n(r)=-\frac{1}{\pi}\int_r^\infty \frac{d}{dp}\left[\frac{I_n(p)}{p^{|n|-2}}\right]\frac{dp}{\sqrt{p^2-r^2}}. \tag{37}$$

Substituting (36) into (37) and differentiating with respect to r,

$$\frac{d}{dr}\left[\frac{H_n(r)}{r^{|n|-2}}\right]+\frac{A_n}{r}\left[\frac{H_n(r)}{r^{|n|-2}}\right]=\frac{-1}{\pi}\frac{d}{dr}\int^\infty \frac{d}{dp}\left[\frac{I_n(p)}{p^{|n|-2}}\right]\frac{dp}{\sqrt{p^2-r^2}}. \tag{38}$$

But (38) is a linear first-order differential equation in the unknown function $H_n(r)/r^{|n|-2}$, which can be solved explicitly for $H_n(r)$ by the usual formula, and the arbitrary constant evaluated from the condition that it vanishes at $r=\infty$. This determines the functions H_2, H_{-2}, H_3, H_{-3} uniquely, as was to be proved.

7. Summary

The electron-optical shadow method of field mapping has been used at the Bureau for 3 years to study such diverse and otherwise inaccessible fields as the fringe fields of ferromagnetic domains of single crystals and collodial particles, space-charge fields in magnetrons, and the external fields of magnetic recording wire. The over-all accuracy of the method depends upon the analysis of the experimental data, and, in favorable cases, has been as good as 5 percent although 10 or 100 times greater error may result in the more unfavorable cases. But in any case, the method opens a new magnitude of fields to study and measure.

In addition to those mentioned in the text and notes, the following nembers, past and present, in the Electron Physics Section, National Bureau of Standards, have by their efforts advanced the work reported: H. Mendlowitz, H. Ernst, J. Stewart, A. A. Nargizian, D. Schubert, P. Weinzierl, L. Greene, A Dauses, and L. Mann. We express our appreciation for their help.

WASHINGTON, March 17, 1953.